Journal of Structural Biology 196 (2016) 260–287

Contents lists available at ScienceDirect

Journal of Structural Biology

journal homepage: www.elsevier.com/locate/yjsbi

Nonclassical crystallization *in vivo et in vitro* (II): Nanogranular features in biomimetic minerals disclose a general colloid-mediated crystal growth mechanism

Carlos Rodríguez-Navarro [a,*], Encarnación Ruiz-Agudo [a], Joe Harris [b], Stephan E. Wolf [b,c]

[a] Dpto. Mineralogía y Petrología, Universidad de Granada, Fuentenueva s/n, 18071 Granada, Spain
[b] Department of Materials Science and Engineering, Institute of Glass and Ceramics (WW3), Friedrich-Alexander-University Erlangen-Nürnberg, Martensstrasse 5, 91058 Erlangen, Germany
[c] Interdisciplinary Center for Functional Particle Systems (FPS), Friedrich-Alexander University Erlangen-Nürnberg (FAU), Haberstrasse 9a, 91058 Erlangen, Germany

ARTICLE INFO

Article history:
Received 29 January 2016
Received in revised form 5 September 2016
Accepted 7 September 2016
Available online 9 September 2016

Keywords:
Biomimetics
Calcium carbonate
Amorphous precursor
Dense liquid precursors
PILP
Nanogranular
Nonclassical crystallization
Nanoparticle-mediated crystal growth

ABSTRACT

Recent research has shown that biominerals and their biomimetics (i) typically form via an amorphous precursor phase, and (ii) commonly display a nanogranular texture. Apparently, these two key features are closely related, underlining the fact that the formation of biominerals and their biomimetics does not necessarily follow classical crystallization routes, and leaves a characteristic nanotextural imprint which may help to disclose their origins and formation mechanisms. Here we present a general overview of the current theories and models of nonclassical crystallization and their applicability for the advance of our current understanding of biomineralization and biomimetic mineralization. We pay particular attention to the link between nonclassical crystallization routes and the resulting nanogranular textures of biomimetic $CaCO_3$ mineral structures. After a general introductory section, we present an overview of classical nucleation and crystal growth theories and their limitations. Then, we introduce the Ostwald's step rule as a general framework to explain nonclassical crystallization. Subsequently, we describe nonclassical crystallization routes involving stable prenucleation clusters, dense liquid and solid amorphous precursor phases, as well as current nonclassical crystal growth models. The latter include oriented attachment, mesocrystallization and the new model based on the colloidal growth of crystals via attachment of amorphous nanoparticles. Biomimetic examples of nanostructured $CaCO_3$ minerals formed via these nonclassical routes are presented which help us to show that colloid-mediated crystal growth can be regarded as a wide-spread growth mechanism. Implications of these observations for the advance in the current understanding on the formation of biomimetic materials and biominerals are finally outlined.

1. Introduction

Biominerals display complex shapes, a hierarchical structure, and an exquisite organization at multiple length-scales, which along with the right combination of rigid (mineral) and elastic/-plastic (organic) materials, provide them with unmatched functionality and physical-mechanical properties (Cölfen and Yu, 2005; Gómez-Morales et al., 2015; Gower, 2008; Hendley et al., 2015; Lowenstam and Weiner, 1989; Mann, 2001; Meldrum and Cölfen, 2008; Nudelman and Sommerdijk, 2012). These features enable biominerals to, for instance, offer protection and structural support (Lowenstam and Weiner, 1989), act as equilibrium, optical or sensing (orientation or navigation) devices (Aizenberg et al., 2001; Faivre and Schüler, 2008; Lowenstam and Weiner, 1989), provide structural color (Li et al., 2015), and act as ion reservoirs (Sato et al., 2011). Inspired by nature and in a quest to reproduce *in vitro* the superior properties and functionality of biominerals, chemists and material scientists have tried to replicate them in the laboratory via bottom-up, mild synthesis routes (Aizenberg and Fratzl, 2009; Arakaki et al., 2015; Imai et al., 2006; Liu and Jiang, 2011; Meldrum and Cölfen, 2008; Munch et al., 2008; Sanchez et al., 2005; Sommerdijk and de With, 2008; Wegst et al., 2015; Xu et al., 2007; Yao et al., 2014). This bio-inspired or biomimetic synthesis approach is not only aimed at replicating abiotically the size, shape, orientation, composition and hierarchical organization of existing biominerals, but also strives to learn guiding principles and ideas that nature has mastered through

* Corresponding author.
E-mail address: carlosrn@ugr.es (C. Rodríguez-Navarro).

http://dx.doi.org/10.1016/j.jsb.2016.09.005
1047-8477/

billion years of evolution (since early microbial biomineralization; see for instance Wright and Oren, 2005) and use them for the synthesis of novel functional materials (Xu et al., 2007). Indeed, as indicated by Gómez-Morales et al. (2015) "what is really important in biomimetic and bio-inspired studies is not the devices themselves, but to understand the mechanisms that life uses to produce them". Interestingly, the synthesis and analysis of biomimetic minerals is in turn yielding important results that are helping to shed light on the mechanisms of biomineralization. Some of these results, particularly those referring to the nanotextural features of biomimetic calcium carbonate minerals and their relationship to nonclassical crystallization routes, are reviewed here.

Growing experimental evidence is showing that biominerals and their biomimetic counterparts commonly display two key features that seem to be related and might be general (Gal et al., 2014, 2015; Gower, 2008): they form via amorphous precursor phases (Addadi et al., 2003; Aizenberg et al., 2003; Beniash et al., 1997, 2009; DeVol et al., 2015; Gal et al., 2010; Gong et al., 2012; Gower, 2008; Killian et al., 2009; Lowenstam and Weiner, 1985; Mahamid et al., 2008; Politi et al., 2004, 2008; Rodriguez-Navarro and Ruiz-Agudo, 2013; Rodriguez-Navarro et al., 2015a,b; Seto et al., 2012; Towe and Lowenstam, 1967), and display a nanogranular texture, typically made up of oriented nanocrystals less than 100 nm in size (for an extended list of contributions, see the first part of this review and references therein -Wolf et al., 2016a, or, for instance Böhm, 2016; Dauphin, 2001, 2008; Cuif et al., 2011; Gal et al., 2013, 2014, 2015; Miyajima et al., 2015; Oaki et al., 2006; Rodriguez-Navarro et al., 2015b; Ruiz-Agudo et al., 2016; Sethmann et al., 2006; Seto et al., 2012; Sondi et al., 2011; Stolarski and Mazur, 2005; Wolf et al., 2012, 2015a). These two key features underline the fact that the formation of biominerals and their biomimetics does not seem to follow classical crystallization routes/pathways. Furthermore, their nonclassical crystallization and subsequent coarsening via an aggregation-based growth mechanism where precursor nanoparticles, liquid or solid, amorphous or crystalline, are the building blocks, as opposed to monomers (as postulated by classical crystallization theory), leaves a characteristic nanotextural imprint (Fig. 1) which may help to disclose their formation mechanisms and may also aid in the recognition of biotic signatures in the geologic record.

Here we review some of the key structural and textural (nanogranular) features of biomimetic minerals, as well as their nonclassical nucleation and growth mechanisms. For this, we first present a brief description of the fundamentals of classical nucleation (CNT) and growth (CGT) theories. Afterwards we introduce the Ostwald's step rule, and discuss the different (thermodynamic and kinetic) theories put forward to explain its origins. The Ostwald's step rule helps us to put into context the following sections in which we present the current models for nonclassical nucleation (stable prenucleation clusters, liquid and solid amorphous precursors) and colloid-mediated, aggregation-based nonclassical crystal growth. We show that the formation of amorphous (liquid and solid) precursor phases, in conjunction with the presence (and effects) of organic additives, along with a general colloid-mediated nonclassical crystal growth mechanism, helps to explain the nanogranular features of a range of biomimetic minerals. Several examples of biomimetic materials with nanogranular features are presented and described here which help us to show that a colloid-mediated crystal growth might be a general growth mechanism *in vitro* (and *in vivo*, too; see Wolf et al., 2016a). We focus our review on calcium carbonate biomimetic minerals for two main reasons: (i) calcium carbonates are the most abundant biominerals and their biomimetics have been the subject of extensive research; and (ii) significant progress in our current understanding of nonclassical crystallization has recently taken place studying the $CaCO_3$-H_2O system. Finally, implications of these observations for the advance in the current understanding on the formation of biomimetic materials and biominerals are outlined.

2. Classical crystallization theory

Crystallization in solution is a first order phase transition which takes place via two distinctive processes: a) nucleation of a solid phase (a crystal embryo) and b) its subsequent spontaneous growth (Mullin, 2001). According to classical nucleation theory (CNT), as defined among others by Volmer and Weber (1926) and Becker and Doring (1935), based on Gibbs's works (Gibbs, 1876, 1878), the driving force for nucleation is the overall reduction in Gibbs free energy of a system, ΔG which can be expressed as:

$$\Delta G = -\frac{\frac{4}{3}\pi r^3}{v} kTln\left(\frac{IAP}{k_{sp}}\right) + 4\pi r^2\gamma \quad (1)$$

where r is the radius of a cluster (assumed to be spherical), v its molecular volume, k is the Boltzmann's constant, T is the absolute temperature, IAP is the ion activity product, and k_{sp} is the solubility product (of a relevant phase), being $\ln(IAP/k_{sp})$ defined as the supersaturation, σ of the system, and γ the interfacial (or surface) energy of the crystal embryo in contact with the solution. The first term of Eq. (1) accounts for the energy released by the formation of the bulk solid phase (due to the reduction in chemical potential upon incorporation of a monomer into a cluster), while the second term accounts for the energy penalty associated with the creation of a solid-solution interface. The competition between bulk and surface free-energy terms leads to the existence of a free-energy barrier that has to be overcome for a cluster to grow (via incorporation of monomers) rather than to shrink. This free energy barrier, $\Delta G*$ is overcome when the clusters reach a critical radius, that is, when $d\Delta G/dr = 0$, and is given by (García-Ruiz, 2003):

$$\Delta G^* = \frac{16\pi v^2\gamma^3}{3\left[kT\ln\left(\frac{IAP}{k_{sp}}\right)\right]^2} \quad (2)$$

Eq. (2) enables the calculation of the free energy barrier for homogeneous nucleation in solution. In most systems, however, a preexisting surface or an interface typically exists (e.g., solid particles, membranes or organic matrices). In these cases, the heterogeneous nucleation of crystal embryos on a substrate is favored. The presence of an interface significantly reduces the Gibbs free energy barrier for nucleation (Sommerdijk and de With, 2008). This occurs because the relevant surface free energy term is the sum of the nucleus-liquid and nucleus-substrate interfacial energies minus that of the liquid-substrate interface, whereas in the case of homogeneous nucleation the only relevant interfacial energy is that of the nucleus-liquid interface (Travaille et al., 2005). Heterogeneous nucleation is thus the generally preferred crystallization route in a range of biomineralization and biomimetic scenarios (e.g., template-directed crystallization, see for instance Aizenberg et al., 1999; Mann, 2001; Sommerdijk and de With, 2008; Tremel et al., 2007).

According to CNT, it is assumed that clusters are spherical (which is not the case for polyhedral crystals) and their γ equals that of the bulk macroscopic crystals. The latter is the so-called "capillary assumption" (Dillmann and Meier, 1989, 1991; Ford et al., 1993; Gebauer et al., 2014), which is largely responsible for the strong deviations between calculated and experimental values of nucleation rates, J^* given by (García-Ruiz, 2003; Mullin, 2001),

$$J^* = Aexp\left(-\frac{\Delta G^*}{kT}\right)exp\left(-\frac{E_a}{kT}\right) \quad (3)$$

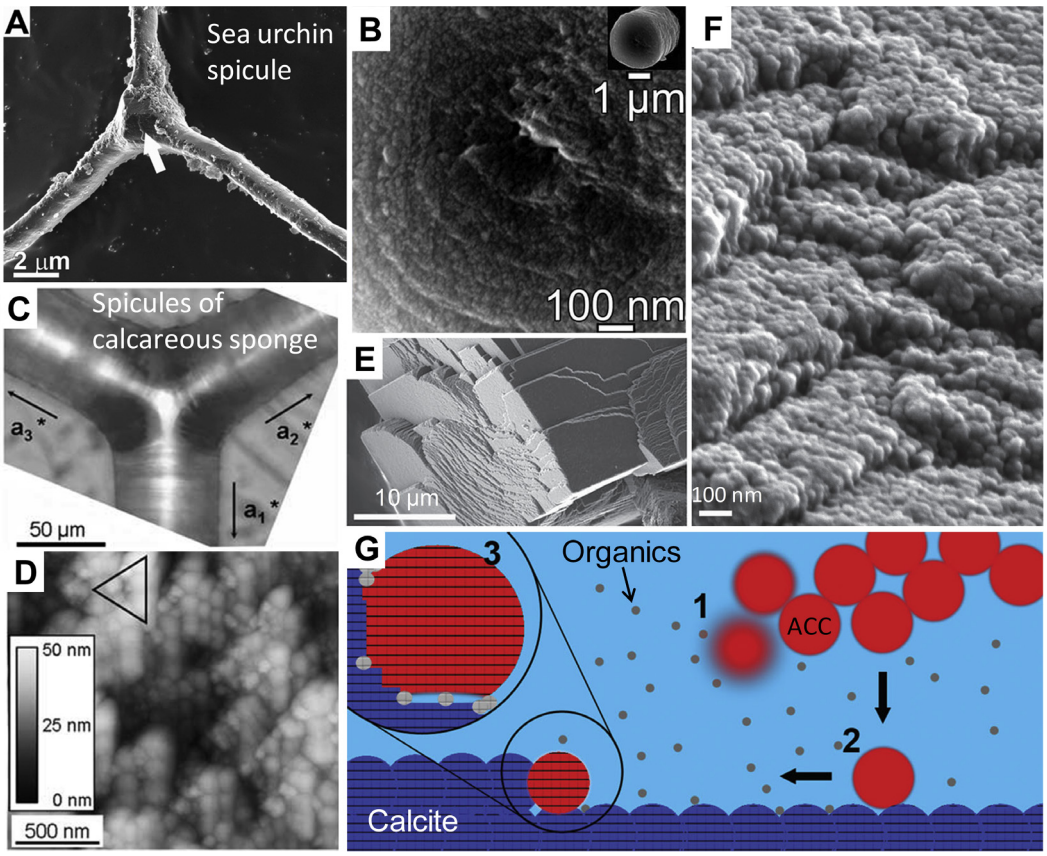

Fig. 1. Amorphous precursors and nanogranular textures in $CaCO_3$ biominerals and their biomimetics. Spicules of sea urchin (A and B) and calcareous sponge (C and D) form via ACC precursors and display a nanogranular texture (B and D). Arrow in (A) shows the initial rhombohedral calcite seed. Inset in (B) shows the fractured spicule, displaying a nanogranular texture in the magnified view. Faceted calcite rhombohedron (E) formed *in vitro*, in the presence of organics, via ACC nanoparticle aggregation displaying a nanogranular texture (F). (G) Model for calcite growth via incorporation of organic-stabilized ACC (1) onto calcite (2) and final fusion with the carbonate structure (3) resulting in the nanogranular texture depicted in (F). Figure (A) reprinted from Gal et al. (2015), with permission from The Royal Society of Chemistry; Figure (B) from De Yoreo et al. (2015). Reprinted with permission from AAAS. Figures (C) and (D) reprinted from Sethmann et al. (2006), with permission from Elsevier; Figures (E, F, and G), reprinted with permission from Gal et al. (2014). Copyright Wiley.

where A is a constant (the so-called pre-exponential factor, which depends on the properties of a particular system), and E_a is the activation energy needed to overcome the kinetic barrier for nucleation (which depends, among other factors, on ion desolvation and structural rearrangements) (Habraken et al., 2013; Vekilov and de Yoreo, 2003). J^* is strongly dependent on T and supersaturation and, of course, interfacial energy, and is given by an Arrhenius-type equation because monomer-by-monomer clustering is associated with inelastic collisions leading to density fluctuations which are stochastic in nature. The contribution of the second exponent in Eq. (3) is typically neglected due to the difficulty of determining the kinetic barrier (Baumgartner et al., 2013; Gebauer et al., 2014).

According to classical crystal growth theory (CGT), once a post-critical crystal embryo is formed in solution, it will continue to grow via a layer-by-layer process that takes place by step generation and spreading (via monomer-by-monomer incorporation at kink sites), either at emerging dislocations or after 2 dimensional (2D) and/or 3D surface nucleation (i.e., terrace-ledge-kink – TLK-model) (Burton et al., 1951; De Yoreo et al., 2009; Frank, 1949; Kossel, 1927; Teng et al., 1998). Note that at the typical, relatively low T of crystallization from solutions in relevant biomineralization or biomimetic systems, normal or continuous growth via direct attachment of monomers is rather uncommon (Chernov, 1984). Standard stepwise layer-by-layer growth of faceted crystals in solution according to the model first delineated by Kossel (1927), involves the following steps: (i) ions/molecules diffuse towards the surface of a crystal where they are adsorbed, (b) they undergo 2D surface diffusion towards an energetically favorable site (kink), and (c) they are incorporated into the crystal lattice following desolvation (Myerson, 2002). As in the case of nucleation, the driving force for crystal growth is the overall reduction in free energy of the system, that is, the free energy of the solvent and the growing crystals (Vekilov and De Yoreo, 2003). In order to minimize the overall surface energy of the system, the largest crystals will tend to growth at the expense of the smallest. This classical coarsening process is called Ostwald's ripening, and is associated with the increased solubility of particles with decreasing size (Gibbs-Thompson effect) (Mullin, 2001).

Despite its enormous merit and the advances that the application of classical crystallization theory has brought about, experimental, computational and theoretical results have shown, however, that strong deviations from CNT and CGT occur in several systems (De Yoreo et al., 2015; Gebauer et al., 2014; Mullin, 2001; Navrotsky, 2004; Nielsen et al., 2014; Vekilov and De Yoreo, 2003). The existence of stable pre-nucleation clusters (Gebauer et al., 2008), as well as dense liquid and solid amorphous precursor phases (Bewernitz et al., 2012; Gower, 2008; Rodriguez-Navarro et al., 2015b), shows that "nonclassical" nucleation pathways can take place in relevant biomineralization and biomimetic systems. Similarly, crystal growth via (nano)particle (amorphous or crystalline) coalescence, aggregation or attachment has been demonstrated (De Yoreo et al., 2015; Killian et al., 2009; Meldrum and Cölfen, 2008; Penn and Banfield, 1998; Wang et al., 2013a; Woehl et al., 2014), which does not fit within the "classical" picture

of crystal growth (i.e., monomer-by-monomer addition). These "nonclassical" crystallization routes, which will be described and discussed in the following sections and are schematically represented in Fig. 2, are dramatically changing our current understanding on the formation of biominerals and biomimetic materials.

3. The Ostwald's step rule: kinetics vs. thermodynamics

3.1. The Ostwald's step rule

One of the founding stones of classical crystallization theory is that two order parameters, namely densification and long-range order, have to emerge simultaneously (Sleutel and van Driessche, 2014). This is, however, not the case in many systems, as Ostwald already pointed out more than 100 years ago. Ostwald (1897) stated that in a system, which is about to undergo phase transition and which can form multiple phases, both stable and metastable, does not go directly to the thermodynamically stable phase. Instead, the system prefers to select intermediate stages and, consequently, less stable phases form prior to the thermodynamically stable phase. Ostwald predicts that the first phase to appear would be the one with a free energy (and structure) closest to the parent phase (e.g., the solution). Stranski and Totomanov (1933) restated this rule indicating that the phase that emerges first is the one separated from the parent phase by the smallest free energy barrier. According to Ostwald, the first phase formed from a supersaturated homogenous solution should be a (dense) liquid phase. Subsequently, the metastable solid phase(s) formed after the (dense) liquid phase may undergo consecutive phase transformation (e.g., via dissolution-reprecipitation) (Ogino et al., 1987) until the thermodynamically stable phase (for a given set of conditions) is formed. This multi-step precipitation sequence is called the Ostwald's step rule (also known as the Ostwald-Lussac or Ostwald-Weber rule of stages) (De Yoreo et al., 2015; Gower, 2008; Meldrum and Cölfen, 2008). Although its validity as a general rule has been questioned, there are numerous examples where this empirical rule is followed (Threlfall, 2003). This is, for instance, the case of the $CaCO_3$-H_2O system, where the following precipitation sequence has been observed (if precipitation takes place at a sufficiently high supersaturation): (dense liquid precursor) → ACC → (ikaite) → (monohydrocalcite) → vaterite → (aragonite) → calcite (phases in parenthesis are not commonly detected or formed at STP conditions) (Ogino et al., 1987; Rodriguez-Navarro et al., 2015b). This precipitation sequence, which follows a downhill energy landscape, can be further complicated by the existence of additional metastable ACC phases with different degrees of hydration and structural order as well as enthalpy/surface energy: e.g., synthetic more dissordered hydrated ACC, less dissordered hydrated ACC, and more ordered anhydrous ACC (Radha et al., 2010; Rodriguez-Navarro et al., 2015b) or biogenic hydrated and anhydrous ACC (DeVol et al., 2015; Gong et al., 2012; Politi et al., 2008).

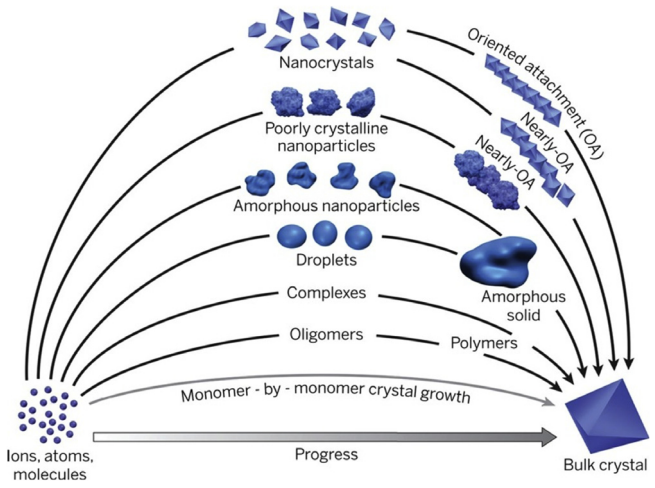

Fig. 2. Classical and nonclassical crystallization. According to CNT, nucleation proceeds by monomer-by-monomer addition (ions or molecules) to a single cluster finally forming a faceted crystal (bottom). Non-classical mechanisms involve nucleation of a liquid (droplets) or amorphous solid (possibly formed after aggregation of stable prenucleation clusters). The nucleated amorphous solid phase subsequently crystallizes to generate the final stable crystal product. Once nanocrystals have been formed, they can continue to grow either via incorporation of monomers (CGT) or via non-classical processes involving coalescence (aggregation or attachment) of individual poorly-crystalline or crystalline nanoparticles (nearly-oriented or oriented attachment). From De Yoreo et al. (2015). Reprinted with permission from AAAS.

3.2. Origins of the Ostwald's step rule

The origin of the Ostwald's step rule has been a matter of controversy (Nývlt, 1995). Ostwald's tentative explanation was based on classical thermodynamics, suggesting that the metastable zone of metastable and stable phases could overlap, enabling the formation of the former prior to the later. This has been, however, considered incorrect (Threlfall, 2003). Several alternative hypotheses have been proposed, that are based either on thermodynamics or on kinetics, or on both.

Based on irreversible thermodynamics, it has been suggested that entropic changes can favor the formation of intermediate metastable phases over the direct formation of the stable one (van Santen, 1984; Threlfall, 2003). However, the role of entropy changes for Ostwald's step rule – as proposed by van Santen (1984) –, has been questioned (Casey, 1988). An alternative explanation for the Ostwald's step rule was proposed by Nývlt (1995). The author suggested that the structure of the solution contributes to select which phase is formed first. The author indicated that the so-called "structuring" of the solution might be related to "varying average clusters size of the solute". Unfortunately, the author did not explain the notions or origins of "structure of the solution" or the "varying clusters size of the solute". However, Nyvlt's hypothesis seems to point indirectly to the entropic gain upon phase transition (crystallization) as the key parameter for the formation of metastable precursor phases. At first sight, this is counterintuitive as a crystal has a lower entropy than the solution from which it crystallizes, so crystallization seems not to obey the second law of thermodynamics (Frenkel, 2015). However, the disorder achieved by the solvent (i.e., changes in the solvent "structuring") and the heat released by the nucleation of a condensed phase (dense liquid or solid) with a higher order, can lead to an overall increase in entropy; then the second law is followed. If we consider the overall system (solution and newly formed solid or dense liquid phase) a higher entropic gain can be achieved by forming a metastable (less ordered) precursor phase instead of a stable crystalline phase. This process is favored if, concurrently, the solvent becomes less ordered. Note that aqueous solutions can display a certain degree of water structuring (i.e., short- or medium-range order) depending on the type and concentration of solute species (i.e., structure-breakers or structure-builder ions) (Marcus, 2009; Ruiz-Agudo et al., 2011), as well as on the amount of bound (oriented) water molecules (Dorvee and Veis, 2013). Thus, one can assume that any process that weakens the solution's structuring, e.g., nucleation of a new phase incorporating the structure-builder ions, will be entropically favored (Dove and Craven, 2005; Ruiz-Agudo et al., 2011). Furthermore, crossovers between the entropy of crystallization of stable and metastable phases can take place at a given T, which will favor the crystallization of a metastable phase. Keislich et al. (2015) reported that in the case of a metal-organic framework (MOF), a metastable polymorph

could crystallize prior to the stable one above a certain *T* at which the entropy of crystallization of the metastable phase is higher than that of the stable phase. For this to occur, the authors emphasized that the enthalpy difference between stable and metastable phases has to be minimal (0.07 eV).

An alternative approach to explain the Ostwald's step rule, which is also based on thermodynamics, was presented by Navrotsky (2004). At sufficiently small crystal sizes (<100 nm), an inversion in the ordering of stability of the different phases in a system may occur due to the size-dependent variation of the enthalpic contribution to the free energy of a particular precursor phase (the entropic contribution was considered irrelevant). This requires that the enthalpy difference between the different phases is sufficiently low (1–10 kJ/mol, see Fig. 3a) which is actually the case of the anhydrous $CaCO_3$ polymorphs. Such an effect, possibly in parallel with impurity effects, may allow for the initial formation of the less stable phase, vaterite, followed by aragonite and, finally, calcite. Furthermore, computer simulations show that at sufficiently small diameters (<4 nm) ACC could be the thermodynamically stable phase (Raiteri and Gale, 2010), thus offering a plausible explanation why, under high supersaturation conditions, ACC typically precedes the formation of any crystalline $CaCO_3$ polymorph (Ihli et al., 2014; Nielsen et al., 2014; Ogino et al., 1987; Rodriguez-Navarro et al., 2015b). Note, however, that the precipitation of amorphous and crystalline phases in the $CaCO_3$ system can involve both direct and indirect pathways (Nielsen et al., 2014). *In situ* liquid cell TEM analyses have recently shown that ACC can form and then transform into vaterite or aragonite (parent and product phases being physically in contact during the transformation) according to the Ostwald's rule, while simultaneously calcite can directly nucleate from solution along with vaterite (or, possibly, ACC) (Nielsen et al., 2014), an effect that cannot be easily explained by the Ostwald's step rule. However, in this case, possible artifacts associated with the e-beam (resulting in the observed deviation from the Ostwald's step rule) cannot be ruled out.

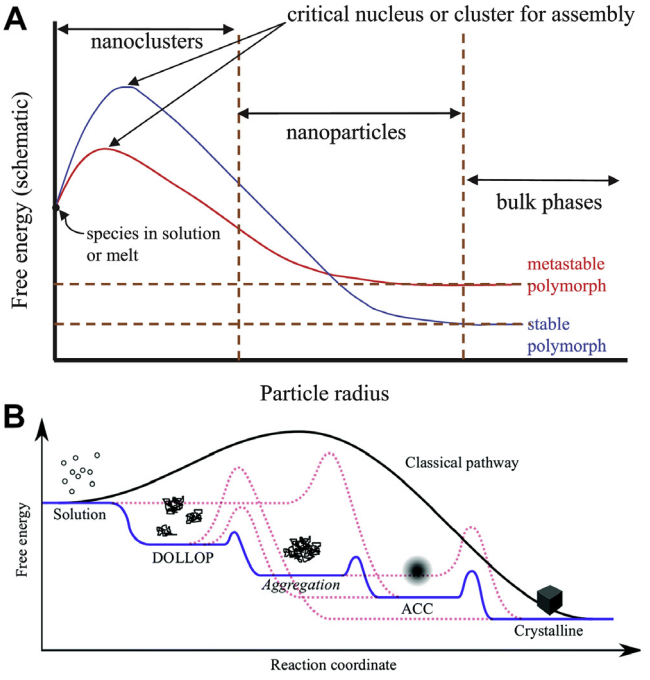

Fig. 3. The Ostwald's step rule: Thermodynamic and kinetic effects. A) Free-energy landscape vs. particle radius for stable and metastable polymorphs. A crossover in free energy (enthalpic contribution) occurs at a sufficiently small particle size, which enables the initial formation of the metastable phase. Reprinted with permission from Navrotsky (2004). Copyright National Academy of Sciences, USA; B) Free energy landscape for crystallization pathways under thermodynamic (classical pathway) and kinetic control (solution → DOLLOP/PNCs → ACC → stable crystal). Whether the system follows one pathway (black line) or the other (blue line) (or the alternative pathways depicted by dashed pink lines) depends on the free energy barrier for nucleation and growth. Reprinted from Harding et al. (2014). With permission of The Royal Society of Chemistry.

An argument similar to the one presented above explaining the Ostwald's step rule on the basis of size-dependent enthalpy crossovers can be made resting on size-dependent variations of the interfacial energy (and surface free energy) of metastable and stable phases. This was suggested for the first time for the Al_2O_3 system (McHale et al., 1997). At a sufficiently small size, a crossover of interfacial energy can facilitate the nucleation of the metastable phase(s) if its interfacial energy is smaller than that of the stable phase.

Size-independent solvent-mineral interactions (inducing surface (re)structuring) also appear to play a role in determining what is the actual surface free energy of a nanosized mineral phase, as shown by Zhang et al. (2003) for the case of ZnS nanoparticles. Such a solvent effect may determine which phase forms first. It follows that during crystallization from solution, the selection of a particular phase according to the Ostwald's step rule may not only depend on size-related surface energy effects, but also on the interactions between a specific (precursor) phase and water molecules. In other words, size-independent structural/compositional changes may also play a critical role in selecting which (metastable or stable) phase nucleates first. This idea is consistent with the so-called "generalized Gibbs approach" which suggests that the barrier for nucleation is overcome mainly via changes in the structure (and composition) of the precursors phase (not in equilibrium with the solution) at a nearly constant size (Schmelzer et al., 2010).

Kinetics, however, have been traditionally considered as the main cause for the existence of the Ostwald's step rule. Stranski and Totomanov (1933) elaborated the first kinetic approach to the interpretation of the Ostwald's step rule. They proposed that a (metastable) phase will form first in a system if the formation rate of supercritical clusters of this phase is higher than that of all other possible metastable or stable phases. Based on the Arrhenius equation, the authors calculated the nucleation rate of the different phases in a system, where the critical step was to overcome the free energy barrier for nucleation that, according to Eq. (2), is strongly dependent on the surface energy of the nucleating phase. The authors concluded that because the free energy barriers for the formation of metastable phases were smaller than the free energy barrier for the direct formation of the stable phase, the nucleation rate of the former would be higher than that of the latter. In other words, the system would prefer to choose a kinetic crystallization pathway rather than a thermodynamic one, as depicted in the energy landscape shown in Fig. 3b. This energy landscape can help to explain why metastable phases (liquid- and solid-amorphous, see below) form earlier (at a higher rate) than the stable one under kinetically-controlled crystallization (Cölfen and Mann, 2003; Gower, 2008; Harding et al., 2014).

It can be concluded that the fundament of Ostwald's step rule is not yet fully understood and may rest on a tight interplay of thermodynamic and kinetic phenomena (Navrotsky, 2004). In any case, the fact that most biomineralization- and biomimetic-relevant systems follow the Ostwald's rule and feature liquid and/or solid amorphous metastable precursor phases indicates that nonclassical crystallization might be a general phenomenon, rather than the exception.

3.3. Phase transitions within the Ostwald's crystallization sequence

Once a metastable solid precursor phase forms, how does it subsequently transform into a more stable one? What is the

mechanism of this phase transformation? Two basic mechanisms have been proposed: a) solid-state transformation, and b) dissolution-reprecipitation. Under typical biogenic/biomimetic conditions, i.e. from solution at relatively low *T*, a solid-state transformation does not seem to be the relevant process because the diffusion rates in solid state are very low. However, there is no general consensus on this. For instance, in the case of the $CaCO_3$-H_2O system, some researchers propose a solid-state transformation for biotic and abiotic low-*T* ACC-to-crystalline conversion (e.g., Addadi et al., 2003; Politi et al., 2008), while others propose a dissolution-reprecipitation process (Giuffre et al., 2015; Rodriguez-Navarro et al., 2015a,b), or a combination of an initial solid-state transformation followed by a dissolution-reprecipitation (Ihli et al., 2014). It should be noted that for the case of ACC-to-crystalline transformation in some biominerals (e.g., sea urchin spicules) where anhydrous ACC is present in the interior, no water would apparently be present for a dissolution-precipitation to take place, so a solid-state transformation would be the most likely mechanism (Gong et al., 2012; Politi et al., 2008). However, Radha et al. (2010) showed that even "anhydrous ACC" (both biogenic and synthetic) included a small amount of water (~0.2 mol H_2O per formula unit). Therefore, during the ACC-to-crystalline transformation, water present in "anhydrous ACC" could be released and contribute to the progress of the phase transformation via a dissolution-precipitation mechanism (Gal et al., 2014; Rodriguez-Navarro et al., 2015b). But a question remains unanswered: What does trigger the initial ACC-to-crystalline transformation in this case? Ihli et al. (2014) underlined that at the very early stages of ACC-to-crystalline transformation a solid-state process could trigger the phase transition, which afterwards would proceed via a dissolution-precipitation mechanism. Hence, it could be possible that in some biominerals both processes play a role.

It has been suggested that in a solution supersaturated with respect to both stable and metastable phases, nuclei of all possible solid phases can form (Cardew and Davey, 1985). Indeed, one could envision that instable nucleation clusters preceding nucleation, or just approaching/reaching their critical size, are highly solvated dynamic entities (Mullin, 2001), which could adopt different (proto)structures: the one which develops and grows fastest should be the one first crystallizing. In other words, nucleation clusters with the structure of the less stable phase can eventually reach the critical size earlier (i.e., its growth rate being fastest due to its lower surface energy or its lower nucleation barrier) than those of the more stable phase. As crystallization progresses, nuclei of the more stable (less soluble) phase can reach the critical size and continue to growth. This reduces the supersaturation of the system, enabling the dissolution of the first formed metastable and more soluble phase at the expense of the growth of the more stable, less soluble one (Schiro et al., 2012). Basically this is similar to an Ostwald's ripening process, but not driven by size-dependent solubility differences (Gibbs-Thomson effect), but by phase-dependent solubility differences. Importantly, the crystallization rate of the stable phase will be proportional to the solubility difference between metastable and stable phases (i.e., the growth rate of the stable phase will be related to the system supersaturation, which in turn is marked by such a solubility difference) (Cardew and Davey, 1985). We will see below that such solubility differences appear to be critical for the final development of a particular crystalline phase after an amorphous precursor (Zou et al., 2015), a phase transition which is fundamental for the formation of many biominerals and their biomimetics. Interestingly, *in vitro*, this phase transformation can proceed in a pseudomorphic fashion, as shown for the case of ACC-to-calcite transformation in Fig. 4. Pseudomorphism, denoting the replacement of a phase by another preserving the overall morphology of the parent phase, has been commonly associated with a solid-state mineral transformation, as exemplified by the proposed solid-state conversion of ACC into crystalline $CaCO_3$ (aragonite or calcite) in biominerals and calcium carbonate biomimetics (Addadi et al., 2003; Politi et al., 2008). However, such a pseudomorphism can readily result from an interface-coupled dissolution-precipitation replacement reaction (Putnis, 2009, 2014), and the only requisites for this to occur are the existence of an interfacial fluid between parent and product phase, and a solubility difference between them as a driving force (Ruiz-Agudo et al., 2016). The fact that this process does not require a large solution reservoir, operates at room *T* at a much higher speed than solid-state diffusion, and does not need to overcome any significant free-energy barrier, suggests that it could be an important process in biomineralization and in biomimetic synthesis, if the Ostwald's step rule is at work and metastable precursors exist (Rodriguez-Navarro et al., 2015b).

4. Nonclassical nucleation: PNCs and the role of organics

Studying the $CaCO_3$-H_2O system, Gebauer et al. (2008) showed that the nucleation of (amorphous) calcium carbonate is preceded by the formation of "stable prenucleation clusters" (PNCs). Remarkably, such PNCs were present in undersaturated solutions, and fell within an energy minimum (valley) in the free energy landscape describing $CaCO_3$ crystallization. Polymeric nanoclusters preceding the formation of stable nuclei were previously observed in other systems, as in the case of silicic acid solutions (Navrotsky,

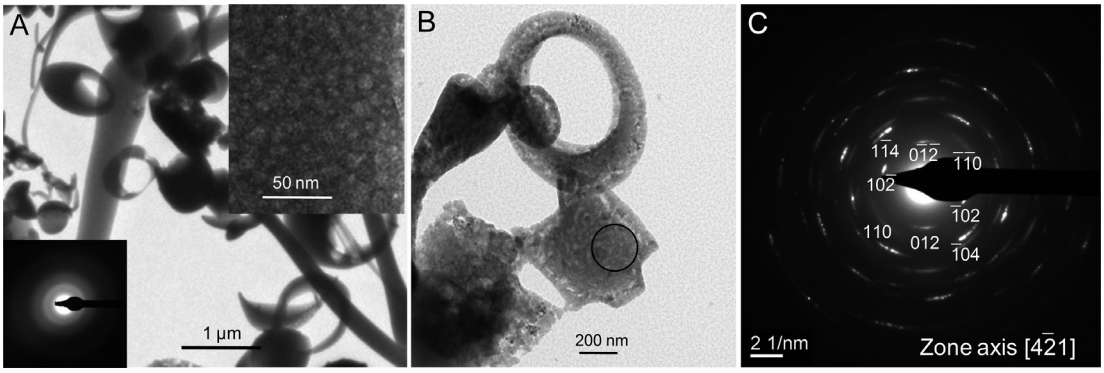

Fig. 4. ACC-to-calcite conversion: A) 2D (ribbons or plates) and 3D (ring-like) ACC structures (lower left inset: SAED pattern showing the diffuse rings of the amorphous phase; upper right: nanogranular structure of ACC); B) ACC structures after pseudomorphic transformation in humid air via an interface-coupled dissolution-precipitation. The resulting porous calcite structures diffract electrons as a mesocrystal (SAED in (C)). Reprinted from Rodriguez-Navarro et al. (2015b), with permission from The Royal Society of Chemistry.

2004). However, such clusters formed via polymerization in saturated or supersaturated solutions. In the case of ionic crystals, such as ammonium sulfate or ammonium dihydrogen phosphate, formation of (apparently stable) non-crystalline subcritical clusters under supersaturated conditions was also reported and such species were considered to play an important role in crystallization (see Dorvee and Veis, 2013; Mullin, 2001, and references therein). Posner's clusters (i.e., subcritical aggregates of calcium phosphate) also fall within this category (Eanes et al., 1965). However, the formation of stable prenucleation species in undersaturated electrolyte solutions was not considered thermodynamically possible until the contribution of Gebauer et al. (2008). Using a titration system (constant pH), the authors demonstrated that the free calcium detected using an ion-selective electrode was systematically lower than the calcium dosed to a carbonate buffer solution (Fig. 5a). Ion pairing could not account for such a "reduced" free calcium concentration. At the same time, no solid phase was detected during the early stages of the titration process. These results, in combination with analytical ultracentrifugation showing

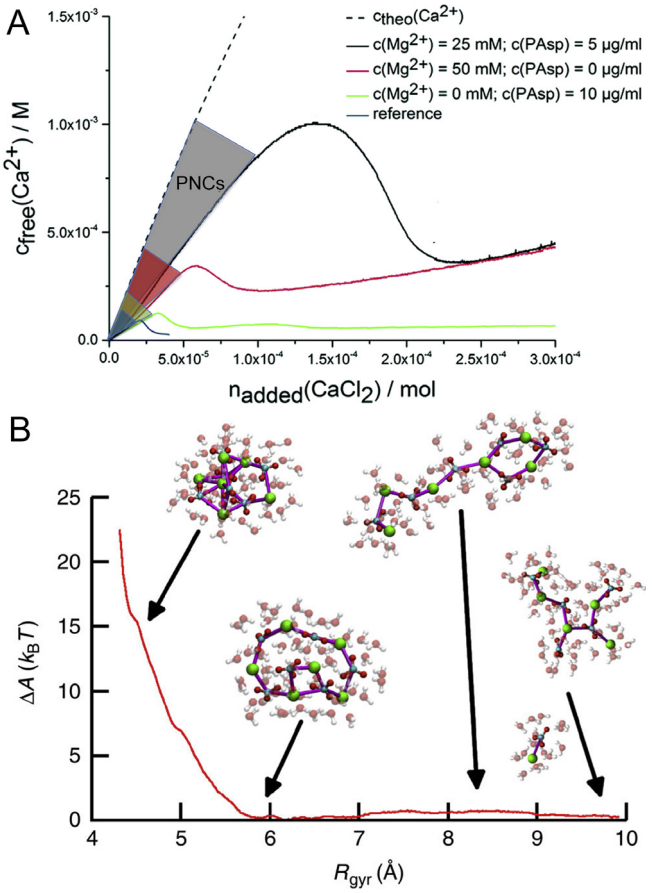

Fig. 5. PNCs and $CaCO_3$ crystallization. A) Evolution of free calcium concentration upon addition of $CaCl_2$ solution with and without additives (as indicated) into 10 mM carbonate buffer (pH 9.75) at a rate of 100 μl min^{-1} (note that this crystallization diagram is similar to the classical LaMer and Dinegar (1950) concentration-reaction time curve). A lower amount of free calcium than that dosed (marked by the dashed line) is systematically detected at the pre-nucleation stage, which is due to the formation of PNCs. Both inorganic (Mg) and organic (PAA) additives have a profound effect on the width of PNC stability field (color-shaded areas) and on the onset of nucleation (which is marked by the inflection point of the different curves). Modified from Wolf et al. (2015b), with permission from The Royal Society of Chemistry. B) MD computer simulation of solvated Ca (green)-carbonate (blue :C; red: O) ion associates (PNCs or DOLLOPS) present at different values of Helmholtz free energy (ΔA), which is plotted as a function of the radius of gyration (R_{gyr}). Reprinted by permission from Macmillan Publishers LTD: Demichelis et al. (2011). Copyright 2011.

the existence of clusters ~2 nm in size (only detected in supersaturated solutions) formed by an average of ~70 ions/cluster, led the authors to conclude that stable clusters with size below the critical size were present in solution prior to the formation of amorphous calcium carbonate (ACC). Gebauer et al. (2008) also indicated that the fact that PNCs are stable relative to individual ions in solution is not related to enthalpy factors, but to the variation of entropy associated with water solvation of the clusters. The authors suggested that subsequent ACC formation likely occurred through cluster aggregation. Because the system supersaturation is greatly reduced by the formation of PNCs, classical nucleation of a new solid phase via monomer-by-monomer addition would be unlikely: thus, a new (dense-liquid or solid) condensed phase should form by aggregation of PNCs, a process which would be facilitated by agitation (fostering cluster-cluster interaction) and which has to involve desolvation as speculated by Dorvee and Veis (2013). Further evidence regarding the existence of PNCs was claimed by Pouget et al. (2009). Using cryo-TEM, the authors showed particles 0.6 to 1.1 nm in size, which were believed to be PNCs. A critical point is that PNCs are considered to be solute species, that is, they do not have a solid character, nor a surface (or surface tension), and they are stable, because an equilibrium constant of cluster formation existed (Gebauer and Cölfen, 2011; Gebauer et al., 2014). This casts some doubts about the actual nature of the putative PNCs observed by Pouget et al. (2009), which according to their cryo-TEM images were individual nanoparticles. Note, however, that Dorvee and Veis (2013) suggest that the existence of slow moving bound water around PNCs may serve as a phase boundary. Interestingly, Pouget et al. (2009) observed that nearby of an organic template (stearic acid monolayer), ACC nanoparticles (~30 nm) formed in the bulk solution via coalescence/aggregation of PNCs. They were not observed to heterogeneously nucleate on the template, a process that, as indicated in Section 2, should be energetically favored according to CNT. This observation can be rationalized considering that, as indicated above, PNCs are solute species (with no interfacial energy), a feature that would not favor the heterogeneous nucleation of liquid-like or solid ACC on a substrate; rather, PNCs would form ACC precursors (liquid or solid) via reorganization of the clusters or, more likely, aggregation after random collisions (associated with Brownian motion) in the bulk solution. ACC nanoparticles would later on attach to the template where they could subsequently transform into a crystalline $CaCO_3$ phase with an orientation imposed by the template. Although such a nonclassical template-directed crystallization involving an ACC precursor was first postulated by Cölfen and Mann (2003), it was not experimentally demonstrated until the work by Pouget et al. (2009).

Subsequent studies have shown that PNCs are not exclusive of the $CaCO_3$-H_2O system (Gebauer and Cölfen, 2011). Dey et al. (2010) reported the formation of PNCs (~0.87 nm in size) preceding the formation of calcium phosphate. PNCs can also precede the formation of calcium oxalate, iron(oxy)(hydr)oxides, silica, and aminoacids (Gebauer et al., 2014). These observations suggest that the formation of PNCs in solution may be a general phenomenon, being thus likely involved in the formation of many biominerals and their biomimetics.

Recent experimental work and computer simulations have provided a more complete and complex picture regarding the nature and (possible) structure of PNCs (Demichelis et al., 2011; Wallace et al., 2013). One important point is that PNCs are highly dynamic entities, which can change configuration and degree of polymerization (and solvation) at very short timescales (picoseconds). Molecular dynamics simulations have shown that PNCs are not just ion-pairs (i.e., dimers), rather, they typically are larger associates, which have been termed DOLLOPs (dynamically ordered liquid-like oxyanions polymers) (Demichelis et al., 2011). DOLLOPs dis-

play a combination of linear chains, rings and branched structures with a high degree of solvation (inset in Fig. 5b). More recent computational work has suggested that these PNCs can become a dense liquid phase, preceding the formation of ACC (Wallace et al., 2013), as it will be discussed below. An attempt to unite the novel nonclassical nucleation route involving the formation of PNCs and CNT was proposed for the calcium phosphate system, assuming that pre-nucleation species were ion-association complexes which displayed characteristics of a "solid" phase (Habraken et al., 2013). The latter idea, however, does not fully fit within the concept of PNCs, which, as stated above, are considered as solutes by Gebauer et al. (2008, 2014).

4.1. The role or organics

The existence of PNCs is changing our current understanding on the effects of organic (e.g., polymers and acidic proteins) and inorganic (e.g., ions such as phosphates or Mg^{2+}) additives on the crystallization from solution of a range of minerals (Gebauer et al., 2009). Additives are known to play critical roles in the nucleation and growth of minerals and biominerals as well as their biomimetics (Gower, 2008; Rodriguez-Navarro and Benning, 2013; Song and Cölfen, 2011). Additives can inhibit or promote nucleation (nucleation inhibitors or promoters, respectively), and/or modify crystals morphology (habit modifiers). They can also stabilize metastable precursor phases (e.g., ACC) or select/stabilize specific polymorphs (Sommerdijk and de With, 2008). Moreover, they can favor the heterogeneous nucleation of a specific phase and determine its crystal orientation (Harding et al., 2014; Mann, 2001). In a pioneering study, Gebauer et al. (2009) showed that poly(acrylic acid) (PAA) has manifold effects on the nucleation and growth of $CaCO_3$ depending on at what stage of the crystallization process PAA acts, and with what species (solute species, liquid precursors, or solid products) it interacts. Up to nine types of independent actions occurring both in pre- and post-nucleation stages were defined and observed in different additive systems (Verch et al., 2011). However, not all these type of interactions have to occur in a specific system, and not all additives display the same type of interaction. For instance, polystyrene sulfonate (PSS), which is known to induce the formation of $CaCO_3$ mesocrystals (Song et al., 2009), mostly acts at the post-nucleation stage of $CaCO_3$, whereas citrate ions destabilize PNCs, thus delaying nucleation of $CaCO_3$ (Verch et al., 2011). Also, these type of interactions are not constrained to organic additives: they are also observed in the case of inorganic additives. For instance, Mg^{2+} acts as a nucleation inhibitor of $CaCO_3$ via PNCs destabilization, an effect that can be potentiated in the presence of PAA (synergistic action) (Wolf et al., 2015b) (Fig. 5a). While stabilization of PNCs by adsorption of additive molecules leading to nucleation inhibition is easily explained because such an adsorption effect prevents PNCs clustering (Picker et al., 2012), similarly to colloidal stabilization, the destabilization of PNCs by additives also leading to nucleation inhibition is somehow a counterintuitive effect. In the case of the $CaCO_3$-H_2O system, such a destabilization increases the measured free Ca^{2+} (i.e., Ca activity) and, as a consequence, the system supersaturation. The later should favor nucleation (see Eq. (2)). However, the opposite effect is observed. This suggests that PNCs are indeed critical for the nucleation of a new phase (via their coalescence). Note, however, that recent *in situ* fluid-cell TEM has shown that the nucleation of ACC in the presence of PSS involves the initial formation of Ca-PSS complexes (with a liquid-like character), the subsequent competition between carbonate ions and PSS for bonded Ca and, finally, the nucleation of ACC nanoparticles within the PSS matrix (Smeets et al., 2015). It is thus unclear whether in this latter system PNCs play a role in the formation of ACC.

4.2. Polyamorphism

One interesting outcome of the study by Gebauer et al. (2008) was the finding that depending on the system pH, ACC with either protovaterite or protocalcite structure (short- to medium-range order) was obtained, which eventually transformed into vaterite or calcite, respectively (Gebauer et al., 2010). The authors suggested that such a protostructure was already imprinted at the prenucleation stage and was conveyed by ACC until the crystalline phase was formed. These observations, along with the identification of ACC with different short-range order in several biominerals (Levi-Kalisman et al., 2002; Politi et al., 2006), have led to the concept of polyamorphism (Cartwright et al., 2012). Note, however, that Zou et al. (2015) have recently reported that synthesis-dependent size-related solubility differences among ACC nanoparticles can lead to $CaCO_3$ polymorph selection. Smaller, more soluble ACC nanoparticles typically resulted in the formation of vaterite, while larger, less soluble ACC nanoparticles favored the formation of calcite after a dissolution-reprecipitation transformation. However, the authors did not report on the possible protostructure of both types of ACC, so it is not clear whether or not polymorph selection was already established at the prenucleation stage (i.e., protostructure) or was solely related to the above mentioned solubility differences.

In summary, growing evidence shows that PNCs can play a key role in the formation of solid phases from solution (both amorphous and crystalline) and may also likely play a key role in the formation of dense liquid precursor phases (see below). They are also key players in the formation of solid phases (and possibly, dense liquid ones) when additives are present in a system. They can thus be critical in biomineralization and in the biomimetic synthesis of functional materials. An interesting, but largely unexplored topic, refers to the role that such pre-nucleation species play in the dissolution of minerals. This is an important issue that can have significant implications in biomineralization and in biomimetics. Note, for instance, that demineralization processes are critical in bone remodeling or in crustacean molting (Ehrlich et al., 2009). Similarly, it is unknown whether or not PNCs directly contribute to the growth of an already formed crystal (Gebauer et al., 2014).

5. Nonclassical crystallization: Liquid and amorphous precursors – PILPs

5.1. Liquid precursors

One particular case of the nonclassical multistage crystallization path above described (Ostwald's step rule) involves the formation of a dense liquid precursor phase. Extensive experimental evidence has accumulated which shows that liquid-liquid phase separation (either via binodal separation or spinodal decomposition) takes place in the biomimetically-relevant $CaCO_3$-H_2O system (both in the presence and absence of organic additives). Faatz et al. (2004) proposed that at sufficiently high supersaturation a binodal liquid-liquid separation could be the first stage in the formation of ACC, but presented no experimental evidence for the formation of such a liquid precursor phase. Evidence for the formation of ACC nanoparticles from a liquid precursor phase in the absence of additives was first claimed by Rieger et al. (2000, 2007). Using X-ray microscopy and TEM, the authors observed an "emulsion-like" structure prior to the formation of ACC. Afterwards, Wolf et al. (2008) reported the formation of solid amorphous calcium carbonate after the initial liquid-liquid separation of a dense liquid precursor. In their experiments the authors avoided any interference or artifacts associated with possible heterogeneous nucleation by observing the formation of new phases in a levitated calcium

bicarbonate solution droplet subjected to evaporation. They showed TEM images of amorphous precursors with no contrast difference between the center and periphery which according to the authors indicates that such flattened structures resulted from the diffluence of liquid droplets. Further evidence for the formation of a liquid precursor phase in the $CaCO_3$-H_2O system in the absence of additives was provided by Bewernitz et al. (2012), who showed that such a liquid precursor phase was bicarbonate biased. More recently, Rodriguez-Navarro et al. (2015b) showed that the formation of ACC nanoparticles at very high supersaturation and in the absence of additives was preceded by the formation of a dense liquid precursor phase. *In situ* polarized light microscopy showed that this liquid precursor displayed the standard bicontinuous phase features of a spinodal decomposition process (Gebauer et al., 2014).

Recently, results from computational studies have provided support for the proposed occurrence of liquid-liquid phase separation based on experimental observations. Molecular dynamics simulations of crystallization pathways and the formation of precursor phases in the $CaCO_3$-H_2O system led Wallace and co-workers (2013) to conclude that the formation of ACC could be preceded by the formation of a dense liquid precursor phase after a process of spinodal decomposition (Fig. 6). The green horizontal line in Fig. 6 represents a constant temperature slice through the stability fields as the solution ion activity product is increased. The solubility of all polymorphs is represented by a single solubility line (SL), which bounds the blue undersaturated solution field. This simplification highlights that the solid phases of $CaCO_3$ (calcite, aragonite, vaterite, and presumably ACC) all display the same general retrograde solubility behavior. The SL curve separates the undersaturated bulk solution from the field in which the solution is metastable against the formation of a solid phase by a binodal process.

For binodal formation of a new phase, an energy barrier has to be overcome, for instance by spontaneous and uncoupled density fluctuations that enable the formation of randomly scattered crystal embryos. This process is also well known as nucleation. Basically the binodal marks the solubility curve of the solid phases. In this field of metastability (n.b., against solid-liquid decomposition), we find another binodal line that demarks the region in which the solution becomes unstable to liquid-liquid phase separation by nucleation processes. Note that the binodal marking the formation of dense liquid droplets is always in the solid-liquid zone of metastability (Gebauer et al., 2014). In the region bounded by the spinodal line, the solution is unstable to density fluctuations and liquid-liquid separation can occur spontaneously without overcoming a free energy barrier. This process is called spinodal decomposition and for it to occur the system has to cross the metastable field without phase separation taking place (or the spinodal regime must be directly reached through the critical point). Spinodal decomposition leads to characteristic two-phase bicontinuous patterns because the density fluctuations are coupled by a characteristic wavelength. This wavelength is the hallmark of spinodal decompositions and a straight way to prove its occurrence. However, such a wavelength has not been reported for the $CaCO_3$-H_2O system.

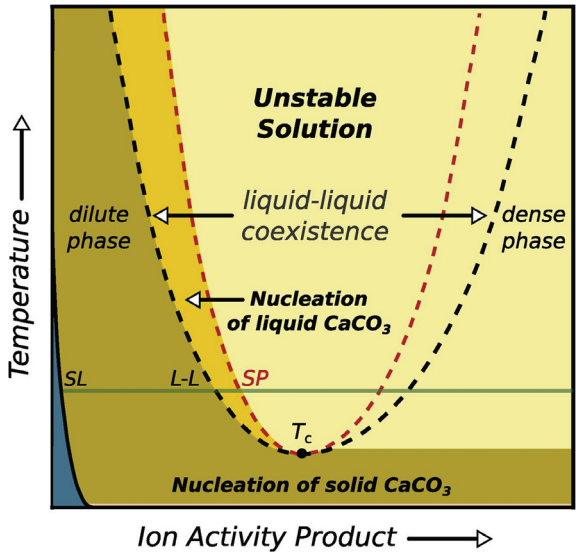

Fig. 6. Phase relationships in the $CaCO_3$-H_2O system. SL represents the (retrograde) solubility of solid phases (ACC, vaterite, aragonite and calcite), which separates the undersaturated and saturated solution fields. Note that due to such a retrograde solubility, the critical point, Tc is at the bottom of the diagram (although more recent experimental results suggest that Tc is at the top of the diagram: see Zou et al., 2016). If the system increases its concentration at constant *T* (marked by the green line) it can reach the binodal at L-L (black dashed line) leading to liquid-liquid separation. If no separation occurs at the binodal, the spinodal line (red dashed line) can be reached at point SP and liquid-liquid spinodal decomposition can take place. Reprinted from Wallace et al. (2013). With permission from AAAS.

Wallace et al. (2013) have shown that, based upon molecular dynamics simulations, the spinodal line appears to be easily accessible and within the common range of concentrations at which the formation of a liquid-condensed phase was either observed or speculated (Faatz et al., 2004; Rieger et al., 2007; Rodriguez-Navarro et al., 2015b; Wolf et al., 2008). In these concentration ranges, formation, growth and coalescence of dense liquid (prenucleation) clusters spontaneously take place and the constituents feature the characteristic polymeric structure that inspired Demichelis et al. (2011) to dub them DOLLOPs. The bottom line of the work of Wallace et al. (2013) is clear: the formation of a liquid-condensed mineral precursor in the calcium carbonate system is not in contradiction with classical models of phase separation; the spinodal is within our experimental range. Their results further imply that the basic constituents of the liquid-condensed phase are prenucleation clusters, further corroborating the previous independently made speculation of Wolf and Gebauer (Gebauer et al., 2014; Wolf et al., 2012).

5.2. Polymer-induced liquid precursors (PILPs)

While the liquid-liquid phase separation event is yet to be experimentally observed *in situ*, at high magnification, post hoc TEM analysis has shown "emulsion-like" or "liquid-like" amorphous calcium carbonate precursor phases in the presence of polymeric additives (e.g., Rieger et al., 2007; Wolf et al., 2011a,b). This dense liquid precursor resembles the so-called polymer-induced-liquid-precursor (PILP), a term first introduced by Gower and Odom (2000). In a series of pioneering studies Gower and co-workers indicated that the presence of poly(aspartic acid) or poly(acrylic acid) in solution with Ca^{2+} and carbonate ions leads to the separation of dense liquid droplets which precede the formation of crystalline $CaCO_3$, typically via a solid amorphous precursor phase (Gower, 2008). The acidic polymers mimic the action of the highly charged macromolecules present within the biomineralization cellular milieu, and suppress classical nucleation, thereby giving access to the condensed liquid phase. These colloidal liquid droplets become the key component of the crystallization, undergoing coalescence and aggregation, prior to dehydration, which leads to solidification yielding a solid amorphous precursor phase. This phase undergoes pseudomorphic crystallization, resulting in the formation of crystalline non-equilibrium morphologies with nanogranular fine structure (see review by Gower, 2008). Such morphologies are derived from the concentrated aggregation of mineral droplets (liquid-like ACC) to growing crystal fronts yielding mineral bodies shaped as wires (Olszta et al.,

2004), helices (Gower and Odom, 2000), films (Gower and Odom, 2000; Xu et al., 2004), and tablets (Amos et al., 2007) (see Fig. 7b-e). Macromolecules of varying molecular structures and Coulombic charges have been employed in PILP syntheses such as the negatively charged protein ovalbumin (Wolf et al., 2011a), and anionic polypeptides (Schenk et al., 2012a). Interestingly, positively charged synthetic polymers (Cantaert et al., 2012) and the positively charged protein lysozyme have also been found to induce the PILP phase (Wolf et al., 2011b) for the $CaCO_3$ system. Moreover, the PILP system is not confined solely to calcium carbonate: analogous metallic carbonate systems (such as Sr, Ba, Mn, Cd and Pb) (Homeijer et al., 2010; Wolf et al., 2011b; Zhu et al., 2015), calcium phosphates (Olszta et al., 2007) and molecular crystals (amino acids and dye pigments) (Ma et al., 2009; Wohlrab et al., 2005), have all been observed to have crystallized following the PILP-mediated pathway. The variety of systems applicable to the PILP process adds weight to the claims of Gower's group that a PILP-mediated mineralization could be of relevance for a range of processes: from mollusk shell formation to the mineralization of bone (Olszta et al., 2003). Such assertions gain weight when the properties of the PILP phase and the subsequently formed crystals are further examined. First, the liquid like character of the PILP phase affords the synthesis of non-equilibrium geometries within confined volumes via infiltration of the dense colloidal liquid droplets. This property has been evidenced by the formation of both high-aspect ratio calcite nanowires within the pores of track etched membranes (Kim et al., 2011) and hydroxyapatite crystallites within the voids of collagenous templates (Olszta et al., 2007). In both cases this is thought to occur by the effect of capillarity drawing the fluidic mineral precursor into the pores. When considered in the context of biomineralization such a property could explain a synthetic route to the space-filling mineral structures observed in mollusks and other biominerals (Yang et al., 2011). Second, AFM analysis of PILP films shows that at the nanoscale they are composed of globular granules between 30 and 150 nm in diameter (Kim et al., 2007) (see Fig. 7a). This granular nanostructure, which provides evidence that the PILP process occurs by colloidal attachment, is shared with biominerals that are commonly observed to comprise nanoscopic granules typically aligned into a crystallographic register. For an extensive overview and the respective process-structure-property relationship in biominerals, please confer the first part of this review (Wolf et al., 2016a). Third, the pseudomorphic crystallization process observed in PILP films is analogous to that proposed to occur within biominerals (Harris et al., 2015). In some instances, the crystallographic alignment of the granules in PILP formed wires is such that they are ordered with a low angle spread (Cantaert et al., 2013), as observed in mesocrystalline biogenic crystals (Seto et al., 2012). In alternate systems the crystallization can follow spherulitic mechanisms leading to complex crystallographic features such as lattice tilting which are also present within biominerals (Harris et al., 2015; Olson et al., 2013b) (see Fig. 7f).

5.3. PILP vs. coacervation

The PILP pathway is commonly misconstrued as a coacervation process, due to the perceived role of the polyelectrolyte in mediating phase separation. Coacervation describes the

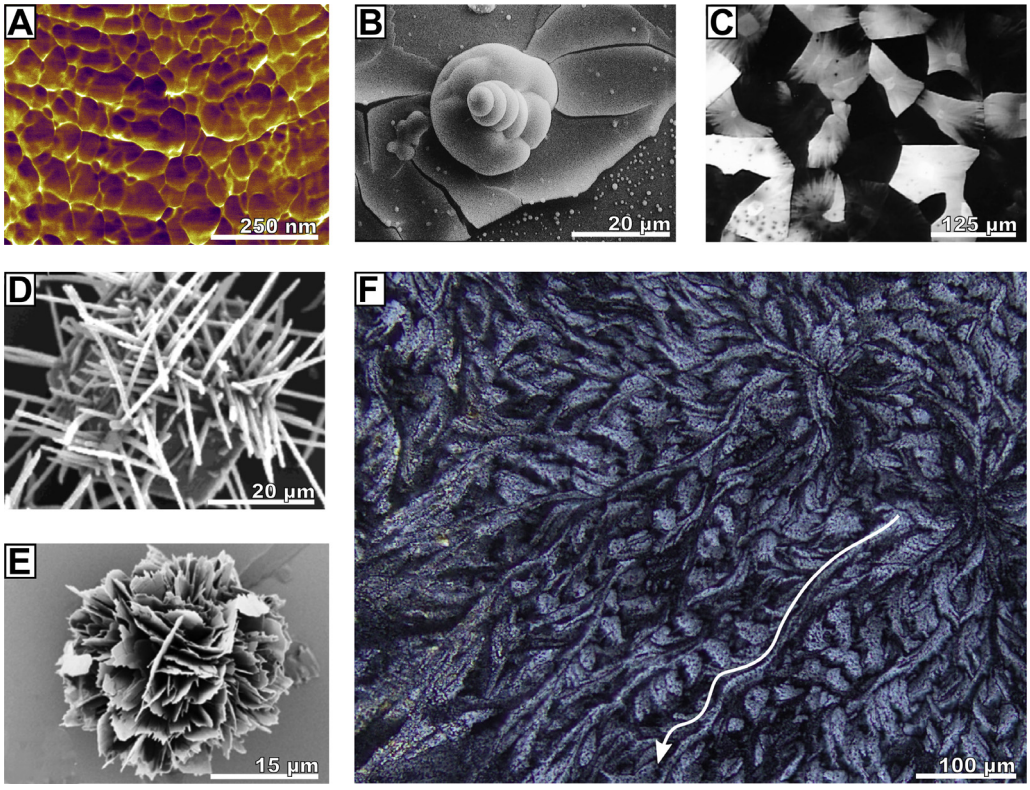

Fig. 7. Nanoscopic fine structure and non-equilibrium morphologies generated by means of the polymer-induced liquid-precursor process. (A) The phase image of an atomic force micrograph reveals the characteristic nanogranularity of a PILP product suggesting its non-classical mode of growth. (B) Helical protrusion emerging from a thin calcium carbonate film. (C) A mosaic mesocrystalline film of calcium carbonate. (D) Nanofibrillar calcite of 100–800 nm growing on calcite substrates. (E) Hierarchical microspheres of amino acids. (F) Calcite thin films exhibiting crystal lattice tilting similar to that known from biominerals (Harris et al., 2015). Subfigures (A) and (F) are taken from Harris et al. (2015). Published by the Royal Society of Chemistry; Subfigures (B) and (C) reprinted from Gower and Odom (2000), with permission from Elsevier; Subfigure (D) reprinted with permission from Olszta et al. (2004). Copyright 2004 American Chemical Society; Subfigure (E) reprinted with permission from Jiang et al. (2011). Copyright 2011 American Chemical Society.

liquid-liquid phase separation of a homogenous solution of charged colloids into a dense colloid-rich phase (the coacervate) and a colloid-deficient phase (the equilibrium phase) as a result of intra- or intermolecular associative interactions (Bungenberg de Jong, 1949). The two phases have the same solvent, yet are immiscible and in thermodynamic equilibrium (Gupta and Bohidar, 2005). Importantly, and in contrast to the PILP phase, the coacervate phase is thermodynamically stable, whereas PILP is only kinetically stable (Jiang et al., 2012). The polymer complexes that constitute the coacervate have a lower solvent affinity, which leads to the observed phase separation, but do not completely desolvate; the coacervate remains as a liquid phase in equilibrium with the solvent. Contrastingly, in the PILP system, after formation of the dense liquid droplets dehydration of the phase occurs resulting in precipitation of the solid precursor (Gower, 2008). Some confusion between the coacervate and PILP syntheses may still exist. This is because solutions of PAA and calcium ions are often used in PILP syntheses, and this is a system known to undergo coacervation (Kaempfe et al., 2013). However, in PILP crystallization the polymer is clearly below the critical coacervation concentration (i.e., the concentration required for phase separation to be thermodynamically favorable) therefore, although complexes form, demixing is energetically forbidden and coacervation does not occur.

6. Nonclassical aggregation-based growth: Oriented attachment and mesocrystals

Recent research has extensively shown that crystals do not necessarily grow in solution via the classical layer-by-layer model proposed by Kossel (1927) (see Section 2). Indeed, growing evidence shows that particle-mediated or aggregation-based growth of crystals is more common than previously thought (Cölfen and Mann, 2003; Cölfen and Antonietti, 2008; De Yoreo et al., 2015; Zhang et al., 2014). Two main mechanisms for such an aggregation-based growth have been proposed: a) oriented attachment (Penn and Banfield, 1998), and b) mesocrystal formation (Cölfen and Mann, 2003; Cölfen and Antonietti, 2008; Niederberger and Cölfen, 2006) (Fig. 8). In both cases, nanoparticulate building blocks aggregate along specific [*hkl*] directions forming single crystals. Although there are some commonalities between these two aggregation-based growth processes, there are, however, some key differences (De Yoreo et al., 2015; Meldrum and Cölfen, 2008).

6.1. Oriented attachment

The term "oriented attachment" (OA), equivalent to "oriented aggregation" (Penn and Soltis, 2014), was coined by Penn and Banfield (1998) to describe the particle-mediated growth of single crystals via the spontaneous self-assembly of nanocrystalline particles which move, interact, rotate, and re-arrange in order to fuse along equivalent crystallographic faces, that is, sharing two common crystallographic directions (Li et al., 2012; Penn and Soltis, 2014; Zhang et al., 2014). Such a reduction of interfaces was initially considered as the driving force for OA, because it ultimately contributed to an overall reduction of the system free energy. However, it was argued that such an interface elimination is achieved "after" attachment, so it was unclear what was the (long-range) driving force leading to attachment, that is, operating "before" and "during" attachment. Alternative phenomena proposed as the driving force for OA include van der Waals and/or dipole-dipole interactions, as well as interatomic Coulombic interactions (Zhang and Banfield, 2014). While it would seem that OA should favor the growth of 1D structures, 2D and 3D structures have also been claimed to form via OA (Meldrum and Cölfen, 2008). The nanoscale features of such a nonclassical crystal growth mechanism were first disclosed using HRTEM (Penn and Banfield, 1998). More recently, the movement of iron oxyhydroxide nanocrystals in solution until they approached, rotated and fused along specific homologous crystal faces was directly observed using *in situ* HRTEM equipped with a fluid cell (Li et al., 2012). Inherent to such a growth mechanism is the notion that nanoparticles have to be crystalline. However, it has been recently suggested that OA could also operate in the case of poorly crystalline or, even, amorphous phases, provided that sufficient degree of anisotropy (e.g., dipolar moment) exists (Zhang et al., 2014). Indeed, Rodriguez-Navarro et al. (2015b) claimed that OA of ACC nanoparticles led to the formation of 1D, 2D and 3D ACC structures. The authors showed that ACC nanoparticles displayed calcitic medium-range order. Such a medium-range order was considered critical to enable OA of ACC nanoparticles forming the structures shown in Fig. 4. Their calcitic medium-range order made the ACC particles partially anisotropic, so that they could undergo OA, likely via dipole-dipole interactions.

It should be pointed out that (under different names) growth via OA was first described more than 100 years ago to explain the growth of a range of crystals spanning from oxy-hydroxides, sulfides, carbonates, sulfates and phosphates, to organic (molecular) crystals. However, these pioneering works, which were recently reviewed by Ivanov et al. (2014), lacked the appropriate high resolution electron microscopy techniques in use nowadays to show the key (nano)features which define growth via OA. This and the fact that most of the early literature on OA was in Russian may help to explain why OA is considered as a "new" nonclassical crystal growth mechanism.

6.2. Mesocrystals

The term "mesocrystal" is an abbreviation for "mesoscopically structured crystals" (Cölfen and Antonietti, 2005, 2008). They are colloidal crystals made up of individual crystalline nanoparticles arranged in crystallographic register via mesoscale aggregation and alignment (Meldrum and Cölfen, 2008; Niederberger and Cölfen, 2006). This term has been expanded to include structures that can form by aggregation of amorphous nanoparticles, which upon amorphous-to-crystalline transformation retain a textural memory of the original individual precursor nanoparticles (Song and Cölfen, 2010). As a consequence of their ordered structuring, mesocrystals diffract x-rays or electrons as a single crystal (Fig. 9), despite the fact that they consist of individual nanoparticle building units, typically separated by amorphous organic or inorganic layers (Bergström et al., 2015). Similarly, they can display birefringence under the polarized optical microscope. However, and in contrast to single crystals (either formed via a classical crystallization process or via OA), they typically display a very small coherent domain length (or crystallite size) and forbidden faces (i.e., not consistent with the crystal symmetry of a particular mineral, as it is the case of calcite mesocrystals with octahedral form), or negatively curved faces (Song et al., 2009) (Fig. 9a and b). The fact that mesocrystals are made up of nanoparticle building units (Fig. 9c) is evidenced by their rough nanogranular surfaces (Fig. 9d) or their internal nanostructure. Indeed, mesocrystals are the epitome of biomimetic structures displaying a nanogranular surface texture, which according to Song et al. (2009) can result from the aggregation of amorphous precursor nanoparticles. However, while it has been proposed that once amorphous nanoparticles coalesce into a mesostructure they undergo amorphous-to-crystalline transformation reaching the standard crystalline features of a mesocrystal (Gower, 2008; Seto et al., 2012; Wolf et al., 2012), little is known regarding how such an amorphous-to-crystalline transformation takes place, or how amorphous nanoparticles can arrange forming a faceted mesocrystal. We will come to these critical questions later on.

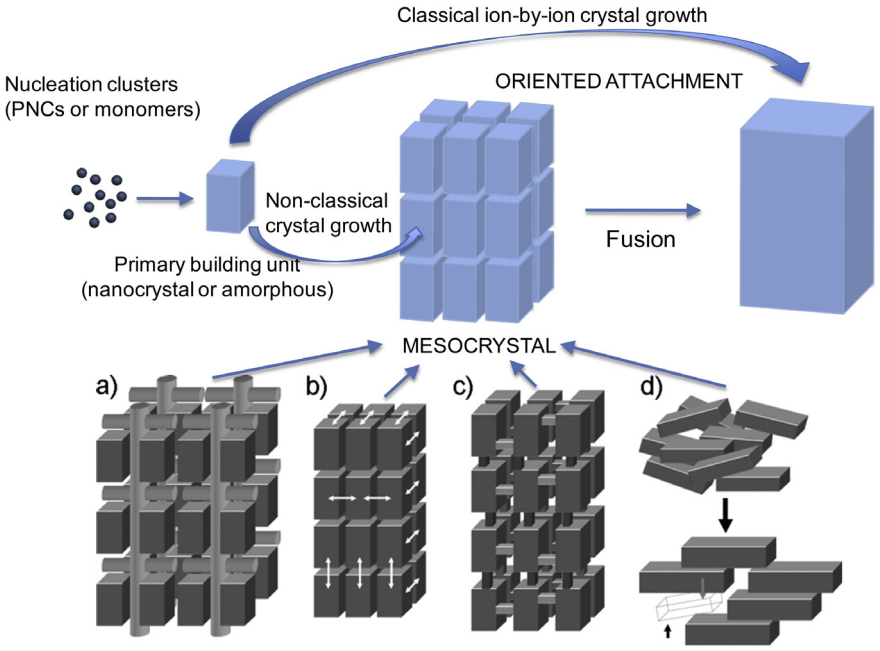

Fig. 8. Classical vs. non-classical crystal growth involving OA and/or mesocrystallization. The four known mechanisms for mesocrystal formation are indicated (a-d). a) alignment of nanoparticles by a templating oriented matrix; b) by an external field or by mutual alignement of identical faces (i.e., OA); c) by epitaxial growth through mineral bridges; d) by spatial constraints. See text for details. Scheme based on Zhou and O'Brian (2012). Figures (a)-(d) reproduced with permission from Song and Cölfen (2010). Copyright Wiley.

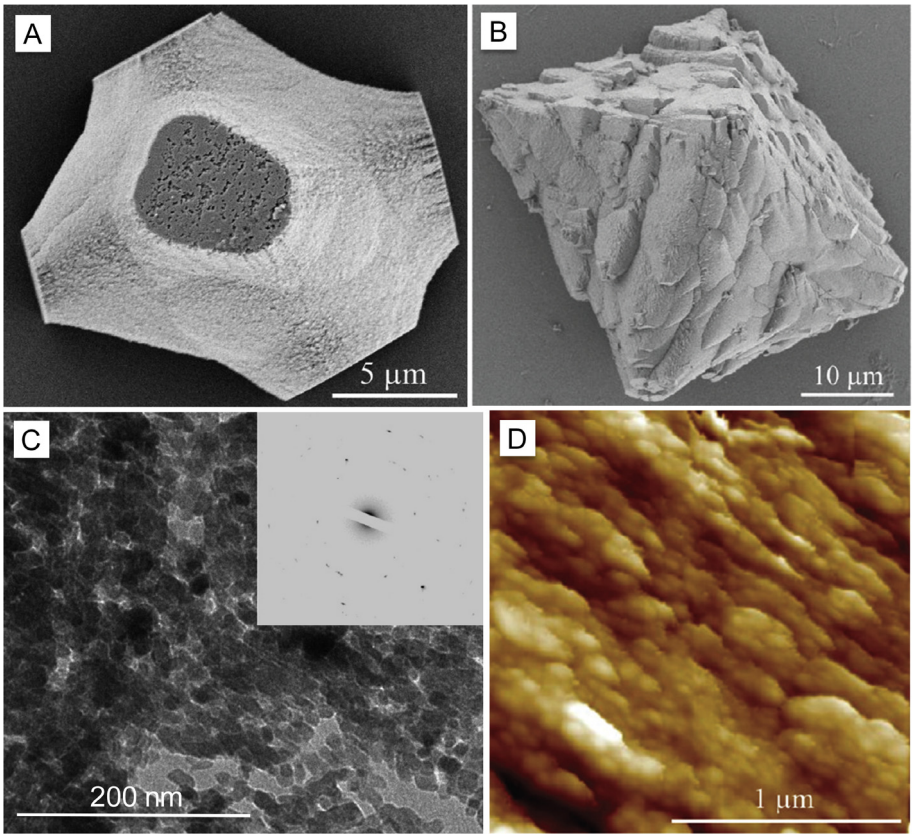

Fig. 9. Morphology and structure of mesocrystals. Negatively curved P-surfaces (A) and octahedral (B) calcite mesocrystals. (C) TEM image of a calcite mesocrystal slice showing it is made up of a porous oriented aggregate of nanocrystals diffracting electrons as a single crystal (SEAD in inset). (D) AFM image showing the (oriented) nanogranular surface features of the calcite mesocrystal in (B). Reprinted with permission from Song et al. (2009). Copyright 2009 American Chemical Society.

An important point for mesocrystal formations (although not mandatory) is the presence of an organic additive (Cölfen and Yu, 2005). The presence of organics is also of general importance in biomimetic materials, which are in many cases suggested to form via mesocrystal assemblage. The organic additive reduces the interfacial tension between the nanocrystal building units and the solution to enable their self-assembly (Meldrum and Cölfen, 2008). Thus, mesocrystals typically include organics, which are adsorbed on each individual nanoparticle subunit. However, as pointed out by Gower (2008), the presence of organics lining the nanocrystal subunits of a mesocrystal, does not prove that the organic was directing the self-assembly or that an organic matrix arranged crystalline nanoparticles. According to Gower (2008), it could be that pseudomorphic crystallization of an amorphous precursor left behind remnant of polymer-encapsulated nanoparticles. The latter is consistent with the reported formation of mesocrystals after amorphous precursor nanoparticles (Zhou and O'Brian, 2008). Note also that in some cases "mineral bridges" exist between nanoparticles (Imai et al., 2006; Oaki et al., 2006), which, according to the authors, enable crystallographic information to be "transmitted" among nanoparticles, not requiring an organic template-directing agent (Zhou and O'Brien, 2012). The lack of perfect fusion among nanoparticles, in part associated with the entrapped organic molecules or the existence of mineral bridges, or the presence of minor amorphous phases between nanocrystal subunits (Bergström et al., 2015), leads to the reported high surface area of mesocrystals (Zhou and O'Brian, 2008).

Currently, up to four possible mechanisms for 3D alignment of already crystalline nanoparticles to a mesocrystal have been proposed (Song and Cölfen, 2010) (Fig. 8a-d): a) alignment of nanoparticles by an oriented organic matrix, b) nanoparticle alignment by physical fields or mutual alignment of homologous crystal faces (basically, this last process also operates in OA), c) epitaxial growth via mineral bridges, and d) nanoparticle alignment by spatial constraints (similar to colloidal crystal formation using anisotropically shaped particles). In some cases, combination of the above mechanisms can take place. For instance, nanoparticles in a mesocrystal may not be initially connected, but they finally connect via mineral bridges.

Some biominerals, such as sea urchin spines, corals, eggshells and nacre, are thought to be mesocrystals (Bergström et al., 2015; Seto et al., 2012; Vielzeuf et al., 2010, 2008; Wolf et al., 2012). Indeed, their outstanding physical-mechanical and optical properties have been related to their mesocrystalline structure (Bergström et al., 2015). In parallel, biomimetic mesocrystals have been shown to display a range of exceptional properties that are finding applications in the rational design of, for instance, photocatalysts, electrodes, optoelectronics, and biomedical materials (Song and Cölfen, 2010; Zhou and O'Brien, 2012).

It has been suggested that the formation of a mesocrystal is a required intermediate step of OA (Schwahn et al., 2007) (Fig. 8). Furthermore, Kulak et al. (2007) reported that single crystals, mesocrystals and polycrystalline $CaCO_3$ aggregates all form in the presence of a copolymer by a common nonclassical aggregation-based mechanism (involving the aggregation of precursor subunits). A key result that points to a common origin for mesocrystals and single crystals grown via OA was presented by Yuwono et al. (2010). Their cryo-TEM study showed that individual goethite nanocrystals approached and aligned along specific crystallographic directions, but did not physically touch during the early stages of aggregation. The resulting rod-like structure (Fig. 10) displayed a faceted contour and resembled a mosaic of oriented nanocrystals (mesocrystal stage) separated by solvent. Over time the nanoparticles fused and transformed into a microscopic single crystal. Importantly, when the vitrified water was sublimated after cryo-TEM observation, each mesocrystal broke apart into individual primary nanoparticles. The latter demonstrated that the amorphous material between each primary nanoparticle (see HRTEM image in Figure10c) was water. Further evidence for the existence of hydration layers mediating the coalescence of nanoparticles was provided by Anand et al. (2015). Using *in situ* fluid-cell TEM, the authors showed that Au nanoparticles displayed a hydration shell which mediated coalescence and prevented the direct contact between nanoparticle pairs during the early stages of aggregation. Subsequent removal of the hydration layers resulted in attachment. The results by Yuwono et al. (2010) show that an interplay between long-range attractive and repulsive forces helps to build such an oriented mesocrystalline structure (basically a colloidal crystal). Most important, these results show that water adsorbed on each individual nanoparticle can act as a bridge that "communicates/transmits" the crystallographic information of one nanoparticle to the surrounding ones. This underlines the fact, which growing evidence is confirming, that water at the (nano)crystal-solution interface adopts a medium-range ordered structure which is imposed by the field created by the crystal substrate, as has been shown using frequency-modulated AFM for the case of water adsorbed on mica (Kobayashi et al., 2013) and calcite surfaces (Imada et al., 2013). Structuring of water by a solid substrate has been also demonstrated for biomineralization-relevant systems such as calcium phosphates (Wang et al., 2013b). Solvent ordering/structuring leads to its layering at the solid-solution interface as shown by experiments and molecular modeling (see Sathiyanarayanan et al., 2011, and references therein). This results in force oscillations both attractive and repulsive so that nanoparticles can reside in an attractive free energy minimum without aggregating prior to form a fused mesocrystalline structure (Sathiyanarayanan et al., 2011). The system described by Yuwono et al. (2010), however, displays key features of mesocrystals, but appears to lack organic or mineral (amorphous or crystalline) "bridges" which are claimed to be necessary for nanoparticle 3D self-assembly in crystallographic registry during mesocrystallization.

Recently, the whole "mesocrystal" concept was challenged, at least for the case of the $CaCO_3$-H_2O system. Kim et al. (2014) showed that a single crystal of calcite placed in a supersaturated solution dosed with PSS, can develop curved faces and a high surface area, typical of mesocrystals, under conditions where no nucleation of individual nanocrystals or precursor ACC nanoparticles was expected, and where an ion-by-ion classical growth mechanism should take place. Moreover, the authors underlined that only a thin shell of the "mesocrystals" was made up of nanoparticles. Nonetheless, the authors reported that aging of the "mesocrystals" formed under conditions resulting in the initial precipitation of ACC led to a significant restructuring and surface area reduction, which is fully consistent with the concept of mesocrystals (Song and Cölfen, 2010). Furthermore, it is unclear whether or not (crystalline or even amorphous) nanoparticles formed (and attached to the crystalline substrate) in runs where solutions undersaturated with respect to hydrated ACC, but supersaturated with respect to calcite (and vaterite, as well as anhydrous ACC: see Rodriguez-Navarro et al., 2015b) were used. Further studies are thus required to disprove that the typical rough (nanogranular) surface features and curved or unexpected faces of calcite mesocrystals are not the result of an assembly of nanoparticles.

7. Nonclassical crystallization by Colloid Attachment and Transformation (CAT): A new route for crystal growth driven by amorphous colloids

Another important but largely unknown aspect of the nonclassical aggregation-based growth of crystals refers to the possibility of growth of an already formed crystal via the incorporation of col-

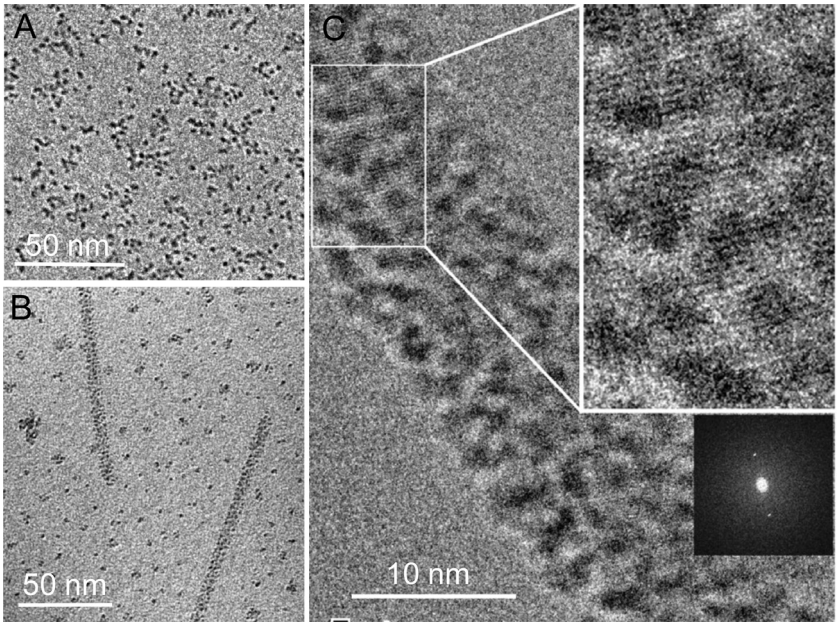

Fig. 10. Cryo-TEM imaging of the early stages of oriented attachment of goethite nanoparticles. (A) Nanoparticle dispersion of precursor ferrihydrite. (B) Oriented aggregation of goethite nanoparticles forming elongated crystal precursors (mesocrystals). Note that the individual nanoparticles in the elongated structure are surrounded by the solvent. (C) HRTEM image showing individual nanoparticles (detail of (0 1 2) lattice fringes in upper inset). The FFT pattern (lower right inset) shows that the whole structure diffracts as a single crystal. Reproduced with permission from Yuwono et al. (2010). Copyright (2010) American Chemical Society.

loids, particularly amorphous nanoparticles. This situation is highly relevant in biomineralization, where biomineral growth typically occurs sequentially as the organism develops (e.g., growth of the calcitic spicule of sea urchins or mollusk nacre), and it commonly proceeds via amorphous precursors (Addadi et al., 2003, 2006; Weiner and Addadi, 2011). It is also of interest in the formation of biomimetic materials, especially in those cases where a multilayer growth, resembling nacre, is sought (Finnemore et al., 2012). Note that if growth occurs via the incorporation of nanoscopic amorphous colloids, growth rates can be increased by orders of magnitude compared to classical ion-mediated growth (Rodriguez-Navarro et al., 2015a). Furthermore, the growth of inorganic ionic crystals with the characteristics of colloidal crystals can be achieved, which opens a whole range of possibilities for the rational design and synthesis of novel functional biomimetic materials. We recently coined the term "colloid attachment and transformation – CAT" in order to denote this nonclassical crystallization process (Wolf et al., 2016b), which represents – as we are going to detail in the following section – one important route to poly- and mesocrystalline bodies with both equilibrium and non-equilibrium shapes.

Using cryo-TEM, Baumgartner et al. (2013) showed that magnetite crystals can grow from solution via precursor nanoparticles (2 nm in size), apparently amorphous (they displayed no lattice fringes). Upon attachment onto a particular (*hkl*) face of magnetite these nanoparticles undergo restructuring and fusion with the crystalline lattice of the substrate. This observation (somehow overlooked by the authors) points to the possibility that an amorphous nanoparticle can directly interact with a crystalline substrate and contribute to its growth. This is intriguing, and could potentially explain a whole set of observations regarding the role of amorphous nanoparticle precursors on the aggregation-based growth of different biominerals and their biomimetics (De Yoreo et al., 2015) as well as in other minerals with a range of technological applications (e.g., zeolites: Kumar et al., 2015; Lupulescu and Rimer, 2014). In this respect, Gal et al. (2013, 2014, 2015) showed that calcite rhombohedra growing in the presence of different organic additives typically display rough surfaces, corresponding to specific (*hkl*) faces, made up of nanogranular structures (they called them "nanoglobular") (Fig. 1f). Such a nanogranular texture points to a growth process that does not proceed via a classical ion-mediated mechanism. The authors suggested that ACC nanoparticles were stabilized by organic additives (or inorganic additives, i.e., phosphate ions), and subsequently attached onto calcite faces and, after 2D diffusion, got incorporated into (i.e., fused with) the crystalline structure of the substrate (Fig. 1g), a growth model similar to that proposed by several authors (e.g., by Politi et al., 2007; Cuif et al., 2010; Gower, 2008; Seto et al., 2012; or Wolf et al., 2012) for the growth of calcium carbonate biominerals. In 2015, Gal et al. also then proposed that such an ACC-mediated aggregation-based mechanism could explain the commonly observed nanogranular features of several biominerals.

Rodriguez-Navarro et al. (2016) reported that calcite growth along specific crystallographic directions can occur via a nonclassical growth mechanism mediated by colloidal ACC which mirrors ion-mediated growth at the nanoscale, and involves the layer-by-layer attachment of ACC nanoparticles, followed by their restructuring and fusion with the substrate in perfect crystallographic registry. The process was directly observed using *in situ* AFM both in the absence and presence of organic additives (poly(acrylic acid), PAA). Most interesting was the observation that ACC nanoparticles attached on the surface of calcite {10.4} faces tended to display a flattened spherical morphology. Such a flattening is fully consistent with the idea that ACC can form after a dense liquid (what has been termed "liquid-like" ACC). Xu et al. (2005) showed that the liquid-like character of ACC precursors was responsible for the formation of hemispheres on Si surfaces following the deposition of initially spherical droplets. Rodriguez-Navarro et al. (2016) also observed the faceted calcite crystals formed via ACC nanoparticle attachment in the absence of additives initially displayed nanoglobular rough surfaces, but upon aging and dissolution-recrystalization, smooth surfaces resulted, similar to those observed following classical ion-mediated calcite growth. Conversely, crystals subjected to ACC nanoparticle-

mediated growth in the presence of PAA displayed nanoglobular surface textures upon aging in a humid environment and conversion of ACC into calcite. The preservation of the nanogranular structure was associated with the accumulation of organic molecules (PAA) at the nanoparticles' surface upon ACC-to-calcite conversion via an interface-coupled dissolution-precipitation (i.e., pseudomorphic replacement), a conversion mechanism that must not be confused with the dissolution of ACC followed by the bulk reprecipitation of calcite, which does not result in a pseudomorph (Rodriguez-Navarro et al., 2015b). A similar "exclusion" of organics following ACC-to-crystalline conversion (after a PILP phase) was described by Dai et al. (2008). Note, however, that the accumulation of organics along specific crystal planes in biogenic nanogranular calcite formed after ACC, may be explained by the same exclusion mechanism resulting in the so-called "transition bars" formed during the pseudomorphic transformation of ACC (after a PILP phase) into calcite (Dai et al., 2008).This novel particle-mediated growth mechanism, depicted in Fig. 11, may help to explain the nanogranular textural features of both $CaCO_3$ biominerals and their biomimetics. It may also offer a plausible explanation for the growth of $CaCO_3$ crystals via propagation of macrospirals observed in several biominerals (e.g., nacre and semi-nacre). Such macrospirals display steps which are orders of magnitude thicker than the molecular level spiral expected for classical growth at a dislocation, and thus likely form from colloid attachment.

It should be pointed out that the above-described "colloid attachment and transformation – CAT" nonclassical crystallization process may also proceed when nanoparticles form by Ca binding to organics as precursor for the formation of ACC, according to the model presented by Smeets et al. (2015). Indeed, a recent study by Gal et al. (2016) shows that the *in vitro* growth of the calcitic structures formed on the base plate of coccoliths proceeds via attachment of nanoparticles made up of Ca bound to specific biomacromolecules involved in coccolith biomineralization.

8. Biomimetic nanogranular structures

In this section we will present some examples which demonstrate that nanogranular structures are common for a range of biomimetic minerals that form via different nonclassical growth

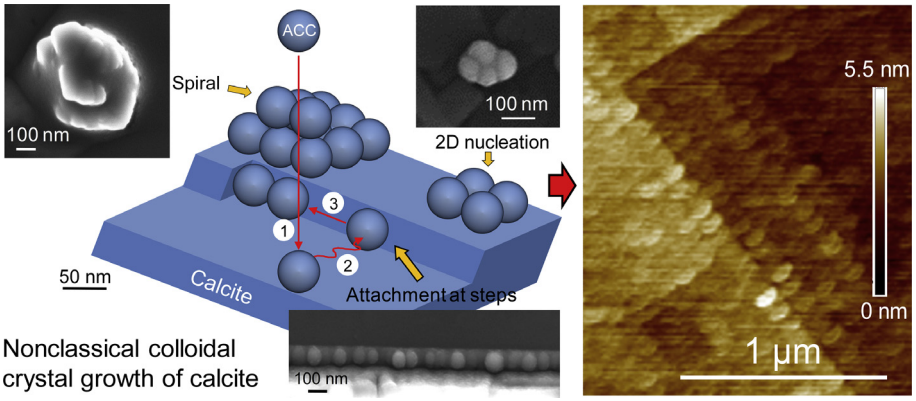

Fig. 11. Model for nonclassical layer-by-layer growth of calcite via a particle-mediated mechanism involving the attachment and restructuring of ACC nanoparticles. Growth progresses via spiral growth and 2D nucleation of ACC nanoparticles on $(10.4)_{calcite}$. Growth involves ACC nanoparticle bulk diffusion (1), surface diffusion (2) and final diffusion/attachment to a (macro)kink (3) where restructuring and fusion with the calcite substrate occurs. This stepwise growth results in faceted calcite crystals that display nanogranular surface features (AFM image on the right), similar to those observed in several biominerals, if growth occurs in the presence of organics. Reprinted with permission from Rodriguez-Navarro et al. (2016). Copyright (2016) American Chemical Society.

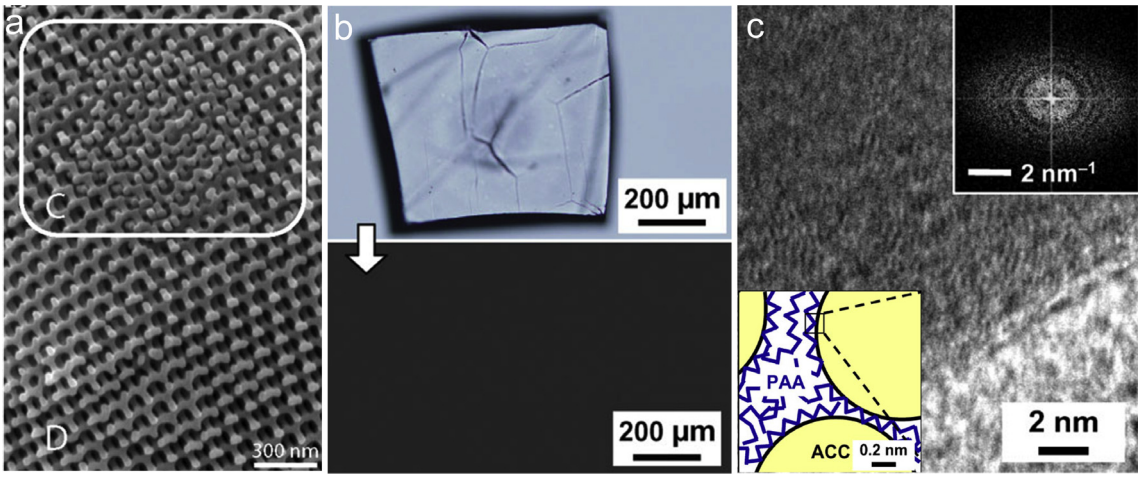

Fig. 12. Biomimetic ACC structures: a) porous gyroid structure made after infiltration of ACC nanoparticles into a colloidal crystal template (subsequently eliminated). Two interpenatrated gyroids are observed (the second one is marked by the squared area). From Finnemore et al. (2009). Copyright Royal Society of Chemistry; b) Stable ACC-PAA transparent thin film. Its amorphous nature is shown by the lack of birefringence under cross-polars (bottom); c) HRTEM image of the film structure made up of ACC nanoparticles (see scheme in lower inset).The FFT image (upper inset) shows its amorphous nature. Reprinted with permission from Oaki et al. (2008). Copyright Wiley.

routes that share in common the existence of liquid precursors and/or amorphous precursor nanoparticles. The literature on these topics is extensive, so we focus on the $CaCO_3$-H_2O system and on recent relevant publications (i.e., papers published over the last decade).

8.1. ACC

Biomimetic routes for the synthesis of novel functional materials based on the use of a precursor liquid or amorphous (solid) phase have been thoroughly explored (Gower and Tirrell, 1998; Gower and Odom, 2000; Gower, 2008; Meldrum and Cölfen, 2008). Aizenberg et al. (2003) used a dispersion of ACC nanoparticles placed onto a micropatterned template organically modified as a precursor for the synthesis of micropatterned calcite single crystals. The authors demonstrated that an ACC-based route for biomimetic crystalline materials was feasible. Xu et al. (2006) showed that ACC thin films preserved the nanogranular morphology of the amorphous precursor nanoparticles once transformed into calcite, either by heating (100–300 °C) or exposure to humid air at room *T*. Li and Qi (2008) used a colloidal dispersion of ACC nanoparticles for the fabrication of 3D ordered macroporous calcite single crystals, following infiltration of an ACC dispersion into a colloidal crystal, and the subsequent calcination-induced ACC-to-calcite conversion (involving the elimination of the colloid crystal template). Very similar results were obtained by Finnemore et al. (2009) infiltrating colloidal crystals (prepared by self-assembly of diblock-copolymers) with $CaCl_2$ solutions and exposing them to NH_3 and CO_2 vapors (from solid $(NH_4)_2CO_3$) that led to the precipitation of ACC nanoparticles within the porous 3D scaffold. Upon ACC crystallization (and elimination of the colloidal template), single crystalline calcite porous structures replicating the diblock copolymer gyroid morphology were obtained (Fig. 12a).

In contrast to the previous cases where the final biomimetic composite material included a crystalline $CaCO_3$ phase, in their pioneering work, Xu et al. (1998) achieved the formation of a (stable) ACC film using a porphyrin template. Remarkably, the film displayed a nanogranular morphology, suggestive of an aggregation-based growth mechanism. More recently, Li et al. (2010) succeeded in the synthesis of (stable) ACC films with a honeycomb pattern. They used a PILP route and a colloidal template (polystyrene nanoparticles self-assembled at the air-solution interface) to form the films that upon elimination of the colloidal template displayed a green structural color. The latter suggests that these structures can have applications as photonic materials. Another type of novel ACC-based functional material was synthesized by Lee et al. (2012). The authors achieved the synthesis of stable ACC microlens arrays following self-assembly of ACC nanoparticles at the air-solution interface. These structures were shown to be highly effective as antireflective coatings. The microlens-array mimicked the structure of the optical devices present in brittlestars. However, in the above-mentioned studies (with exception of the study by Xu et al., 1998), the authors did not present details of the nanostructure of ACC precursors (or the resulting calcite biomimetics). It is very likely that all these structures were made up of ACC nanograins as in the case of other ACC films or 3D (porous) structures prepared via a PILP route (Gower, 2008). Transparent and stable ACC thin films stabilized by organic additives (e.g., PAA) showing a nanogranular structure made up of ACC nanoparticles have been synthesized (Maruyama et al., 2011; Oaki et al., 2008) (see Fig. 12b and c). It is likely that in these cases, film formation took place via a colloidal self-assembly of ACC nanoparticles involving their aggregation and coalescence in the presence of an organic additive as proposed by Zhong and Chu (2009). Using the layer-by-layer approach commonly used for the biomimetic synthesis of nacre (see below), Huang et al. (2014) also obtained transparent, free-standing multilayer films (up to 710 nm in thickness) made up of ACC nanoparticles which were stabilized by PAA prior to their application as a dispersion onto the "organic" layer(s) (poly(diallyldimethyl ammonium chloride)). SEM analyses showed that the film also displayed a nanogranular structure corresponding to the ACC nanoparticle aggregate.

Inspired by the exceptional physical-mechanical properties of crustacean exoskeleton (high flexibility and bending strength) (Grunenfelder et al., 2014), which is formed by a combination of organic biomacromolecules and amorphous calcium carbonate and calcium phosphate phases (Al-Sawalmih et al., 2009; Sato et al., 2011), some researchers have investigated the possibility of synthesizing flexible ACC-based thin films. Saito et al. (2014) reported on the synthesis of freestanding, transparent, stiff and flexible ACC-PAA films reinforced with nanofibrilar cellulose (CACell). These structures were obtained by percolation a colloidal ACC-PAA precursor into a hydrogel sheet of CACell, followed by drying. The resulting structure was made up of stable ACC nanograins embedded within the organic framework. Remarkably, some of the mechanical properties of such a nanostructured biomimetic material outperformed those of the exoskeleton of the shrimp *Marsupenaeus japonicus*.

Other stable ACC-organic biomimetic composite structures have been reported, including peptoid nanosheets that were mineralized (layer-by-layer) with ACC nanoparticles forming a "sandwich structure" (Jun et al., 2015). Such nanosheets, which display a surface nanogranular structure due to the aggregation of ACC nanoparticles on the self-assembled peptoid layer, were considered to be applicable for the biomimetic synthesis of nacre-like materials. More recently, stretchable, moldable and self-healing hydrogels made up of ACC nanoparticles physically crosslinked to PAA, forming transparent and rigid free standing 2D and 3D objects once dried, have been achieved, which were called "mineral plastics" (Sun et al., 2016).

8.2. Vaterite

Vaterite formation is not only relevant for biomineralization (e.g., some tunicates form vaterite spicules: Kabalah-Amitai et al., 2013; Pokroy et al., 2015), but also for the biomimetic synthesis of $CaCO_3$ structures with a range of applications expanding from plastic fillers to drug delivery. Its formation has been a matter of debate, with two schools of thought. While some researchers consider that it forms via classical (spherulitic) growth, other support an aggregation-based growth (Andreassen, 2005). Most recent results suggest that an aggregation-based growth is the dominant mechanism, and it likely involves an amorphous precursor (Gehrke et al., 2005a; Pouget et al., 2009, 2010). Indeed, the formation of vaterite mesocrystals, which typically display a nanogranular surface texture, and commonly form in the presence of additives (ammonia or organics), has been shown to involve several stages of nanoparticle self-assembly (oriented attachment) as well as an ACC-to-crystalline transformation (Aziz et al., 2011; Gehrke et al., 2005a; Hu et al., 2012; Pouget et al., 2009, 2010). Gehrke et al. (2005a) suggested that lens-shaped hexagonal vaterite structures formed via oriented attachment of vaterite nanoplatelets. Interestingly, the authors pointed out that the field created by the crystalline structure was strong enough to attract amorphous intermediates, resulting in the observed nanogranular surface texture (nanograins with size ~20 nm). Hu et al. (2012) suggested that such a nanogranular texture (Fig. 13a and b) resulted from the random aggregation of nanoparticles that latter on lined up along specific crystallographic orientations (concurrent with a transition from poorly crystalline to crystalline) (Fig. 13c). Zhu et al. (2009) reported that complex pancake- or doughnut-like vaterite superstructures made up of flake-like building units formed after

self-assembly of ACC and early crystalline vaterite nanoparticles (HRTEM showed coexistence of both amorphous and crystalline nanoparticles), followed by a mesoscale transformation into vaterite nanocrystals. The whole process was controlled by the presence of organics (cetyltrimethyl ammonium bromide). Overall, these observations are fully consistent with the nonclassical colloid-mediated crystal growth mechanism presented in the previous section. Note, however, that an alternative explanation for the formation of hexagonal vaterite plates (in the presence of NH_4^+ ions) was suggested by Pouget et al. (2010). Using cryo-TEM the authors reported that after an initial aggregation of ACC nanoparticles, a solid-state transformation led to the formation of vaterite. It is however not clear how perfectly faceted hexagonal vaterite crystals can be formed via a solid-state amorphous-to-crystalline transformation from shapeless (mostly) spherical aggregates of ACC nanoparticles. This may be explained if one considers that precursor ACC nanoparticle can self-assemble forming a colloidal crystal. For this to occur, some degree of anisotropy must be present in the amorphous building units. In other words, the ACC nanoparticles must have a (vaterite) proto-structure (medium-range order). This is consistent with the model presented by Rodriguez-Navarro et al. (2015b) for the formation of 1D, 2D and 3D structures via the oriented attachment (self-assembly) of ACC nanoparticles with a proto-calcite structure. Interestingly, the cryo-TEM study of Pouget et al. (2009) showed that some hexagonal-shaped structures of vaterite had a faceted crystalline core (displaying strong lattice contrast) surrounded by an overgrowth with very low contrast and curved surface features. Such features were also observed by Pouget et al. (2010) (Figs. 13d and e). These observations suggest that the overgrowth was ACC and point to the growth of the vaterite core via attachment of ACC nanoparticles (present in the bulk solution), followed by their fusion with the crystalline substrate forming a faceted crystal (Fig. 13f), in agreement with the model proposed by Rodriguez-Navarro et al. (2016) (see Section 7).

Further evidence for the growth of vaterite via attachment of nanoparticle precursors was presented by Li and Zeng (2012). The authors tried to replicate the structure of nacre in lackluster pearls, which is made up of vaterite platelets. They succeeded in preparing the classic "mortar-and-brick" layered structure of nacre using vaterite nanoplates and an organic that enabled their self-assembly. However, their synthesis route resulted in vaterite nanoplates oriented with their c-axis normal to the layered structure, while vaterite plates in lackluster pearls have their b-axes normal to the layered structure. In any case, the nanoplates displayed nanogranular morphology (Fig. 14), suggestive of an aggregation-based growth mechanism involving ACC precursor nanoparticles. Nanogranular structures have also been commonly observed in vaterite thin films deposited, for instance, on a polymer matrix (Zhu et al., 2014), as well as in vaterite spheres formed in the presence of PSS (Imai et al., 2012). In these examples, the two key features, (i) amorphous precursor and (ii) nanogranular texture were closely linked, and pointed to colloidal self-assembly as the growth mechanism.

One key question in the biomimetic precipitation of vaterite after ACC is the following: What is the actual mechanism of polymorph selection? Some authors suggest that the existence of a particular proto-structure in ACC (short- or medium-range order) is critical for the selection of a particular polymorph upon amorphous-to-crystalline conversion (Gebauer et al., 2010). However, as indicated in section 3, recent results by Zou et al. (2015) point to size-related stability and solubility differences among different ACC precursors as the key parameter regulating polymorph selection (in solution). While this effect may explain the formation of vaterite in additive-free solution, it is not clear whether it also plays a role in additive-inclusive solutions where stabilization of this polymorph by different organics reportedly occurs (Rodriguez-Navarro et al., 2007).

8.3. Aragonite

Nacre is an example of the exceptional mechanical properties that the right combination of organic and inorganic (aragonite)

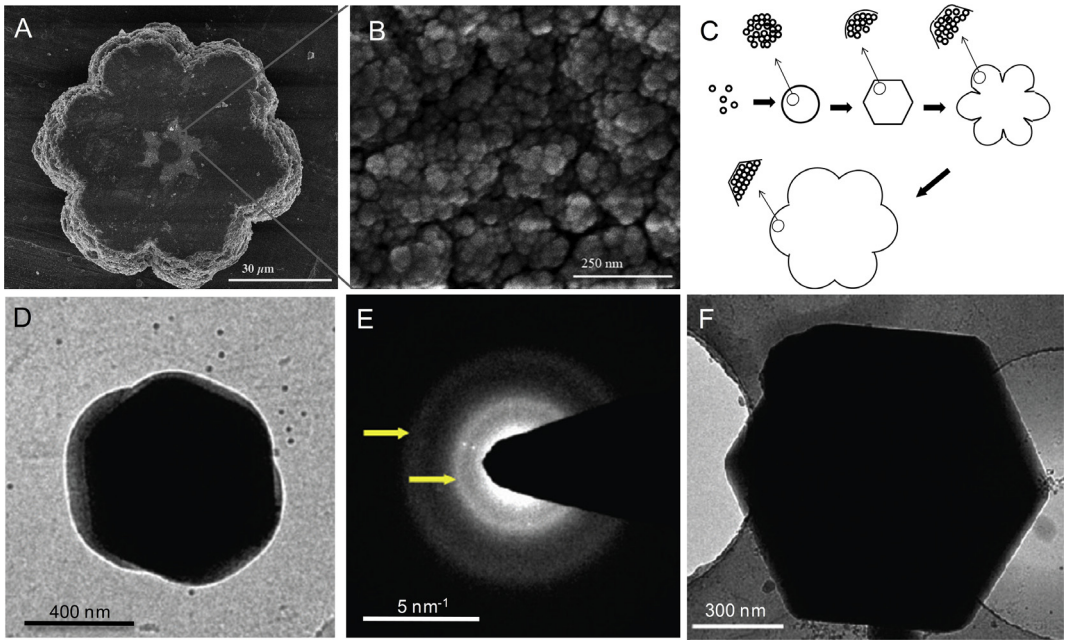

Fig. 13. Vaterite structures. A) Vaterite mesocrystal; B) detail of the nanogranular structure; C) model for the formation of the structure in (A) via aggregation of nanoparticles (see text for details). Reprinted with permission from Hu et al. (2012). Copyright Mineralogical Society of America. D) Cryo-TEM image of early vaterite formed by a crystalline core (dark-contrast inner hexagonal shaped area) and an ACC shell. E) The SAED pattern of the structure in (D) shows diffuse rings (yellow arrows) corresponding to ACC, and a few spots corresponding to vaterite; F) well-developed hexagonal vaterite. Reprinted with permission from Pouget et al. (2010). Copyright (2010) American Chemical Society.

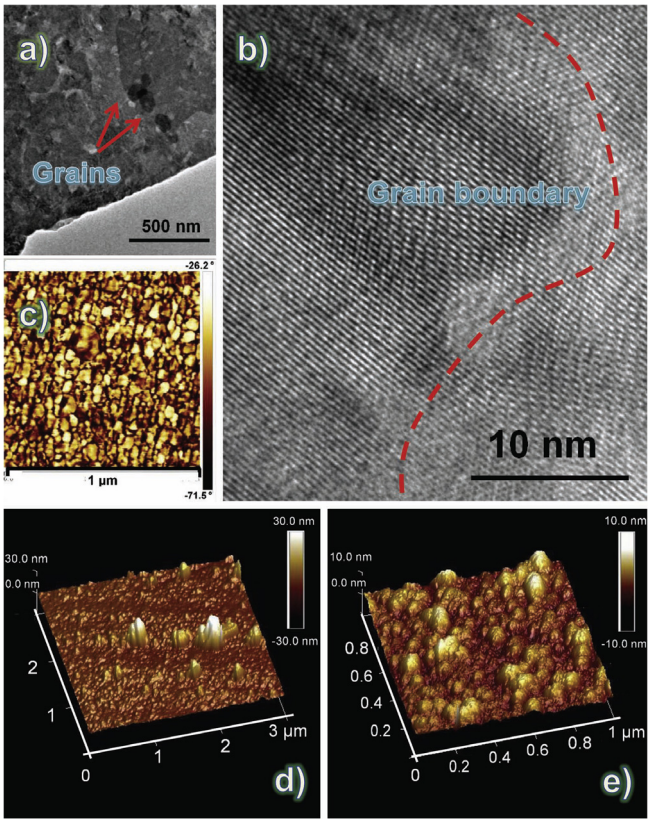

Fig. 14. Nanostructure of vaterite nanoplates used for the biomimetic synthesis of structures resembling nacre-like in lackluster pearls. a) TEM image of a nanoplate. b) HR-TEM image of a nanoplate showing the boundary between individual vaterite nanoparticles. c) AFM image of crystallite grains on a nanoplate. d,e) AFM images of the topography of a nanoplate surface showing the nanogranular structure. From Li and Zeng (2012). Copyright Wiley.

components can reach when properly arranged hierarchically at different length scales into a "brick-and-mortar" structure (Addadi et al., 2006; Lowenstam and Weiner, 1989; Yao et al., 2014). Indeed, the ultimate compression and tensile strength, hardness, and toughness (work of fracture) of nacre can be orders of magnitude higher than those of its individual components: the minor (~5 vol%) organic (bio)macromolecules (mainly polysaccharides, proteins and lipids) forming the "mortar" (Tseng et al., 2014) and the main inorganic phase, aragonite, forming the "bricks", which also includes (bio)macromolecules (Lowenstam and Weiner, 1989; Takahashi et al., 2004). Note, however, while aragonite is recognized as the main inorganic phase in nacre, nacre-like structures made up of vaterite (e.g., nacre in lackluster pearls) and calcite (e.g., semi-nacre in *Novocrania* sp.) have also been reported (Li and Zeng, 2012; Williams et al., 1999). Due to its extraordinary mechanical properties, nacre has been a source of inspiration for the biomimetic synthesis of stiff and tough composite materials (Bonderer et al., 2008; Ortiz and Boyce, 2008; Sellinger et al., 1998; Wegst et al., 2015; Yao et al., 2014). However, the *in vitro* replication of nacre involving the formation of pure, oriented aragonite platelets surrounded by organics and displaying a nanogranular structure of aragonite building blocks (nanogranules ~30 nm in size), which has been related to the exceptional toughness of nacre (Li et al., 2006), has not been achieved. The presence of a nanogranular structure strongly suggests that amorphous precursor nanoparticles play a critical role on the formation of nacre (Addadi et al., 2006), as recently demonstrated by DeVol et al. (2015), and gives important clues for the synthesis of its biomimetics. In their pioneering work, Gehrke et al. (2005b) achieved the retrosynthesis of nacre by the infiltration of a PILP phase within the organic matrix of demineralized nacre. The authors observed the formation of calcite after precursor ACC nanoparticles. This study demonstrated that a PILP phase (in this case, induced by PAA addition) and amorphous precursor nanoparticles could play a critical role during the formation of nacre *in vivo*. However, the formation of oriented aragonite platelets was not achieved and no details on the possible nanogranular structure of the final crystalline $CaCO_3$ mineral were presented. Apparently, the presence of adequate organic macromolecules is critical for the formation of aragonite (Falini et al., 1996). Using different organics (e.g., polyaspartate, polyacrylic acid, poly(vinyl alcohol), poly(vinyl alcohol)-co-(vinyl acetate)) with or without Mg^{2+} (a well-known additive inducing the formation of aragonite) the formation of aragonite nanorods or thin-films with nanogranular features somehow resembling nacre platelets have been achieved, in some cases after assembly of ACC precursor nanoparticles (Kajiyama et al., 2014; Sakamoto et al., 2009; Sugawara and Kato, 2000). Interestingly, Amos et al. (2007) observed the formation of aragonite tablets (~600 nm thick) following deposition of an ACC film underneath a Langmuir monolayer. In this case, the formation of the amorphous precursor was induced by PAA plus Mg^{2+} (i.e., PILP route). Multilayered aragonite structures (with shuttle-like shape) were obtained by Wang et al. (2010) who used a polysaccharide, alginate, to induce the nucleation and growth of $CaCO_3$ (Fig. 15). Initially, vaterite formed after a liquid-like ACC phase, and upon its dissolution, it released alginate, as well as Ca and carbonate ions, which favored the formation of aragonite. This latter phase grew via aggregation of nanoparticles (30 nm in size) whose crystalline or amorphous nature was not determined. Remarkably, the nanoparticles aggregated along preferred directions (vectorial alignment) forming multilayers (each layer ~100 nm thick) with mesocrystal features (SAED spot patterns with a few degrees' angular spread). Apparently, the presence of alginate was of paramount importance for the formation of these aragonitic structures that resembled nacre. Metzler et al. (2010) used N16N, an acid–protein fragment inspired by a protein (N16) in the nacre layer of *Pinctada fucata*, for biomimetic aragonite mineralization. Remarkably, they obtained a lamellar aragonite structure with interspersed N16N layers that strongly resembled natural nacre. However, micrometer-sized structures with only a few "nacre-like" layers were obtained. Layered organic-aragonite composites resembling nacre were also synthesized (via the Kitano method) by Munro and McGrath (2012). Notably, the presence of PAA and an organic matrix (chitin) was a prerequisite for aragonite formation, which displayed a layered, nanogranular nacre-like structure. However, no pure aragonite was obtained; instead, a 4:1 aragonite:calcite ratio was detected.

Some additional clues on the mechanisms of nacre growth have been achieved by performing nacre regrowth experiments *in vitro*. Although no exact replication of all the above-mentioned features of natural nacre could be achieved, some insights into the formation of nacre have been gained. Qiao et al. (2008) performed growth experiments using freshwater pearls that were immersed into $CaCl_2$ solution and exposed to NH_3 and CO_2 gases for mineralization to occur. The authors observed the growth of hexagonal platelets of aragonite that were very similar in morphology, size and orientation to those of the underlying substrate. Aragonite growth proceeded by the simultaneous development of nanometer sized "christmas tree"-like structures on the aragonite substrates, which suggested that crystal growth occurred via a classical 2D surface nucleation. The authors postulated that growth involved the formation of ACC precursor nanoparticles. However, their SEM observations and Raman analyses did not conclusively show what role (if any) ACC played in the development of the observed structures. Hayashi et al. (2010) used a natural nacre substrate for

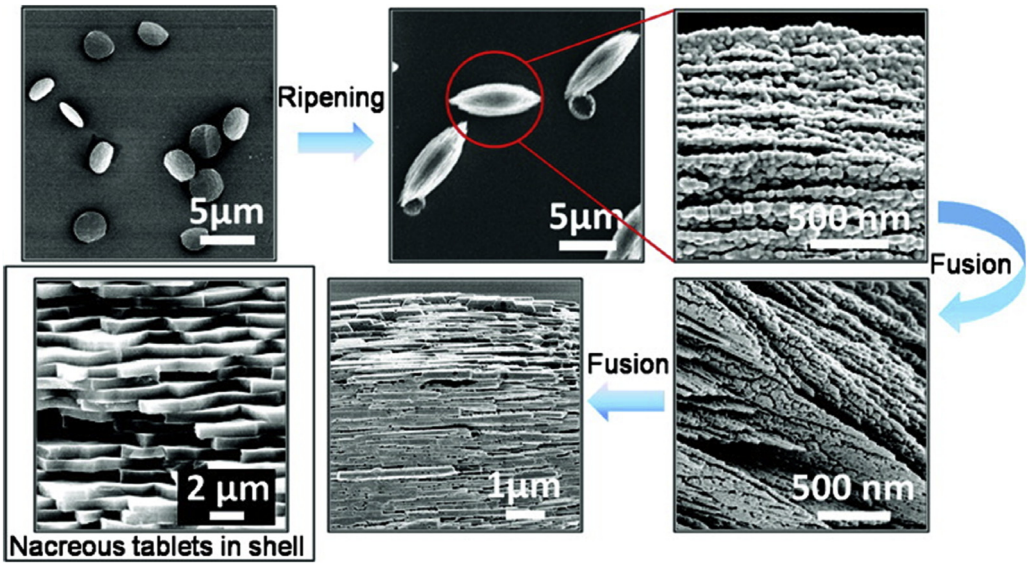

Fig. 15. Steps involved in the formation of nacre-like multilayered aragonite structures (with shuttle-like morphology) from hexagonally shaped vaterite (involving "ripening").The layers are made up of nanoparticle. Reprinted with permission from Wang et al. (2010). Copyright (2010) American Chemical Society.

the overgrowth of nacre-like aragonite/PAA multilayer films. The authors first induced the epitaxial growth of an aragonite layer on the nacre substrate and subsequently drop-coated a film of PAA. Note that near-epitaxial growth of aragonite layers appears to be a general feature of natural nacre (Olson et al., 2013a). By repeating these two steps, the multilayer structure, nearly identical to that of the natural substrate, was achieved according to the authors. However, although a nanogranular structure was evident, the aragonite plates in the overgrowth displayed an irregular contour, with no clear limit between platelets. Other researchers have also performed regrowth experiments using nacre as a substrate, observing that irrespective of the growth solution composition or the precipitation method, aragonite overgrowths with nanogranular textures typically developed (Zuykov et al., 2012).

Gries et al. (2012) achieved the re-mineralization of the insoluble organic matrix of abalone nacre. Aragonite platelets were obtained upon mixing of $NaHCO_3$ and $CaCl_2$ solutions in contact with demineralized insoluble organic matrix. Interestingly, the authors found mineral bridges (the so-called "Checa bridges") between aragonite layers that are considered instrumental for crystallographic alignment (Checa et al., 2011). However, Gries et al. (2012) gave no orientation of aragonite crystals on these layers, so it is unclear whether the $[001]_{aragonite}$ orientation normal to the aragonite platelets was achieved. They also provide no indication regarding the existence or absence of a nanogranular texture.

8.4. Magnesian calcite

Mg-calcite is a thermodynamically unstable variety of calcite (i.e., same space group) that includes Mg substituting Ca in concentrations that typically vary from 4 up to 45 mol% (Morse et al., 2007). Other metastable phases with higher Mg concentration are termed either proto-dolomite (with ~50 mol% Mg) or Mg-deficient magnesite (with ⩾50–55 mol% Mg) (Radha et al., 2012; Xu et al., 2013). The formation of high Mg-calcites (i.e., those with Mg concentrations >10 mol%) has been thoroughly studied due to the fact that several marine organisms (e.g., foraminifera, echinoderms, calcareous sponges, and some corals, serpulids, and calcareous algae) currently build their exoskeletons using such a thermodynamically unstable carbonate (see review by Long et al., 2014). Also, from a biomimetic, material-application perspective, it is important to underline that Mg-calcite biominerals show mechanical properties that exceed those of geologic calcite (Moureaux et al., 2010). Remarkably, *in vitro* synthesis of Mg-calcite in the absence of organic additives (or solvents) have typically failed to reproduce the high Mg content present in some biominerals (up to 45 mol%) (Killian et al., 2009). Conversely, high Mg-calcites have been synthesized in the laboratory using different organic additives and/or solvents (Xu et al., 2013), most of them involving the formation of amorphous precursors, as also occurs in many biogenic Mg-calcite biominerals (e.g., spicules of sea urchins or spicules of calcareous sponges, and sea urchin tooth) (Killian et al., 2009; Politi et al., 2008; Sethmann et al., 2006). Indeed, in their pioneering work, Raz et al. (2000) demonstrated that the formation of Mg-calcite *in vitro* involved an amorphous precursor. Cheng et al. (2007) were able to synthesize thin films of high Mg-calcite (30 mol% Mg) using a PILP route, which involved the precipitation and assembly of Mg-ACC nanoparticle precursors. Mg likely played a key role during thin film formation due to its well-known capacity to stabilize ACC precursors (Lin et al., 2015; Politi et al., 2010). This stabilization effect may not only be pivotal in the formation of Mg-calcite biominerals via an amorphous precursor, but also offers many possibilities for using Mg-ACC colloidal dispersions for the synthesis of biomimetic materials without the shortcomings associated with unwanted early ACC-to-crystalline conversion during material processing. Mg also induces and stabilizes PILPs (Schenk et al., 2012a), and appears to tune the wettability of liquid precursors (favoring their spreading as thin films, or their penetration into porous structures) (Berg et al., 2013). The use of PAA in Cheng et al. (2007) experiments was not only important for the formation of the PILP phase, but, likely, also favored the stabilization and self-assembly of the precursor ACC forming the film. Furthermore, organics such as PAA are known to favor the incorporation of Mg initially into ACC and later on into Mg-calcite because they facilitate the dehydration of such strongly hydrated ion (Wang et al., 2009). It is therefore not unexpected that most Mg-calcites with very high Mg contents (>20 mol % Mg) have been synthesized in the presence of organics. In fact, Long et al. (2011) reported that the presence of polymers in the growth solution used for the synthesis of a Mg-ACC precursor was pivotal to obtain Mg-calcite with up to 40 mol% Mg. Interestingly, the Mg-calcite microspheres the authors synthesized,

displayed a nanogranular surface texture suggestive of a nonclassical aggregation-based growth mechanism. Another example of the importance of organics in the synthesis of high Mg-calcite was reported by Lenders et al. (2012). Using a mixed-solvent synthesis approach, the authors achieved a very high Mg-content in Mg-calcite (53 mol% Mg; basically a "protodolomite" phase). They showed that the formation of high Mg-calcite mesocrystal structures was achieved via the formation of Mg-ACC nanoparticles (some tenths of nm in size) in a non-aqueous solvent (Fig. 16). The Mg-ACC aggregates were subjected to an amorphous-to-crystalline transformation in the presence of water. As a result of this transformation, almond-like Mg-calcite structures made up of individual nanoparticles that diffracted electrons as a single crystal, but with a relatively high angular spreading (~16°), were obtained. Such features are consistent with those of a mesocrystal. Interestingly, some aggregates of ACC nanoparticles were observed (using TEM) attached to the mesocrystals, but not already integrated into the structure. These observations suggest that the formation of such mesocrystals likely took place via attachment of the amorphous nanoparticle precursors and fusion with the crystalline substrate, in agreement with the nonclassical growth model presented in Section 7.

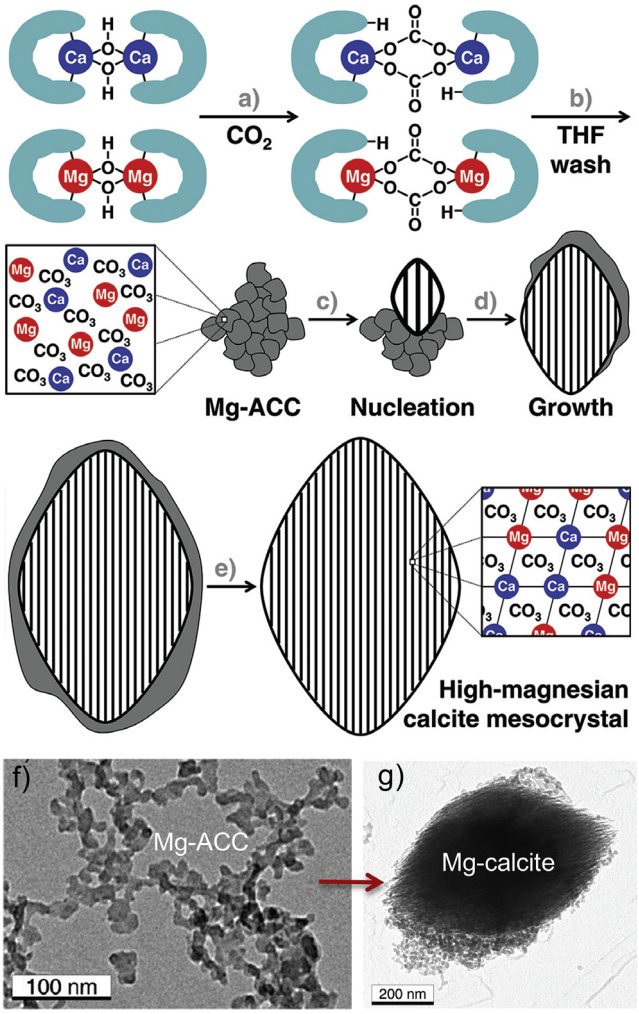

Fig. 16. Model for the formation of high Mg-calcite mesocrystals. a) Reaction of Ca and Mg in the organic solvent with CO_2 leading to the formation of a gel including $(CaCO_3)_2$ and $(MgCO_3)_2$ units and the protonated organic ligand LH. b) THF washing leads to the precipitation of aggregated Mg-ACC nanoparticles. c) Nucleation of high Mg-calcite from Mg-ACC preserving the Mg/Ca ratios present in the precuror. d) Growth by attachment of Mg–ACC nanoparticles onto the crystal surface and co-oriented crystallization into a fibrous substructure. e) Crystalline/amorphous core/shell intermediates precede the final crystalline high Mg-calcite. TEM images of precursor Mg-ACC (f) and Mg-calcite mesocrystal (g), still surrounded by (amorphous) nanoparticles. Reprinted with permission from Lenders et al. (2012). Copyright (2012) American Chemical Society.

8.5. Calcite

Calcitic structures are by far the most common and most thoroughly studied $CaCO_3$ materials formed via biomimetic precipitation routes (Gower, 2008; Meldrum and Cölfen, 2008). Despite extensive research, there are some key points about their formation mechanism(s) that still are not fully understood. Two of these key points are how the commonly reported nanogranular morphology of calcite biomimetic structures forms and what role liquid and/or amorphous precursor nanoparticles play in their growth. In their seminal *in situ* AFM study, Sethmann et al. (2005) showed that at a high supersaturation and in the presence of poly(aspartate), calcite growth progressed after the initial formation of a "gelatinous film" that subsequently transformed into an aggregate of nanometer sized clusters. Such clusters eventually evolved into triangular shaped nanosized structures. Long et al. (2013) observed similar nanostructural features using *in situ* AFM during calcite growth in the presence of PAA. Gower (2008) pointed out that the "gelatinous film" observed by Sethmann et al. (2005) likely was a PILP that transformed into ACC prior to the formation of crystalline $CaCO_3$. The same nanogranular morphologies were observed in the ossicles of sea urchins (Sethmann et al., 2005), in the spicules of calcareous sponges (Sethmann et al., 2006) (see Fig. 1c and d), and in the calcite prisms that form the prismatic layer in mollusk shells (Dauphin, 2002; Gilbert et al., 2011; Nudelman et al., 2007). These observations suggest that a nanocluster-mediated attachment (of liquid-like ACC nanoparticles) might be a general mechanism for $CaCO_3$ biomineralization. Indeed, the *ex situ* AFM analysis by Zhu et al. (2013) showed that the (10.4) faces of calcite formed in the presence of a polypeptide-based copolymer were made up of nanogranular aggregates (nanoparticle size ~100 nm) that somehow resembled the morphology and size of precursor ACC. Nonetheless, the authors concluded that the calcite structures formed via nanocrystal assembly (i.e., mesocrystallization). The latter study is representative of most published results on $CaCO_3$ mesocrystallization that generally neglect the possibility that ACC nanoparticles can directly attach on a crystalline substrate contributing to its growth. The exception is the seminal study by Song et al. (2009). The authors showed that calcite mesocrystals with octahedral forms or even with P-surfaces formed from a precursor ACC, which was assumed to be liquid-like. The surfaces of these calcite mesostructures were characterized by a distinctive nanogranular structure as shown by TEM and AFM analysis (nanoparticles with an average size of 100 nm) (see Fig. 9). Interestingly, the authors indicated that it was quite probable that OA of ACC nanoparticles onto the crystalline mesostructure took place during mesocrystal growth. However, no details on the actual mechanism of ACC attachment onto the calcite substrate via OA were presented. In line with the previous study, Schenk et al. (2012b) reported on the formation of calcite mesocrystals synthesized in the presence of PSS. Their study demonstrated that such mesocrystals displayed a hierarchical structure spanning from the nano- to the macro-scale. The smallest units were nanoparticles ~30 nm in size, arranged into larger, 100 nm layered nanostructures that, in turn, constituted the building-units of micrometer sized calcite crystals. Their x-ray diffraction analysis showed that the coherent size of calcite was ca. 155 nm, larger by a factor of five than the size of the smallest building units observed with SEM and AFM. The authors concluded that, likely, the smallest units were initially ACC that upon fusion and amorphous-to-crystalline transformation resulted

in the larger calcite domains. Remarkably, a simple molecule such as PSS was able to interact with the calcite structure at several levels, directing its self-assembly, and leading to its final hierarchy, being finally incorporated into the mesocrystal. All in all, the resulting structures displayed several key features that are common to calcite biominerals.

Calcite films have been produced by different routes, which typically involved the initial deposition of an amorphous precursor on a substrate (amorphous or crystalline) or on an organic template, including Langmuir monolayers, SAMs, or even polymer templates (Han et al., 2005; Xu et al., 1998). Kotachi et al. (2004) reported on the formation of films of calcite on a substrate in the presence of PAA. Such films displayed a lozenge-shape (i.e., parallelograms with edges at an angle of 104° or 120°) and were formed by oriented calcite nanocrystal units less than 100 nm in size. These results clearly show that the self-assembly of nanoparticles is at the core of calcite film formation mediated by organics (PAA). However, Kotachi et al. (2004) did not considered the possible formation of such structures via a liquid (Gower, 2008: Volkmer et al., 2005) or solid amorphous precursor (Rodriguez-Navarro et al., 2015b). Kim et al. (2007) reported on the deposition of calcite thin films on patterned SAMs via a PILP route. AFM analysis of the nanoscale features of the films showed a characteristic nanogranular texture consistent with their formation via the deposition of colloidal liquid (PILP) droplets (Fig. 17). Such nanodroplets coalesced to form an amorphous mineral film that subsequently transformed into calcite. The direct nucleation of an ACC phase onto the template was ruled out by performing an elegant experiment. The template was placed vertically in the growth solution and the thickness of the deposited $CaCO_3$ layer was measured using AFM. These measurements showed thicker deposits at the bottom than at the top part of the template, clearly demonstrating that nanoparticle precursors (which concentrated at the bottom of the crystallization dish due to gravity) were formed in solution prior to deposition. Remarkably, the nanogranular structure of the precursor colloidal phase was preserved upon the amorphous-to-crystalline transformation. This is consistent with a pseudomorphic transformation. However, it was not clear if the transformation took place via a solid-state mechanism or via a dissolution-precipitation process. In all these examples, film formation is closely related to and/or promoted by the presence of an organic additive, particularly synthetic organic polymers (as well as Mg ions) (Schenk et al., 2012a). Interestingly, *in vitro* calcite film formation is also induced by biomacromolecules extracted from living organisms (Belcher et al., 1996). Sugawara et al. (2006) reported that matrix peptides isolated from the exoskeleton of a crayfish induced the formation of thin films of oriented calcite. The authors proposed that ACC was stabilized by the peptide and then transformed into oriented calcite, which displayed a nanogranular structure. It is likely that such a nanogranular structure was inherited from the ACC nanoparticle precursor according to the ACC nanoparticle-mediated growth model discussed in Section 7.

Hybrid calcite-chitosan composites with superior mechanical properties (work of fracture) were obtained by Xiao and Yang (2011) using ACC nanoparticle precursors. The authors pointed out that the final nanogranular calcite crystals (nanogranules ~150 nm in size) embedded in the chitosan scaffold were not formed via the direct transformation of the initial hydrated ACC (with no short-or medium-range order). They indicated that hydrated ACC first transformed into anhydrous ACC with protocalcite structure and then, this transient phase, transformed into calcite. Such a sequence of phase transitions, fully consistent with the Ostwald's step rule (see Section 3), has been observed in some biominerals such as sea urchin spicules (Gong et al., 2012) or mollusk nacre (DeVol et al., 2015), as well as in additive-free abiotic systems (Rodriguez-Navarro et al., 2015b).

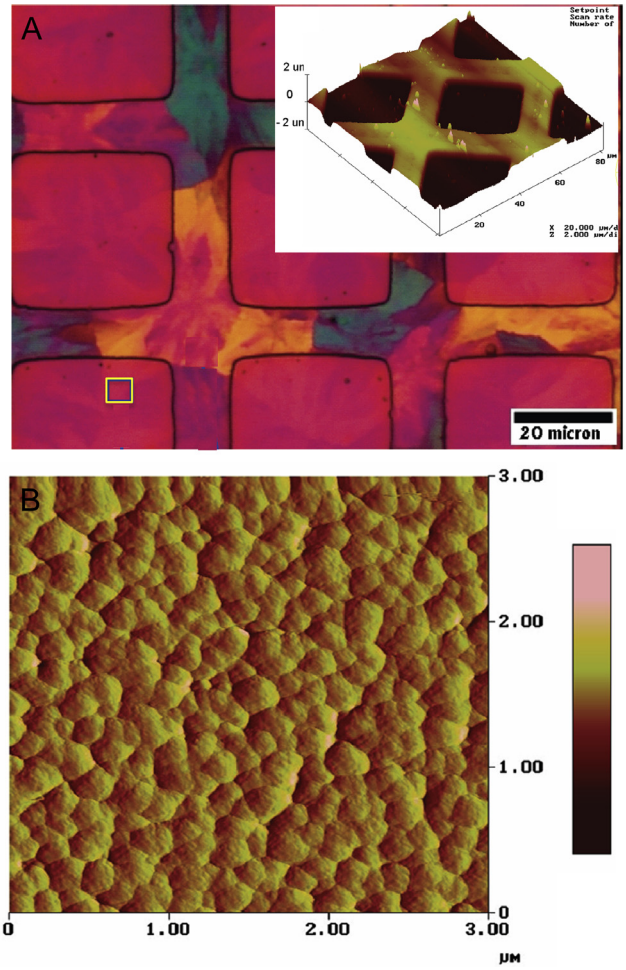

Fig. 17. Nanoscale features of a calcite thin film formed via the deposition of colloidal liquid (PILP) droplets onto a patterned SAM template. A) patterned SAM template covered by the calcite film. The inset shows the AFM image of the surface texture of the patterned template. B) AFM image of the nanogranular features of the calcite film (yellow squared area in (A)). Reprinted with permission from Kim et al. (2007). Copyright (2007) American Chemical Society.

Using the acid soluble organic matter (SOM) from the nacreous layer of *Pinctada margaritifera* pearl oyster shell, Tseng et al. (2014) were able to synthesize $CaCO_3$ layered structures (each layer about 200–400 nm in thickness) which were reminiscent of the nacre structure. Although they obtained calcite instead of aragonite, they observed that each layer was made up of an aggregate of nanoparticles (~20 nm is size) that diffracted as a single crystal. The authors proposed that the organics in SOM were able to stabilize precursor amorphous nanoparticles and induce their self-assembly into the observed 2D structures. This is consistent with the reported capacity of proteins extracted from nacre (n16.3) to organize or assemble calcium carbonate mineral clusters into single crystalline calcite (Perovic et al., 2014). Following an amorphous-to-crystalline transformation, organics were accumulated lining the nanoparticle building blocks, as shown by phase contrast imaging with AFM, a structural feature that was also observed in natural nacre (Fig. 18). Although the authors did not actually indentify ACC in their experiments, basically what they observed is a pseudomorphic ACC-to-crystalline replacement, similar to that reported by Harris et al. (2015). Harris et al. (2015) synthesized complex calcite spherulites displaying bent morphologies and crystal lattice tilting which formed from ACC via the PILP route. The authors concluded that the formation of ACC films could

explain these features. Such films underwent a pseudomorphic transformation into calcite thus resulting in the complex spherulitic structures (Fig. 7e). The structures displayed a nanogranular texture that demonstrated that growth took place via aggregation of the ACC precursor nanoparticles, followed by their pseudomorphic transformation into calcite. These results are consistent with those reported by Rodriguez-Navarro et al. (2015b) and the model presented in Section 7 (Rodriguez-Navarro et al., 2016). For such a pseudomorphic replacement to occur, the presence of organics is of paramount importance. First, organics accumulate around each nanoparticle due to a purification-though-crystallization process taking place during the ACC-to-crystalline conversion. Second, the organics prevent further classical ion-by-ion crystal growth, which otherwise would erase any nanogranular structure, as occurs in the ACC-to-calcite transformation in the absence of organics (Rodriguez-Navarro et al., 2016). Combined, the results of the previous studies strongly suggest that $CaCO_3$ biominerals and their biomimetcs, can develop via a nonclassical crystal growth process involving the attachment and self-assembly of ACC nanoparticles followed by their pseudomorphic transformation into crystalline $CaCO_3$ polymorph, these processes being controlled or mediated by organic (bio)macromolecules.

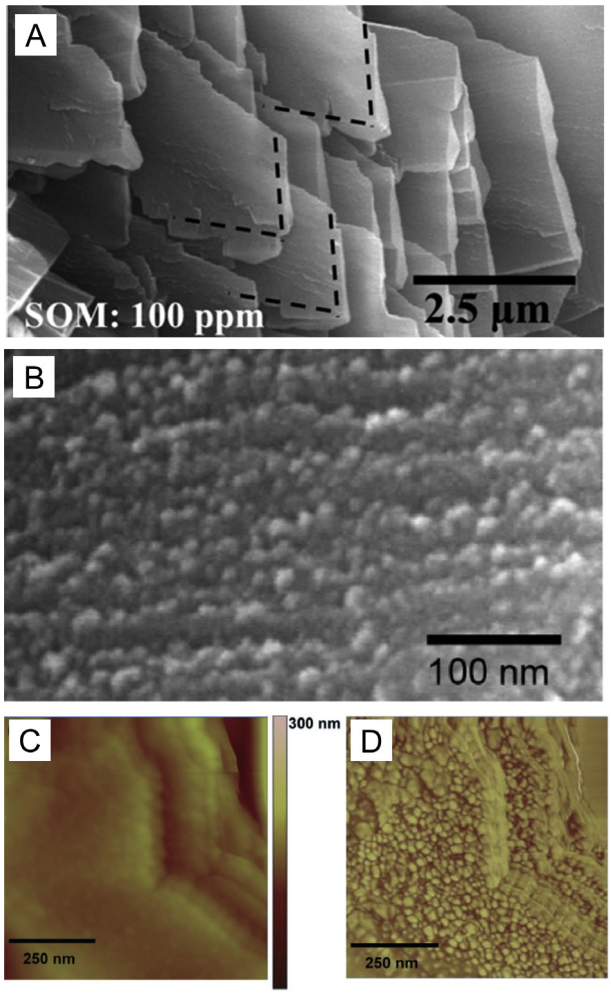

Fig. 18. Plate-like calcite structures formed after ACC in the presence of soluble organic matter (SOM) extracted from nacre. A) SEM image of the calcite structures; B) Detail of the nanogranules making up the structures depicted in (A); Topographic (C) and phase-contrast (D) AFM images of the surface of the calcite structures formed in the presence of 100 ppm SOM. Reprinted from Tseng et al. (2014), with permission from The Royal Society of Chemistry.

Trying to replicate the structure of nacre in the laboratory, Gong et al. (2010) used a PILP route and a block-copolymer and obtained a multilayer organic-inorganic composite that resembled biogenic nacre (Fig. 19). However, three key features of nacre could not be replicated: (i) the authors obtained calcite from ACC, but not aragonite; (2) the inorganic layer was not formed by the typical hexagonal platelets of crystalline $CaCO_3$ with 200–700 nm in thickness and some 1–5 mm in lateral dimensions: In contrast, a mosaic-like structure of shapeless and polydisperse calcite crystals – some of them with lateral dimensions over 100 μm – was obtained; (3) the preferred crystallographic orientation of nacre platelets (aragonite *c*-axis normal to the nacre layers) was not achieved: The XRD pattern of the multilayer was consistent with that of a powder, and the polarized optical microscopy image of the film showed different interference colors among individual crystals making the mosaic-like structure, features not consistent with a [001] preferred orientation. Interestingly, however, the AFM analysis of the PILP phase deposited underneath the block-copolymer layer revealed a nanogranular structure made up of an aggregate of nanoparticles 43 nm in size (i.e., precursor ACC nanoparticles). Finnemore et al. (2012) obtained $CaCO_3$-polymer (poly(acrylic acid) and poly(4-vinol pyridine)) layered structures that displayed the iridescence and toughness (indentation hardness) of natural nacre (Fig. 20). The authors claimed that theirs was the first successful attempt to replicate nacre using $CaCO_3$. However, the fact that their layered structure was made of calcite, rather than aragonite, leaves open the quest for the successful replication of nacre. Interestingly, Finnemore et al. (2012) reported that calcite in their nacre-like structures formed via an ACC precursor phase which left a nanogranular imprint. They also suggested that the preferred orientation of calcite crystals formed from ACC was transmitted across layers (epitaxy) due to the porous structure of the organic films deposited on each $CaCO_3$ layer.

Using a bio-inspired approach, Natalio et al. (2013) were able to synthesize calcite structures which replicated the morphology, size and crystal orientation of calcareous sponge spicules. Remarkably, these 1D biomimetic structures were formed via self-assembly of ACC nanoparticles that later on transformed into mesostructured calcite (with [100] orientation). It is unclear whether the vectorial alignment of ACC was due to OA associated with a calcite protostructure (Rodriguez-Navarro et al., 2015b) or was due to a possible directing role of the silicatein-α protein. The authors showed that these artificial spicules displayed extreme bending strength, surpassing that of natural calcite spicules.

9. Summary and implications in biomineralization

Here we have summarized a large body of experimental results obtained in the last decades that clearly indicates that the formation of biominerals and their biomimetic counterparts does not necessarily follow classical crystallization routes, and it may rather involve the formation of pre-nucleation ion associates and precursor (liquid and solid) amorphous phases as well as aggregation-based growth mechanisms. Such nonclassical processes can explain many of the features and superior properties of biominerals and their biomimetics. The formation of ion associates (PNCs) prior to the formation of solid or liquid precursor phases raises the possibility that the effects of organics (e.g., biomacromolecules) at modulating the growth of biominerals and their biomimetics may start earlier than thought. The presence of (bio)-macromolecules in the precipitation media inhibits nucleation in the classical sense and allows the formation of dense liquid precursor phases at higher driving forces for crystallization. These phases are critical for the mineralization process in biological systems, as their liquid like character allows molding of the final crystalline

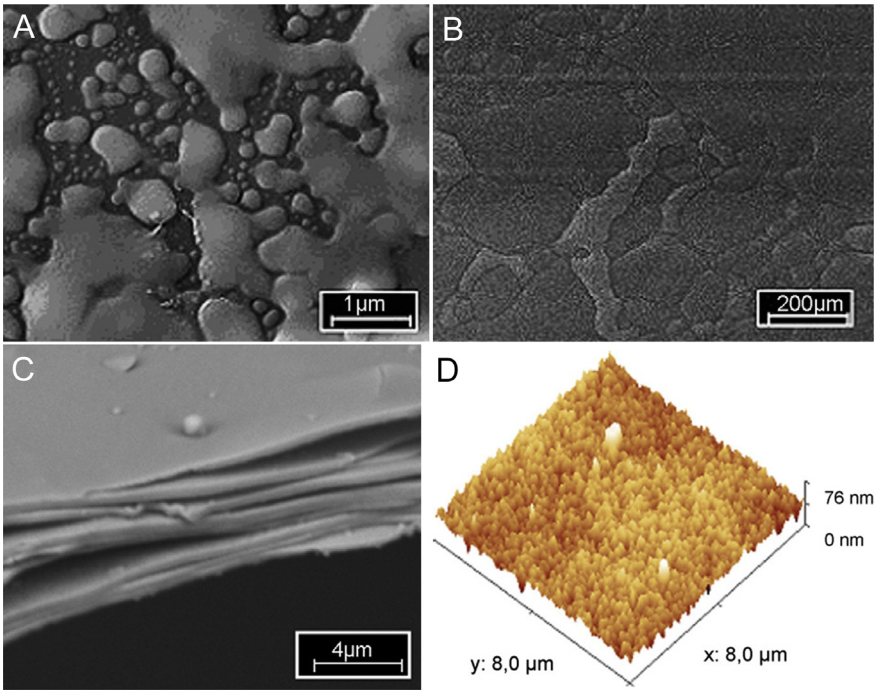

Fig. 19. Nacre-like layered calcite structure synthesized using a PILP route. A) PILP dropplets deposited on a substrate; B) calcite layer formed after the PILP; C) multilayered calcite resembling the structure of nacre; D) AFM image of the surface topography of the multilayer structure showing a nanogranular texture. Reprinted from Gong et al. (2010), with permission from Elsevier.

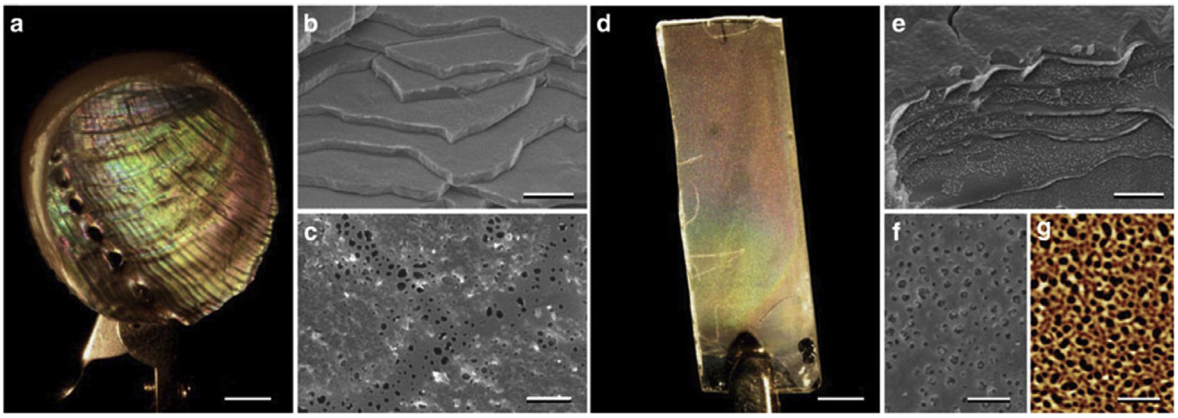

Fig. 20. Iridescence and structural features of natural nacre (a-c) and artificial calcitic nacre-like structure (d-f). Note the similarities in the layered structure (b and e) and the porous structure of the organic layer separating $CaCO_3$ platelets (c vs. f). A detail of the porous organic layer in the artificial nacre is shown by the AFM image in (g). Reprinted by permission from Macmillan Publishers LTD: Finnemore et al. (2012). Copyright (2012).

biominerals into non-equilibrium geometries via infiltration of the precursor condensed liquid phase within confined volumes and subsequent solidification into amorphous phases and pseudomorphic crystallization. This molding capacity is of great advantage for the mineralization of pre-formed biomimetic structures (e.g., using a colloidal crystal template). Additionally, recent experimental results indicate that crystalline materials may as well grow by non-classical mechanisms involving the incorporation of (amorphous) colloidal nanoparticles. This is of relevance for biomineralization processes, in which sequential mineral growth takes place as the organism develops, as well as in the synthesis of multilayered biomimetic materials.

The formation mechanisms described above commonly leave a characteristic nanotextural imprint in both biominerals and their biomimetics that has been studied with the aim of disclosing their origins and formation mechanisms. The frequently observed nanogranular morphology of calcitic, vateritic and aragonitic biominerals or $CaCO_3$-based biomimetic materials apparently results from growth involving amorphous (solid and/or liquid) nanoparticle attachment and restructuring. This nanotexture is typically preserved upon crystallization if organic molecules are present. Such a colloid-like growth mechanism allows a fast supply of material at the growth site, which leads to growth rates orders of magnitude higher than those achieved by classical ion-mediated growth, as it is typically observed in biominerals formed after ACC. It would be enlightening to experimentally prove, *in vivo*, whether or not the nonclassical growth mechanism above mentioned involving PILP phases and/or amorphous nanoparticles

actually operate during biomineral growth. This is a challenging task that, however, is not impossible considering the current development in analytical technologies for *in situ* analysis.

Future research should focus on the analysis of textural and structural features of biominerals and their biomimetics in other systems including phases such as calcium phosphates, calcium oxalates and iron oxides, in order to disclose if the nonclassical amorphous nanoparticle based growth mechanism reviewed here is also at work.

Further research is also necessary to shed light on the ultimate mechanism that leads to the preservation of the nanogranular features of biominerals and their biomimetics once the amorphous-to-crystalline conversion has taken place. Studies should also focus on disclosing how such a conversion preserving the nanogranular shape of the biominerals does not leaves a porous structure (as in mesocrystals) but rather typically results in space-filling materials.

Acknowledgements

CRN and ERA thank funding by the Spanish Government (Grants MAT2012-37584, CGL2012-35992 and CGL2015-70642-R) and the Junta de Andalucía (Research Group RNM-179 and Project P11-RNM-7550). E.R.-A. acknowledges a Ramón y Cajal grant. SEW is beholden to the German Research Foundation for generous financial support in the framework of an Emmy Noether starting grant (DFG, N° WO1712/3-1) and further gratefully acknowledges additional financial support by the Bavarian Research Alliance as well as by the Cluster of Excellence 315 'Engineering of Advanced Materials—Hierarchical Structure Formation for Functional Devices' funded by the German Research Foundation. JH is also beholden of the Cluster of Excellence 315.

References

Addadi, L., Raz, S., Weiner, S., 2003. Taking advantage of disorder: amorphous calcium carbonate and its roles in biomineralization. Adv. Mater. 15, 959–970.
Addadi, L., Joester, D., Nudelman, F., Weiner, S., 2006. Mollusk shell formation: a source of new concepts for understanding biomineralization processes. Chem. Eur. J. 12, 980–987.
Aizenberg, J., Fratzl, P., 2009. Biological and biomimetic materials. Adv. Mater. 21, 387–388.
Aizenberg, J., Black, A.J., Whitesides, G.M., 1999. Control of crystal nucleation by patterned self-assembled monolayers. Nature 398, 495–498.
Aizenberg, J., Tkashenko, A., Weiner, S., Addadi, L., Hendler, G., 2001. Calcitic microlenses as part of the photoreceptor system in brittlestars. Nature 412, 819–822.
Aizenberg, J., Muller, D.A., Grazul, J.L., Hamann, D.R., 2003. Direct fabrication of large micropatterned single crystals. Science 299, 1205–1208.
Al-Sawalmih, A., Li, C., Siegel, S., Fratzl, P., Paris, O., 2009. On the stability of amorphous minerals in lobster cuticule. Adv. Mater. 21, 4011–4015.
Amos, F.F., Sharbaugh, D.M., Talham, D.R., Gower, L.B., 2007. Formation of single-crystalline aragonite tablets/films via an amorphous precursor. Langmuir 23, 1988–1994.
Anand, U., Lu, J., Loh, D., Aabdin, Z., Mirsaidov, U., 2015. Hydration layer-mediated pairwise interaction of nanoparticles. Nano Lett. 16, 786–790.
Andreassen, J.P., 2005. Formation mechanism and morphology in precipitation of vaterite - nano aggregation or crystal growth? J. Cryst. Growth 274, 256–264.
Arakaki, A., Shimizu, K., Oda, M., Sakamoto, T., Nishimura, T., Kato, T., 2015. Biomineralization-inspired synthesis of functional organic/inorganic hybrid materials: organic molecular control of self-organization of hybrids. Org. Biomol. Chem. 13, 974–989.
Aziz, B., Gebauer, D., Hedin, N., 2011. Kinetic control of particle-mediated calcium carbonate crystallization. CrystEngComm 13, 4641–4645.
Baumgartner, J., Dey, A., Bomans, P.H.H., Le Coadou, C., Fratzl, P., Sommerdijk, N.A.J. M., Faivre, D., 2013. Nucleation and growth of magnetite from solution. Nat. Mater. 12, 310–314.
Becker, R., Doring, W., 1935. Kinetische Behandlung der Keimbildung in übersättigen Dämpfen. Ann. Phys. 24, 719–752.
Belcher, A.M., Wu, X.H., Christensen, R.J., Hansma, P.K., Stucky, G.D., Morse, D.E., 1996. Control of crystal phase switching and orientation by soluble mollusc-shell proteins. Nature 381, 56–58.
Beniash, E., Aizemberg, J., Addadi, L., Weiner, S., 1997. Amorphous calcium carbonate transforms into calcite during sea urchin larval spicule growth. Proc. R. Soc. London, Ser. B 264, 461–463.
Beniash, E., Metzler, R.A., Lam, R.S.K., Gilbert, P.U.P.A., 2009. Transient amorphous calcium phosphate in forming enamel. J. Struct. Biol. 166, 133–143.
Berg, J.K., Jordan, T., Binder, Y., Boerner, H.G., Gebauer, D., 2013. Mg^{2+} tunes the wettability of liquid precursors of $CaCO_3$: towards controlling mineralization sites in hybrid materials. J. Am. Chem. Soc.
Bergström, L., Sturm, E.V., Salazar-Alvarez, G., Cölfen, H., 2015. Mesocrystals in biominerals and colloidal arrays. Acc. Chem. Res. 48, 1391–1402.
Bewernitz, M.A., Gebauer, D., Long, J., Cölfen, H., Gower, L.B., 2012. A metastable precursor phase of calcium carbonate and its interactions with polyaspartate. Faraday Discuss. 199, 291–312.
Böhm, C.F. et al., 2016. Structural commonalities and deviations in the hierarchical organization of crossed-lamellar shells: a case study on the shell of the bivalve *Glycymeris glycymeris*. J. Mater. Res. accepted.
Bonderer, L.J., Studart, A.R., Guackler, L.J., 2008. Bioinspired design and assembly of platelet reinforced polymer films. Science 319, 1069–1073.
Bungenberg de Jong, H.G., 1949. Complex colloid systems. In: Kruyt, H. (Ed.), Colloid Science, vol. II. Elsevier, Amsterdam, pp. 335–432.
Burton, W.K., Cabrera, N., Frank, F.C., 1951. The growth of crystals and the equilibrium structure of their surfaces. Philos. Trans. R. Soc. London, A 243, 299–358.
Cantaert, B., Kim, Y.-Y., Ludwig, H., Nudelman, F., Sommerdijk, N.A.J.M., Meldrum, F. C., 2012. Think positive: phase separation enables a positively charged additive to induce dramatic changes in calcium carbonate morphology. Adv. Funct. Mater. 22, 907–915.
Cantaert, B., Verch, A., Kim, Y.-Y., Ludwig, H., Paunov, V.N., Kröger, R., Meldrum, F.C., 2013. Formation and structure of calcium carbonate thin films and nano fibers precipitated in the presence of poly(allylamine hydrochloride) and magnesium ions. Chem. Mater. 25, 4994–5003.
Cardew, P.T., Davey, R.J., 1985. The kinetics of solvent-mediated phase transitions. Proc. R. Soc. London, Ser. A 398, 415–428.
Cartwright, J.H.E., Checa, A.G., Gale, J.D., Gebauer, D., Sainz-Diaz, C.I., 2012. Calcium carbonate polyamorphism and its role in biomineralization: how many amorphous calcium carbonates are there. Angew. Chem. Int. Ed. 51, 11960–11970.
Casey, W.H., 1988. Entropy production and the Ostwald step rule. J. Phys. Chem. 92, 226–227.
Checa, A.G., Cartwright, J.H.E., Willinger, M.G., 2011. Mineral bridges in nacre. J. Struct. Biol. 176, 330–339.
Cheng, X., Vorona, P.L., Olszta, M.J., Gower, L.B., 2007. Biomimetic synthesis of calcite films by a polymer-induced liquid-precursor (PILP) process 1. Influence and incorporation of magnesium. J. Cryst. Growth 307, 395–404.
Chernov, A.A., 1984. Modern Crystallography III, Crystal Growth. Springer, Berlin.
Cölfen, H., Antonietti, M., 2005. Mesocrystals: inorganic superstructures made by highly parallel crystallization and controlled alignment. Angew. Chem. Int. Ed. 44, 5576–5591.
Cölfen, H., Antonietti, M., 2008. Mesocrystals and Nonclassical Crystallization. Wiley, San Francisco, CA.
Cölfen, H., Mann, S., 2003. Higher-order organization by mesoscale self-assembly and transformation of hybrid nanostructures. Angew. Chem. Int. Ed. 42, 350–2365.
Cölfen, H., Yu, S.-H., 2005. Biomimetic mineralization/synthesis of mesoscale order in hybrid inorganic-organic materials via nanoparticle self-assembly. MRS Bull. 30, 727–735.
Cuif, J.-P., Dauphin, Y., Sorauf, J.E., 2011. Biominerals and Fossils Through Time. Cambridge University Press, Cambridge.
Dai, L., Cheng, X., Gower, L.B., 2008. Transition bars during transformation of an amorphous calcium carbonate precursor. Chem. Mater. 20, 6917–6928.
Dauphin, Y., 2001. Nanostructures de la nacre des tests de cephalopodes actuels. Paläontol. Z. 75, 113–122.
Dauphin, Y., 2002. Comparison of the soluble matrices of the calcitic prismatic layer of *Pinna nobilis* (Mollusca, Bivalvia, Pteriomorpha). Comp. Biochem. Physiol. A 132, 577–590.
Dauphin, Y., 2008. The nanostructural unity of Mollusk shells. Miner. Mag. 72, 243–246.
De Yoreo, J.J., Zepeda-Ruiz, L.A., Friddle, R.W., Qui, S.R., Wasylenki, L.E., Chernov, A. A., Gilmer, G.H., Dove, P.M., 2009. Rethinking classical crystal growth models through molecular scale insights: consequences of kink-limited kinetics. Cryst. Growth Des. 9. 5135-3144.
De Yoreo, J.J., Gilbert, P.U.P.A., Sommerdijk, N.A.J.M., Penn, R.L., Whitelam, S., Joester, D., Zhang, H., Rimer, J.D., Navrotsky, A., Banfield, J.F., Wallace, A.F., Michel, F.M., Meldrum, F.C., Cölfen, H., Dove, P.M., 2015. Crystallization by particle attachment in synthetic, biogenic and geologic environments. Science 349. aaa6760-1.
Demichelis, R., Raiteri, P., Gale, J.D., Quigley, D., Gebauer, D., 2011. Stable prenucleation mineral clusters are liquid-like ionic polymers. Nat. Commun. 2, 590.
DeVol, R.T., Sun, C.-Y., Marcus, M.A., Coppersmith, S.N., Myneni, S.C.B., Gilbert, P.U.P. A., 2015. Nanoscale transforming mineral phases in fresh nacre. J. Am. Chem. Soc. 137, 13325–13333.
Dey, A., Bomans, P.H.H., Muller, F.A., Frederik, P.M., de With, G., Sommerdijk, N.A.J. M., 2010. The role of prenucleation clusters in surface-induced calcium phosphate crystallization. Nat. Mater. 9, 1010–1014.
Dillmann, A., Meier, G.E.A., 1989. Homogeneous nucleation of supersaturated vapors. Chem. Phys. Lett. 160, 71–74.
Dillmann, A., Meier, G.E.A., 1991. A refined droplet approach to the problem of homogeneous nucleation from the vapor phase. J. Chem. Phys. 94, 3872.

Dorvee, J.R., Veis, A., 2013. Water in the formation of biogenic minerals: peeling away the hydration layers. J. Struct. Biol. 183, 278–303.
Dove, P.M., Craven, C.M., 2005. Surface charge density on silica in alkali and alkaline earth chloride electrolyte solutions. Geochim. Cosmochim. Acta 69, 4963–4970.
Eanes, E.D., Gillessen, I.H., Posner, A.S., 1965. Intermediate states in the precipitation of hydroxyapatite. Nature 208, 365–367.
Ehrlich, H., Koutsoukos, P.G., Demadis, K.D., Pokrovsky, O.S., 2009. Principles of demineralization: modern strategies for the isolation of organic frameworks: Part II. Decalcification. Micron 40, 169–193.
Faatz, M., Gröhn, F., Wegner, G., 2004. Amorphous calcium carbonate: synthesis and potential intermediate in biomineralization. Adv. Mater. 16, 996–1000.
Faivre, D., Schüler, D., 2008. Magnetotactic bacteria and magnetosomes. Chem. Rev. 108, 4875–4898.
Falini, G., Albeck, S., Weiner, S., Addadi, L., 1996. Control of aragonite and calcite polymorphism by mollusk shell macromolecules. Science 271, 67–69.
Finnemore, A.S., Scherer, M.R.J., Langford, R., Mahajan, S., Ludwigs, S., Meldrum, F.C., Steiner, U., 2009. Nanostructured calcite single crystals with gyroid morphologies. Adv. Mater. 21, 3928–3932.
Finnemore, A., Cunha, P., Shean, T., Vignolini, S., Guldin, S., Oyen, M., Steiner, U., 2012. Biomimetic layer-by-layer assembly of artificial nacre. Nat. Commun. 3, 966.
Ford, I.J., Laaksonen, A., Kulmala, M., 1993. Modification of the Dillmann-Meier theory of homogeneous nucleation. J. Chem. Phys. 99, 764.
Frank, F.C., 1949. The influence of dislocations on crystal growth. Discuss. Faraday Soc. 5, 48–54.
Frenkel, D., 2015. Order through entropy. Nat. Mater. 14, 9–12.
Gal, A., Weiner, S., Addadi, L., 2010. The stabilizing effect of silicate on biogenic and synthetic amorphous calcium carbonate. J. Am. Chem. Soc. 132, 13208–13211.
Gal, A., Habraken, W., Gur, D., Fratzl, P., Weiner, S., Addadi, L., 2013. Calcite crystal growth by a solid-state transformation of stabilized amorphous calcium carbonate nanospheres in a hydrogel. Angew. Chem. Int. Ed. 52, 4867–4870.
Gal, A., Kahil, K., Vidavsky, N., DeVol, R.T., Gilbert, P.U.P.A., Fratzl, P., Weiner, S., Addadi, L., 2014. Particle accretion mechanism underlies biological crystal growth from an amorphous precursor phase. Adv. Funct. Mater. 24, 5420–5426.
Gal, A., Weiner, S., Addadi, L., 2015. A perspective on underlaying crystal growth mechanisms in biomineralization: solution mediated growth versus nanosphere particle accretion. CrystEngComm 17, 2606–2615.
Gal, A., Wirth, R., Kopka, J., Fratzl, P., Faivre, D., Scheffel, A., 2016. Macromolecular recognition directs calcium ions to coccolith mineralization sites. Science 353, 590–593.
García-Ruiz, J.M., 2003. Nucleation of protein crystals. J. Struct. Biol. 142, 22–31.
Gebauer, D., Cölfen, H., 2011. Prenucleation clusters and non-classical nucleation. Nanotoday 6, 564–584.
Gebauer, D., Völkel, A., Cölfen, H., 2008. Stable prenucleation clusters. Science 322, 1819–1822.
Gebauer, D., Cölfen, H., Verch, A., Antonietti, M., 2009. The multiple roles of additives in $CaCO_3$ crystallization: a quantitative case study. Adv. Mater. 21, 435–439.
Gebauer, D., Gunawidjaja, P.N., Ko, J.Y.P., Bacsik, Z., Aziz, B., Liu, L., Hu, Y., Bergström, L., Tai, C.-W., Edán, M., Hedin, N., 2010. Proto-calcite and proto-vaterite in amorphous calcium carbonate. Angew. Chem. Int. Ed. 49, 8889–8891.
Gebauer, D., Kellermeier, M., Gale, J.D., Bergström, L., Cölfen, H., 2014. Pre-nucleation clusters as solute precursors in crystallization. Chem. Soc. Rev. 43, 2348–2371.
Gehrke, N., Cölfen, H., Pinna, N., Antonietti, M., Nassif, N., 2005a. Superstructures of calcium carbonate crystals by oriented attachment. Cryst. Growth Des. 5, 1317–1319.
Gehrke, N., Nassif, N., Pinna, N., Antonietti, M., Gupta, H.S., Cölfen, H., 2005b. Retrosynthesis of nacre via amorphous precursor particles. Chem. Mater. 17, 6514–6516.
Gibbs, J.W., 1876. On the equilibrium of heterogeneous substances (first part). Trans. Connect. Acad. Arts Sci. 3, 108–248.
Gibbs, J.W., 1878. On the equilibrium of heterogeneous substances (concluded). Trans. Connect. Acad. Arts Sci. 16, 343–524.
Gilbert, P.U.P.A., Young, A., Coppersmith, S.N., 2011. Measurement of c-axis angular orientation in calcite ($CaCO_3$) nanocrystals using X-ray absorption spectroscopy. Proc. Natl. Acad. Sci. U.S.A. 108, 11350–11355.
Giuffre, A.J., Gagnon, A.C., De Yoreo, J.J., Dove, P.M., 2015. Isotopic evidence for the amorphous calcium carbonate to calcite transformation by dissolution-reprecipitation. Geochim. Cosmochim. Acta 165, 407–417.
Gómez-Morales, J., Falini, G., García-Ruiz, J.M., 2015. Biological crystalization. In: Nishinaga, T. (Ed.), Handbook of crystal growth, vol. 1. Elsevier, New York, pp. 873–913.
Gong, H., Pluntke, M., Marti, O., Walther, P., Gower, L., Cölfen, H., Volkmer, D., 2010. Multilayer $CaCO_3$/block-copolymer materials via amorphous precursor to crystal formation. Colloids Surf., A: Physicochem. Eng. Aspects 354, 279–283.
Gong, Y.U.T., Killian, C.E., Olson, I.C., Appathurai, N.P., Amasino, A.L., Martin, M.C., Holt, L.J., Wilt, F.H., Gilbert, P.U.P.A., 2012. Phase transitions in biogenic amorphous calcium carbonate. Proc. Natl. Acad. Sci. U.S.A. 109, 6088–6093.
Gower, L.B., 2008. Biomimetic model systems for investigating the amorphous precursor pathway and its role in biomineralization. Chem. Rev. 108, 4551–4627.
Gower, L.B., Odom, D.J., 2000. Deposition of calcium carbonate films by a polymer-induced liquid-precursor (PILP) process. J. Cryst. Growth 210, 719–734.
Gower, L.B., Tirrell, D.A., 1998. Calcium carbonate films and helices grown in solutions of poly(aspartate). J. Cryst. Growth 191, 153–160.
Gries, K.I., Heinemann, F., Rosenauer, A., Fritz, M., 2012. In vitro growth of flat aragonite crystals between the layers of the insoluble organic matrix of the abalone *Haliotis laevigata*. J. Cryst. Growth 358, 75–80.
Grunenfelder, L.K., Herrera, S., Kisailus, D., 2014. Crustacean-derived biomimetic components and nanostructured composites. Small 16, 3207–3232.
Gupta, A., Bohidar, H., 2005. Kinetics of phase separation in systems exhibiting simple coacervation. Phys. Rev. E 72, 011507.
Habraken, W.J.E.M., Tao, J., Brylka, L.J., Freidrich, H., Bertinetti, L., Schenk, A.S., Verch, A., Dmitrovic, V., Bomans, P.H.H., Frederik, P.M., Laven, J., van der Schoot, P., Aichmayer, B., de With, G., De Yoreo, J.J., Sommerdijk, N.A.J.M., 2013. Ion-association complexes unite classical and non-classical theories for the biomimetic nucleation of calcium phosphate. Nat. Commun. 4, 1507.
Han, J.T., Xu, X., Kim, D.H., Cho, K., 2005. Mosaic, single-crystal $CaCO_3$ thin films fabricated on modified polymer templates. Adv. Funct. Mater. 15, 475–480.
Harding, J.H., Freeman, C.L., Duffy, D.M., 2014. Oriented crystal growth on organic monolayers. CrystEngComm 16, 1430–1438.
Harris, J., Mey, I., Hajir, M., Mondeshki, M., Wolf, S.E., 2015. Pseudomorphic transformation of amorphous calcium carbonate films follows spherulitic growth mechanisms and can give rise to crystal lattice tilting. CrystEngComm 17, 6831–6837.
Hayashi, A., Nakamura, T., Watanabe, T., 2010. Fabrication of a nacre-like aragonite/PAA multilayer film on a nacre substrate. Cryst. Growth Des. 10, 5085–5091.
Hendley IV, C.T., Tao, J., Kunitake, J.A.M.R., De Yoreo, J.J., Estroff, L.A., 2015. Microscopy techniques for investigating the control of organic constituents on biomineralization. MRS Bull. 40. 480-480.
Homeijer, S.J., Barrett, R.A., Gower, L.B., 2010. Polymer-induced liquid-precursor (PILP) process in the non-calcium based systems of barium and strontium carbonate. Cryst. Growth Des. 10, 1040–1052.
Hu, Q., Zhang, A., Teng, H., Becker, U., 2012. Growth process and crystallographic properties of ammonia-induced vaterite. Am. Miner. 97, 1437–1445.
Huang, S.-C., Minami, T., Naka, K., Chujo, Y., 2014. Fabrication of amorphous calcium carbonate composite particles-polymer multilayer films by a layer-by-layer method. Polym. Compos., 1–6
Ihli, J., Wong, W.C., Noel, E.H., Kim, Y.-Y., Kulak, A.N., Christenson, H.K., Duer, M.J., Meldrum, F.C., 2014. Dehydration and crystallization of amorphous calcium carbonate in solution and in air. Nat. Commun. 5, 3169.
Imada, H., Kimura, K., Onishi, H., 2013. Water and 2-propanol structured on calcite (104) probed by frequency-modulation atomic force microscopy. Langmuir 29, 10744–10751.
Imai, H., Oaki, Y., Kotachi, A., 2006. A biomimetic approach for hierarchically structured inorganic crystals through self- organization. Bull. Chem. Soc. Jpn. 79, 1834–1851.
Imai, H., Tochimoto, N., Nishino, Y., Takezawa, Y., Imai, Y., 2012. Oriented nanocrystal mosaic in monodispersed $CaCO_3$ microspheres with functional organic molecules. Cryst. Growth Des. 12, 876–882.
Ivanov, V.K., Fedorov, P.P., Beranchikov, A.Y., Osiko, V.V., 2014. Oriented attachment of particles: 100 years of investigations of non-classical crystal growth. Russ. Chem. Rev. 83, 1204–1222.
Jiang, Y., Gower, L.B., Volkmer, D., Cölfen, H., 2011. Hierarchical DL-glutamic acid microspheres from polymer-induced liquid precursors. Cryst. Growth Des. 11, 3243–3249.
Jiang, Y., Gower, L., Volkmer, D., Cölfen, H., 2012. The existence region and composition of a polymer-induced liquid precursor phase for DL-glutamic acid crystals. Phys. Chem. Chem. Phys. 14, 914–919.
Jun, J.M.V., Altoe, M.V.P., Aloni, S., Zuckermann, R.N., 2015. Peptoid nanosheets as soluble, two-dimensional templates for calcium carbonate mineralization. Chem. Commun. 51, 10218–19221.
Kabalah-Amitai, L., Mayzel, B., Kauffmann, Y., Fitch, A.N., Bloch, L., Gilbert, P.U.P.A., Pokroy, B., 2013. Vaterite crystals contain two interspersed crystal structures. Science 340, 454–457.
Kaempfe, P., Lauth, V.R., Halfer, T., Treccani, L., Maas, M., Rezwan, K., 2013. Micromolding of calcium carbonate using bio-inspired, coacervation-mediated process. J. Am. Ceram. Soc. 96, 736–742.
Kajiyama, S., Nishimura, T., Sakamoto, T., Kato, T., 2014. Aragonite nanorods in calcium carbonate/polymer hybrids formed through self-organization process from amorphous calcium carbonate solution. Small 10, 1634–1641.
Keislich, G., Kumagai, S., Butler, K.T., Okamura, T., Hendon, C.H., Sun, S., Yamashita, M., Walsh, A., Cheetham, A.K., 2015. Role of entropic effects in controlling the polymorphism in formate ABX_3 metal-organic frameworks. Chem. Comm. 51, 15538–15541.
Killian, C.E., Metzler, R.A., Gong, Y.U.T., Olson, I.C., Aizenberg, J., Politi, Y., Wilt, F.H., Scholl, A., Young, A., Doran, A., Kunz, M., Tamura, N., Coppersmith, S.N., Gilbert, P.U.P.A., 2009. Mechanism of calcite co-orientation in the sea urchin tooth. J. Am. Chem. Soc. 131, 18404–18409.
Kim, Y.-Y., Douglas, E.P., Gower, L.B., 2007. Patterning inorganic ($CaCO_3$) thin films via a polymer-induced liquid-precursor process. Langmuir 23, 4862–4870.
Kim, Y.-Y., Hetherington, N.B.J., Noel, E.H., Kröger, R., Charnock, J.M., Christenson, H. K., Meldrum, F.C., 2011. Capillarity creates single-crystal calcite nanowires from amorphous calcium carbonate. Angew. Chem. Int. Ed. 50, 12572–12577.
Kim, Y.-Y., Schenk, A.S., Ihli, J., Kulak, A.N., Hetherington, N.B.J., Tang, C.C., Schmahl, W.W., Griesshaber, E., Hyett, G., Meldrum, F.C., 2014. A critical analysis of calcium carbonate mesocrystals. Nat. Commun. 5, 4341.
Kobayashi, K., Oyabu, N., Kimura, K., Ido, S., Suzuki, K., Imai, T., Tagami, K., Tsukada, M., Yamada, H., 2013. Visualization of hydration layers on muscovite mica in aqueous solution by frequency-modulation atomic force microscopy. J. Chem. Phys. 138, 184704.

Kossel, W., 1927. Zur Theorie des Kristallwachstums. Nachr. Gesellschaft Wiss. Göttingen. Math. Phys. Klasse, 135–143.
Kotachi, A., Miura, T., Imai, H., 2004. Morphological evaluation and film formation with iso-oriented calcite crystals using binary poly(acrylic acid). Chem. Mater. 16, 3191–3196.
Kulak, A.N., Iddon, P., Li, Y., Armes, S.P., Cölfen, H., Paris, O., Wilson, R.M., Meldrum, F.C., 2007. Continuous structural evolution of calcium carbonate particles: a unifying model of copolymer-mediated crystallization. J. Am. Chem. Soc. 129, 3729–3736.
Kumar, M., Luo, H., Román-Leshkov, Y., Rimer, J.D., 2015. SSZ-13 crystallization by particle attachment and deterministic pathways to crystal size control. J. Am. Chem. Soc. 137, 13007–13017.
LaMer, V.K., Dinegar, R.H., 1950. Theory, production and mechanism of formation of monodispersed hydrosols. J. Am. Chem. Soc. 72, 4847–4854.
Lee, K., Wagermaier, W., Masic, A., Kommareddy, K.P., Bennet, M., Manjubala, I., Lee, S.-W., Parl, S.B., Cölfen, H., Fratzl, P., 2012. Self-assembly of amorphous calcium carbonate microlens arrays. Nat. Commun. 3, 725.
Lenders, J.J., Dey, A., Bomans, P.H.H., Spielmann, J., Hendrix, M.M.R.M., de With, G., Meldrum, F.G., Harder, S., Sommerdijk, N.A.J.M., 2012. High-magnesian calcite mesocrystals: a coordination chemistry approach. J. Am. Chem. Soc. 134, 1367–1373.
Levi-Kalisman, Y., Raz, S., Weiner, S., Addadi, L., Sagi, I., 2002. Structural differences between biogenic amorphous calcium carbonate phases using x-ray absorption spectroscopy. Adv. Funct. Mater. 12, 43–48.
Li, C., Qi, L., 2008. Bioinspired fabrication of 3D ordered macroporous single crystals of calcite from a transient amorphous phase. Angew. Chem. Int. Ed. 47, 2388–2393.
Li, X.Q., Zeng, H.C., 2012. Calcium carbonate nanotablets: bridging artificial to natural nacre. Adv. Mater. 24, 6277–6282.
Li, X., Xu, Z.-H., Wang, R., 2006. In situ observation of nanograin rotation and deformation in nacre. Nanoletters 6, 2301–2304.
Li, D., Nielsen, M.H., Lee, J.R.I., Frandsen, C., Banfield, J.F., De Yoreo, J.J., 2012. Direction-specific interactions control crystal growth by oriented attachment. Science 336, 1014–1018.
Li, L., Kolle, S., Weaver, J.C., Ortiz, C., Aizenberg, J., Kolle, M., 2015. A highly conspicuous mineralized composite photonic architecture in the translucent shell of the blue-rayed limpet. Nat. Commun. 6, 6322.
Li, C., Hong, G., Yu, H., Qi, L., 2010. Facile fabrication of honeycomb-patterned thin films of amorphous calcium carbonate and mosaic calcite. Chem. Mater. 22, 3206–3211.
Lin, C.J., Yang, S.-Y., Huang, S.-J., Jerry, C.C., Chan, J.C.C., 2015. Structural characterization of Mg-stabilized amorphous calcium carbonate by Mg-25 solid-state NMR spectroscopy. J. Phys. Chem. C 119, 7225–7233.
Liu, K., Jiang, L., 2011. Bio-inspired design of multiscale structures for function integration. Nanotoday 6, 155–175.
Long, X., Ma, Y., Qi, L., 2011. In vitro synthesis of high Mg calcite under ambient conditions and its implication for biomineralization process. Cryst. Growth Des. 11, 2866–2873.
Long, X., Ma, Y., Cho, K.R., Li, D., De Yoreo, J.J., Qi, L., 2013. Oriented calcite micropillars and prisms formed through segregation and recrystallization of poly(acrylic acid) stabilized nanoparticles. Cryst. Growth Des. 13, 3856–3863.
Long, X., Ma, Y., Qi, L., 2014. Biogenic and synthetic high magnesium calcite - A review. J. Struc. Biol. 185, 1–14.
Lowenstam, H.A., Weiner, S., 1985. Transformation of amorphous calcium phosphate to crystalline dahillite in the radular teeth of chitons. Science 227, 51–53.
Lowenstam, H.A., Weiner, S., 1989. On Biomineralization. Oxford University Press, New York.
Lupulescu, A.I., Rimer, J.D., 2014. In situ imaging of silicalite-1 surface growth reveals the mechanism of crystallisation. Science 344, 729–732.
Ma, Y., Mehltretter, G., Plüg, C., Rademacher, N., Schmidt, M.U., Cölfen, H., 2009. PY181 pigment microspheres of nanoplates synthesized via polymer-induced liquid precursors. Adv. Funct. Mater. 19, 2095–2101.
Mahamid, J., Sharir, A., Addadi, L., Weiner, S., 2008. Amorphous calcium phosphate is a major component of the forming fin bones of zebrafish: indications for an amorphous precursor phase. Proc. Natl. Acad. Sci. U.S.A. 105, 12748–12753.
Mann, S., 2001. Biomineralization, Principles. Oxford University Press, Oxford, Concepts in Bioinorganic Materials Chemistry.
Marcus, Y., 2009. Effect of ions on the structure of water: structure making and breaking. Chem. Rev. 109, 1346–1370.
Maruyama, K., Yoshino, T., Kagi, H., 2011. Synthesizing a composite material of amorphous calcium carbonate and aspartic acid. Mater. Lett. 65, 179–181.
McHale, J.M., Aubux, A., Perrotta, A.J., Navrotsky, A., 1997. Surface energies and thermodynamic phase stability in nanocrystalline aluminas. Science 277, 788–791.
Meldrum, F.C., Cölfen, H., 2008. Controlling mineral morphologies and structures in biological and synthetic systems. Chem. Rev. 108, 4332–4432.
Metzler, R.A., Evans, J.S., Killian, C.E., Zhou, D., Churchill, T.H., Appathurai, N.P., Coppersmith, S.N., Gilbert, P.U.P.A., 2010. Nacre protein fragment templates lamellar aragonite growth. J. Am. Chem. Soc. 132, 6329–6334.
Miyajima, R., Oaki, Y., Kogure, T., Imai, H., 2015. Variation in mesoscopic textures of biogenic and biomimetic calcite crystals. Cryst. Growth Des. 15, 3755–3761.
Morse, J.W., Arvidson, R.S., Lüttge, A., 2007. Calcium carbonate formation and dissolution. Chem. Rev. 107, 342–381.
Moureaux, C., Perez-Huerta, A., Compere, P., Zhu, W., Leloup, T., Cusak, M., Dubois, P., 2010. Structure, composition and mechanical relations to function in sea urchin spine. J. Struct. Biol. 170, 41–49.
Mullin, J.W., 2001. Crystallization. Butterworth, Oxford.
Munch, E., Launey, M.E., Alsem, D.H., Saiz, E., Tomsia, A.P., Ritchie, R.O., 2008. Tough, bio-inspired hybrid materials. Science 322, 1516–1520.
Munro, N.H., McGrath, K.M., 2012. Biomimetic approach to forming chitin/aragonite composites. Chem. Commun. 48, 4716–4718.
Myerson, A.S., 2002. Handbook of Industrial Crystallization. Butterworth, Boston.
Natalio, F., Corrales, T.P., Panthöfer, M., Schollmeyer, D., Lieberwirth, I., Müller, W.E. G., Kappl, M., Butt, H.-J., Tremel, W., 2013. Flexible minerals: self-assembled spicules with extreme bending strength. Science 339, 1298–1302.
Navrotsky, A., 2004. Energetic clues to pathways to biomineralization: precursors, clusters, and nanoparticles. Proc. Natl. Acad. Sci. U.S.A. 101, 12096–12101.
Niederberger, M., Cölfen, H., 2006. Oriented attachment and mesocrystals: non-classical crystallization mechanisms based on nanoparticle assembly. Phys. Chem. Chem. Phys. 8, 3271–3287.
Nielsen, M.H., Aloni, S., De Yoreo, J.J., 2014. In situ TEM imaging of $CaCO_3$ nucleation reveals coexistence of direct and indirect pathways. Science 345, 1158–1162.
Nudelman, F., Sommerdijk, N.A.J.M., 2012. Biomineralization as an inspiration for materials chemistry. Angew. Chem. Int. Ed. 51, 6582–6596.
Nudelman, F., Chen, H.H., Goldberg, H.A., Weiner, S., Addadi, L., 2007. Spiers Memorial Lecture Lessons from biomineralization: comparing the growth strategies of mollusc shell prismatic and nacreous layers in *Atrina rigida*. Faraday Discuss. 136, 9–25.
Nývlt, J., 1995. The Ostwald rule of stages. Cryst. Res. Technol. 30, 445–451.
Oaki, Y., Kotashi, A., Miura, T., Imai, H., 2006. Bridged nanocrystals in biominerals and their biomimetics: classical yet modern crystal growth on the nanoscale. Adv. Funct. Mater. 16, 1633–1639.
Oaki, Y., Kjiyama, S., Nishimura, T., Imai, H., Kato, T., 2008. Nanosegregated amorphous composites of calcium carbonate and an organic polymer. Adv. Mater. 20, 3633–3637.
Ogino, T., Suzuki, T., Sawada, K., 1987. The formation and transformation mechanism of calcium carbonate in water. Geochim. Cosmochim. Acta 51, 2757–2767.
Olson, I.C., Blonsky, A.Z., Tamura, N., Kunz, M., Pokroy, B., Romao, C.P., White, M.A., Gilbert, P.U.P.A., 2013a. Crystal nucleation and near-epitaxial growth in nacre. J. Struct. Biol. 184, 454–463.
Olson, I.C., Metzler, R.A., Tamura, N., Kunz, M., Killian, C.E., Gilbert, P.U.P.A., 2013b. Crystal lattice tilting in prismatic calcite. J. Struct. Biol. 183, 180–190.
Olszta, M.J., Odom, D.J., Douglas, E.P., Gower, L.B., 2003. A new paradigm for biomineral formation: mineralization via an amorphous liquid-phase precursor. Connec. Tissue Res. 44, 326–334.
Olszta, M.J., Gajjeraman, S., Kaufman, M., Gower, L.B., 2004. Nanofibrous calcite synthesized via a solution-precursor-solid mechanism. Chem. Mater. 16, 2355–2362.
Olszta, M.J., Cheng, X., Jee, S.S., Kumar, R., Kima, Y.-Y., Kaufman, M.J., Douglas, E.P., Gower, L.B., 2007. Bone structure and formation: a new perspective. Mater. Sci. Eng. Rep. 58, 77–116.
Ortiz, C., Boyce, M.C., 2008. Bioinspired structural materials. Science 319, 1053–1054.
Ostwald, W., 1897. Studien über die Bildung und Umwandlung fester Körper. Z. Phys. Chem. 22, 289–330.
Penn, R.L., Banfield, J.F., 1998. Imperfect oriented attachment: dislocation generation in defect-free nanocrystals. Science 281, 969–971.
Penn, R.L., Soltis, J.A., 2014. Characterizing crystal growth by oriented aggregation. CrystEngComm 16, 1409–1418.
Perovic, I., Chang, E.P., Lui, M., Rao, A., Cölfen, H., Evans, J.S., 2014. A nacre protein, n16.3 self-assembles to form protein oligomers that dimensionally limit and organize mineral deposits. Biochemistry 53, 2739–2748.
Picker, A., Kellermeier, M., Seto, J., Gebauer, D., Cölfen, H., 2012. The multiple effects of amino acids on the early stages of calcium carbonate crystallization. Z. Kristallogr. 227, 744–757.
Pokroy, B., Kabalah-Amitai, L., Polishchuk, I., DeVol, R.T., Blonsky, A.Z., Sun, C.Y., Marcus, M.A., Scholl, A., Gilbert, P.U.P.A., 2015. Narrowly distributed crystal orientation in biomineral vaterite. Chem. Mater. 27, 6516–6523.
Politi, Y., Arad, T., Klein, E., Weiner, S., Addadi, L., 2004. Sea urchin spine calcite forms via a transient amorphous calcium carbonate phase. Science 306, 1161–1164.
Politi, Y., Levi-Kalisman, Y., Raz, S., Wilt, F., Addadi, L., Weiner, S., 2006. Structural characterization of the transient amorphous calcium carbonate precursor phase in sea urchin embryos. Adv. Funct. Mater. 16, 1289–1298.
Politi, Y., Mahamid, J., Goldberg, H., Weiner, S., Addadi, L., 2007. Asprich mollusk shell protein: in vitro experiments aimed at elucidating function in $CaCO_3$ crystallization. CrystEngComm 9, 1171–1177.
Politi, Y., Metzler, R.A., Abrecht, M., Gilbert, B., Wilt, F., Sagi, I., Addadi, L., Weiner, S., Gilbert, P.U.P.A., 2008. Transformation mechanism of amorphous calcium carbonate into calcite in the sea urchin larval spicule. Proc. Natl. Acad. Sci. U.S.A. 105, 17362–17366.
Politi, Y., Batchelor, D.R., Zaslansky, P., Chmelka, B.F., Weaver, J.C., Sagi, I., Weiner, S., Addadi, L., 2010. Role of magnesium ion in the stabilization of biogenic amorphous calcium carbonate: a structure-function investigation. Chem. Mater. 22, 161–166.
Pouget, E.M., Bomans, P.H.H., Goos, J.A.C.M., Frederik, P.M., de With, G., Sommerdijk, N.A.J.M., 2009. The initial stages of template-controlled $CaCO_3$ formation revealed by cryo-TEM. Science 323, 1455–1458.
Pouget, E.M., Bomans, P.H.H., Dey, A., Frederik, P.M., de With, G., Sommerdijk, N.A.J. M., 2010. The development of morphology and structure in hexagonal vaterite. J. Am. Chem. Soc. 132, 11560–11565.

Putnis, A., 2009. Mineral replacement reactions. Rev. Miner. Geochem. 70, 87–124.

Putnis, A., 2014. Why mineral interfaces matter. Science 343, 1441–1442.

Qiao, L., Feng, Q., Lu, S., 2008. In vitro growth of nacre-like tablet forming: from amorphous calcium carbonate, nanostacks to hexagonal tablets. Cryst. Growth Des. 8, 1509–1514.

Radha, A.V., Forbes, T.Z., Killian, C.E., Gilbert, P.U.P.A., Navrotsky, A., 2010. Transformation and crystallization energetics of synthetic and biogenic amorphous calcium carbonate. Proc. Natl. Acad. Sci. U.S.A. 107, 16438–16443.

Radha, A.V., Fernandez-Martinez, A., Hu, Y., Jun, Y.-S., Waychunas, G.A., Navrotsky, A., 2012. Energetic and structural studies of amorphous $Ca(1-x)MgxCO_3{\cdot}nH2O$ $(0 \leqslant x \leqslant 1)$. Geochim. Cosmochim. Acta 90, 83–95.

Raiteri, P., Gale, J.D., 2010. Water is the key to nonclassical nucleation of amorphous calcium carbonate. J. Am. Chem. Soc. 132, 17623–17634.

Raz, S., Weiner, S., Addadi, L., 2000. Formation of high-magnesian calcites via an amorphous precursor phase: possible biological implications. Adv. Mater. 12, 38–42.

Rieger, J., Thieme, J., Schmidt, C., 2000. Study of precipitation reactions by X-ray microscopy: $CaCO_3$ precipitation and the effect of polycarboxylates. Langmuir 16, 8300–8305.

Rieger, J., Frechen, T., Cox, G., Heckmann, W., Schmidt, C., Thieme, J., 2007. Precursor structures in the crystallization/precipitation processes of $CaCO_3$ and control of particle formation by polyelectrolytes. Faraday Discuss. 136, 265–277.

Rodriguez-Navarro, C., Benning, L.G., 2013. Control of crystal nucleation and growth by additives. Elements 9, 203–209.

Rodriguez-Navarro, C., Ruiz-Agudo, E., Niteo, 2013. Carbonates: an overview of recent research. In: Niteo, F., Livi, K.J.T. (Eds.), Minerals at the nanoscale, EMU Notes in Mineralogy, vol. 14. European Mineralogical Union, London, pp. 337–375.

Rodriguez-Navarro, C., Jimenez-Lopez, C., Rodriguez-Navarro, A., Gonzalez-Muñoz, M.T., Rodriguez-Gallego, M., 2007. Bacterially mediated mineralization of vaterite. Geochim. Cosmochim. Acta 71, 1197–1213.

Rodriguez-Navarro, A.B., Marie, P., Nys, Y., Hincke, M.T., Gautron, J., 2015a. Amorphous calcium carbonate controls avian eggshell mineralization: a new paradigm for understanding rapid eggshell calcification. J. Struct. Biol. 190, 291–303.

Rodriguez-Navarro, C., Kudłacz, K., Cizer, Ö., Ruiz-Agudo, E., 2015b. Formation of amorphous calcium carbonate and its transformation into mesostructured calcite. CrystEngComm 17, 58–72.

Rodriguez-Navarro, C., Burgos-Cara, A., Elert, K., Putnis, C.V., Ruiz-Agudo, E., 2016. Direct nanoscale imaging reveals the growth of calcite crystals via amorphous nanoparticles. Cryst. Growth Des. 16, 1850–1860.

Ruiz-Agudo, E., Putnis, C.V., Wang, L., Putnis, A., 2011. Specific effects of background electrolytes on the kinetics of step propagation during calcite growth. Geochim. Cosmichim. Acta 75, 3803–3814.

Ruiz-Agudo, E., Putnis, C.V., Rodriguez-Navarro, C., 2016. Reactions between minerals and aqueous solutions, In: Heinrich, W., Rainer, Abart, R., (Eds.), Mineral reaction kinetics: microstructures, textures, chemical and isotopic signatures. EMU Notes on Mineralogy, vol. 17, ch. 13, pp. 1–49.

Saito, T., Oaki, Y., Nishimura, T., Isogai, A., Kato, T., 2014. Bioinspired stiff and flexible composites of nanocellulose-reinforced amorphous $CaCO_3$. Mater. Horiz. 1, 321–325.

Sakamoto, T., Oichi, A., Nishimura, T., Sugawara, A., Kato, T., 2009. Calcium carbonate/polymer thin-film hybrids: induction of the formation of patterned aragonite crystals by thermal treatment of a polymer matrix. Polym. J. 41, 522–523.

Sanchez, C., Arribart, H., Guille, M., 2005. Biomimetism and bioinspiration as tools for the design of innovative materials and systems. Nat. Mater. 4, 277–288.

Sathiyanarayanan, R., Alimohammadi, M., Zhou, Y., Fichthorn, K.A., 2011. Role of solvent in the shape-controlled synthesis of anisotropic colloidal nanostructures. J. Phys. Chem. C 115, 18983–18990.

Sato, A., Nagasaka, S., Furihata, K., Nagata, S., Arai, I., Saruwatari, K., Kogure, T., Sakuda, S., Nagasawa, H., 2011. Glycolytic intermediates induce amorphous calcium carbonate formation in crustaceans. Nat. Chem. Biol. 7, 197–199.

Schenk, A.S., Zope, H., Kim, Y.-Y., Kros, A., Sommerdijk, N.A.J.M., Meldrum, F.C., 2012a. Polymer-induced liquid precursor (PILP) phases of calcium carbonate formed in the presence of synthetic acidic polypeptides—relevance to biomineralization. Farad. Discuss. 159, 327–344.

Schenk, A.S., Zlotnikov, I., Pokroy, B., Gierlinger, N., Masic, A., Zaslansky, P., Fitch, A. N., Paris, O., Metzger, T.H., Cölfen, H., Fraztl, P., Aichemayer, B., 2012b. Hierarchical calcite crystals with occlusions of a simple polyelectrolyte mimic complex biomineral structures. Adv. Funct. Mater. 22, 4668–4676.

Schiro, M., Ruiz-Agudo, E., Rodriguez-Navarro, C., 2012. Damage mechanisms of porous materials due to in-pore salt crystallization. Phys. Rev. Lett. 109, 265503.

Schmelzer, J.W.P., Fokin, V.M., Abyzov, A.S., Zanotto, E.D., Gutzow, I., 2010. How do crystals form and grow in glass-forming liquids: Ostwald's rule of stages and beyond. Int. J. Appl. Glass Sci. 1, 16–26.

Schwahn, D., Ma, Y., Cölfen, H., 2007. Mesocrystal to single crystal transformation of D, L-alanine evidenced by small angle neutron scattering. J. Phys. Chem. C 111, 3224–3227.

Sellinger, A., Weiss, P.M., Nguyen, A., Lu, Y., Assink, R.A., Gong, W., Brinker, C.J., 1998. Continuous self-assembly of organic-inorganic nanocomposite coatings that mimic nacre. Nature 394, 256–260.

Sethmann, I., Putnis, A., Grassmann, O., Löbmann, P., 2005. Observation of nano-clustered calcite growth via a transient phase mediated by organic polyanions: a close match for biomineralization. Am. Miner. 90, 1213–1217.

Sethmann, I., Hinrichs, R., Wörheide, G., Putnis, A., 2006. Nano-cluster composite structure of calcitic sponge spicules – a case study of basic characteristics of biominerals. J. Inorg. Biochem. 100, 88–96.

Seto, J., Ma, Y., Davis, S.A., Meldrum, F., Gourrier, A., Kim, Y.-Y., Schilde, U., Sztucki, M., Burghammer, M., Maltsev, S., Jäger, C., Cölfen, H., 2012. Structure-property relationships of a biological mesocrystal in the adult sea urchin spine. Proc. Natl. Acad. Sci. U.S.A. 109, 3699–3704.

Sleutel, M., van Driessche, A.E.S., 2014. Role of clusters in nonclassical nucleation and growth of protein crystals. Proc. Natl. Acad. Sci. U.S.A., E546–E553

Smeets, P.J.M., Cho, K.R., Kempen, R.G.E., Sommerdijk, N.A.J.M., De Yoreo, J.J., 2015. Calcium carbonate nucleation driven by ion binding in a biomimetic matrix revealed by in situ electron microcopy. Nat. Mater. 14, 394–399.

Sommerdijk, N.A.J.M., de With, G., 2008. Biomimetic CaCO3 mineralization using designer molecules and interfaces. Chem. Rev. 108, 4499–4550.

Sondi, I., Škapin, S., Jurina, I., Slovenec, D., 2011. A novel concept in the growth and design of anhydrous carbonate minerals: nano-scale aggregation mechanisms. Geol. Croat. 64, 61–65.

Song, R.-Q., Cölfen, H., 2010. Mesocrystals – ordered nanoparticle superstructures. Adv. Mater. 22, 1303–1330.

Song, R.-Q., Cölfen, H., 2011. Additive controlled crystallization. CrystEngComm 13, 1249–1276.

Song, R.Q., Cölfe, H., Xu, A-.W., Hartmann, J., Antonietti, M., 2009. Polyelectrolyte-directed nanoparticle aggregation: systematic morphogenesis of calcium carbonate by nonclassical crystallization. ACS Nano 3, 1966–1978.

Stolarski, J., Mazur, M., 2005. Nanostructure of biogenic versus abiogenic calcium carbonate crystals. Acta Paleontol. Polonica 50, 847–865.

Stranski, I.N., Totomanov, D., 1933. Rate of formation of (crystal) nuclei and the Ostwald step rule. Z. Phys. Chem. 163, 399–408.

Sugawara, A., Kato, T., 2000. Aragonite $CaCO_3$ thin-film formation by cooperation of Mg^{2+} and organic polymer matrices. Chem. Commun., 487–488

Sugawara, A., Nishimura, T., Yamamoto, Y., Inoue, H., Nagasawa, H., Kato, T., 2006. Self-organization of oriented calcium carbonate/polymer composites: effects of a matrix peptide isolated from the exoskeleton of a crayfish. Angew. Chem. Int. Ed. 45, 2876–2879.

Sun, S., Mao, L.-B., Lei, Z., Yu, S.-H., Cölfen, H., 2016. Hydrogels from amorphous calcium carbonate and polyacrylic acid: bio-inspired materials for "mineral plastics". Angew. Chem. Int. Ed. 55. http://dx.doi.org/10.1002/anie.201602849.

Takahashi, K., Yamamoto, H., Onoda, A., Doi, M., Inaba, T., Chiba, M., Kobayashi, A., Taguchi, T., Okamura, T., Ueyama, N., 2004. Highly oriented aragonite nanocrystal–biopolymer composites in an aragonite brick of the nacreous layer of *Pinctada fucata*. Chem. Commun., 996–997

Teng, H.H., Dove, P.M., Orme, C.A., De Yoreo, J.J., 1998. Thermodynamics of calcite growth: baseline for understanding biomineral formation. Science 282, 724–727.

Threlfall, T., 2003. Structural and thermodynamic explanations of Ostwald's rule. Org. Process Res. Dev. 7, 2017–2027.

Towe, K.M., Lowenstam, H.A., 1967. Ultrastructure and development of iron mineralization in the radular teeth of *Cryptochiton stelleri* (Mollusca). J. Ultrastruct. Res. 17, 1–13.

Travaille, A.M., Steijven, E.G.A., Meekes, H., van Kempen, H., 2005. Thermodynamics of epitaxial calcite nucleation on self-assembled monolayers. J. Phys. Chem. B 109, 5618–5626.

Tremel, W., Küther, J., Balz, M., Loges, N., Wolf, S.E., 2007. Template surfaces for the formation of calcium carbonate. In: Bäuerlein, E. (Ed.), Handbook of Biomineralization. Wiley-VCH Verlag GmbH, Berlin, pp. 209–232.

Tseng, Y.-H., Chevillard, C., Dauphin, Y., Guenoun, P., 2014. $CaCO_3$ nanostructured crystals induced by nacreous organic extracts. CrystEngComm 16, 561–569.

van Santen, R.A., 1984. The Ostwald step rule. J. Phys. Chem. 88, 5768–5769.

Vekilov, P.G., De Yoreo, J.J., 2003. Principles of crystal nucleation and growth. Rev. Miner. Geochem. 54, 57–93.

Verch, A., Gebauer, D., Antonietti, M., Cölfen, H., 2011. How to control the scaling of $CaCO_3$: a "fingerprinting technique" to classify additives. Phys. Chem. Chem. Phys. 13, 16811–16820.

Vielzeuf, D., Garrabou, J., Baronnet, A., Grauby, O., Marschal, C., 2008. Nano to macroscale biomineral architecture of red coral (*Corallium rubrum*). Am. Miner. 93, 1799–1815.

Vielzeuf, D., Floquet, N., Chatain, D., Bonneté, F., Ferry, D., Garrabou, J., Stolper, E.M., 2010. Multilevel modular mesocrystalline organization in red coral. Am. Miner. 95, 242–248.

Volkmer, D., Harms, M., Gower, L., Ziegler, A., 2005. Morphosynthesis of nacre-type laminated $CaCO_3$ thin films and coatings. Angew. Chem. Int. Ed. 44, 639–644.

Volmer, M., Weber, A., 1926. Keimbildung in übersättigten Gebilden. Z. Phys. Chem. 119, 277–301.

Wallace, A.F., Hedges, L.O., Fernandez-Martinez, A., Raiteri, P., Gale, J.D., Waychunas, G.A., Whitelam, S., Banfield, J.F., De Yoreo, J.J., 2013. Microscopic evidence for liquid-liquid separation in superpersaturated $CaCO_3$ solutions. Science 341, 885–889.

Wang, D., Wallace, A.F., De Yoreo, J.J., Dove, P.M., 2009. Carboxylated molecules regulate magnesium content of amorphous calcium carbonate during calcification. Proc. Natl. Acad. Sci. U.S.A. 106, 21511–21516.

Wang, T., Leng, B., Che, R., Shao, Z., 2010. Biomimetic synthesis of multilayered aragonite aggregates using alginate as crystal growth modifier. Langmuir 26, 13385–13392.

Wang, F., Richards, V.N., Shields, S.P., Buhro, W.E., 2013a. Kinetics and mechanisms of aggregative nanocrystal growth. Chem. Mater. 26, 5–21.

Wang, Y., Von Euw, S., Fernandes, F.M., Cassaignon, S., Selmane, M., Laurent, G., Pehau-Arnaudet, G., Coelho, C., Bonhomme-Coury, L., Giraud-Guille, M.-M., Babonneau, F., Azaïs, T., Nassif, N., 2013b. Water-mediated structuring of bone apatite. Nat. Mater. 12, 1144–1153.
Wegst, U.G.K., Bai, H., Saiz, E., Tomsia, A.P., Ritchie, R.Q., 2015. Bioinspired structural materials. Nat. Mater. 14, 23–36.
Weiner, S., Addadi, L., 2011. Crystallization pathways in biomineralization. Annu. Rev. Mater. Res. 41, 21–40.
Williams, A., Cusack, M., Brown, K., 1999. Growth of protein-doped rhombohedra in the calcitic shell of craniad brachiopods. Proc. R. Soc., London, Ser. B 266, 1601–1607.
Woehl, T.J., Park, C., Evans, J.E., Arslan, I., Ristenpart, W.A., Browning, N.D., 2014. Direct observation of aggregative nanoparticle growth: kinetic modeling of the size distribution and growth rate. Nano Lett. 14, 373–378.
Wohlrab, S., Cölfen, H., Antonietti, M., 2005. Crystalline, porous microspheres made from amino acids by using polymer-induced liquid precursor phases. Angew. Chem. Int. Ed. 44, 4087–4092.
Wolf, S.E., Leiterer, J., Kappl, M., Emmerling, F., Tremel, W., 2008. Early homogeneous amorphous precursor stages of calcium carbonate and subsequent crystal growth in levitated droplets. J. Am. Chem. Soc. 130, 12342–12347.
Wolf, S.E., Leiterer, J., Pipich, V., Barrea, R., Emmerling, F., Tremel, W., 2011a. Strong stabilization of amorphous calcium carbonate emulsion by ovalbumin: gaining insight into the mechanism of "polymer-induced liquid precursor" process. J. Am. Chem. Soc. 133, 12642–12649.
Wolf, S.E., Müller, L., Barrea, R., Kampf, C.J., Leterer, J., Panne, Hoffmann, T., Emmerling, F., Tremel, W., 2011b. Carbonate-coordinated metal complexes precede the formation of liquid amorphous mineral emulsions of divalent metal carbonates. Nanoscale 3, 1158–1165.
Wolf, S.E., Leiberwirth, I., Natalio, F., Bardeau, J.-F., Delorme, N., Emmerling, F., Barrea, R., Kappl, M., Marin, F., 2012. Merging models of biomineralisation with concepts of nonclassical crystallisation: is a liquid amorphous precursor involved in the formation of the prismatic layer of the Mediterranean Fan Mussel *Pinna nobilis*? Faraday Discuss. 159, 433–448.
Wolf, S.E., Böhm, C., Harris, J., Hajir, M., Mondeshki, M., Marin, F., 2015a. Single nanogranules preserve intracrystalline amorphicity in biominerals. Key Eng. Mater. 672, 47–59.
Wolf, S.L.P., Jähme, K., Gebauer, D., 2015b. Synergy of Mg^{2+} and poly(aspartic acid) in additive-controlled calcium carbonate precipitation. CrystEngComm 17, 6857–6862.
Wolf, S.E., Bohn, C.F., Harris, J., Demmert, B., Jacob, D.E., Mondeshki, M., Ruiz-Agudo, E., Rodriguez-Navarro, C., 2016a. Nonclassical crystallization in vivo et in vitro (I): process-structure-property relationships of nanogranular biominerals. J. Struct. Biol. 196, 244–259.
Wolf, S.E., Lovett, A., Harris, J., Gower, L.B., 2016b. Non-classical crystallization processes: potential relevance to stone formation. In: Coe, F.L., Worcester, E.M., Lingeman, J.E., Evan, A.P. (Eds.), Kidney stones: Medical and surgical management. Jaypee Medical Publishers, Philadelphia, PA. in press.
Wright, D.T., Oren, A., 2005. Nonphotosynthetic bacteria and the formation of carbonates and evaporites through time. Geomicrobiol J. 22, 27–53.
Xiao, J., Yang, S., 2011. Biomimetic synthesis, hierarchical assembly and mechanical properties of calcite/chitosan composites in a three-dimensional chitosan scaffold. Adv. Mater. 13, B32–B40.
Xu, G., Yao, N., Aksay, I.A., Groves, J.T., 1998. Biomimetic synthesis of macroscopic-scale calcium carbonate thin films. Evidence for a multistep assembly process. J. Am. Chem. Soc. 120, 11977–11985.
Xu, X., Han, J.T., Cho, K., 2004. Formation of amorphous calcium carbonate thin films and their role in biomineralization. Chem. Mater. 16, 1740–1746.
Xu, X., Han, J.T., Cho, K., 2005. Deposition of amorphous calcium carbonate hemispheres on substrates. Langmuir 21, 4801–4804.
Xu, X., Han, J.T., Kim, D.H., Cho, K., 2006. Two modes of transformation of amorphous calcium carbonate films in air. J. Phys. Chem. B 110, 2764–2770.
Xu, A.-W., Ma, Y., Cölfen, H., 2007. Biomimetic mineralization. J. Mater. Chem. 17, 415–449.
Xu, J., Yan, C., Zhang, F., Konishi, H., Xu, H., Teng, H.H., 2013. Testing the cation-hydration effect on the crystallization of Ca-Mg-CO_3 systems. Proc. Natl. Acad. Sci. U.S.A. 110, 17750–17755.
Yang, L., Killian, C.E., Kunz, M., Tamura, N., Gilbert, P.U.P.A., 2011. Biomineral nanoparticles are space-filling. Nanoscale 3, 603–609.
Yao, H.-B., Ge, J., Yan, Y.-X., Yu, S.-H., 2014. Artificial carbonate nanocrystals and layered structural nanocomposites inspired by nacre: synthesis, fabrication and applications. Adv. Mater. 26, 163–188.
Yuwono, V.M., Burrows, N.D., Soltis, J.A., Penn, R.L., 2010. Oriented aggregation: formation and transformation of mesocrystal intermediates revealed. J. Am. Chem. Soc. 132, 2163–2165.
Zhang, H., Banfield, J.F., 2014. Interatomic Coulombic interactions as the driving force for oriented attachment. CrystEngComm 16, 1568–1578.
Zhang, H., Gilbert, B., Huang, F., Banfield, J.F., 2003. Water-driven structure transformation in nanoparticles at room temperature. Nature 424, 1025–1029.
Zhang, H., De Yoreo, J.J., Banfield, J.F., 2014. A unified description of attachment-based crystal growth. ACS Nano 8, 6226–6530.
Zhong, C., Chu, C.C., 2009. Acid polysaccharide-induced amorphous calcium carbonate (ACC) films: colloidal nanoparticle self-organization process. Langmuir 25, 3045–3049.
Zhou, L., O'Brian, P., 2008. Mesocrystals: a new class of solid materials. Small 4, 1566–1574.
Zhou, L., O'Brien, P., 2012. Mesocrystals – properties and applications. J. Phys. Chem. Lett. 3, 620–628.
Zhu, Y., Liu, Y., Ruan, Q., Zeng, Y., Xiao, J., Liu, Z., Cheng, L., Xu, F., Zhang, L., 2009. Superstructures and mineralization of laminated vaterite mesocrystals via mesoscale transformation and self-assembly. J. Phys. Chem. 113, 6584–6588.
Zhu, W., Lin, J., Cai, C., Lu, Y., 2013. Biomimetic mineralization of calcium carbonate mediated by a polypeptide-based copolymer. J. Mater. Chem. B 1, 841–849.
Zhu, F., Nishimura, T., Eimura, H., Kato, T., 2014. Supramolecular effects on formation of $CaCO_3$ thin films on a polymer matrix. CrystEngComm 16, 1496–1501.
Zhu, J., Huang, L., Cui, M., Ma, L., Cao, F., 2015. A cationic polyelectrolyte-controlled liquid mineral precursor process in the $BaCO_3$ system. Eur. J. Inorg. Chem., 1819–1826
Zou, Z., Bertinetti, L., Politi, Y., Jensen, A.C.S., Weiner, S., Addadi, L., Fratzl, P., Habraken, W.J.E.M., 2015. Opposite particle size effect on amorphous calcium carbonate crystallization in water and during heating on air. Chem. Mater. 27, 4237–4246.
Zou, Z., Habraken, W.J., Bertinetti, L., Politi, Y., Gal, A., Weiner, S., Addadi, L., Fratzl, P., 2016. On the phase diagram of calcium carbonate solutions. Adv. Mater. Interfaces. 1600076.
Zuykov, M., Pelletier, E., Anderson, J., Cotterell, T.F., Belzile, C., Demers, S., 2012. In vitro growth of calcium carbonate crystals on bivalve shells: application of two methods of synthesis. Mater. Sci. Eng., C 32, 1158–1163.